Universität Konstanz

Activation driven by a non-Markovian heat bath

Bachelorarbeit

vorgelegt von

Elias Kohler

Mathematisch-Naturwissenschaftliche Sektion
Fachbereich Physik

Betreuer 1: Nikolas Ditz

Betreuer 2: Prof. M. Fuchs

Gutachter: Professor Dr. M. Fuchs

überarbeitete Version

16. September 2021

Abstract

Glassy systems are often described as supercooled liquids in which the microscopic disordered structure of a liquid is 'frozen' by rapid cooling. As a result, glassy systems are far from thermal equilibrium. A promising concept to describe glassy systems are effective temperatures. In this thesis, three possible effective temperatures are investigated using a model system developed by Ilg and Barrat [J. Phys.: Conf. Ser. **40**, 76 (2006)]. The system models the thermal non-equilibrium of a glass over two heat baths maintained at different temperatures. The meta-stable character of a glass system is modelled by a double well potential. The first definition of an effective temperature in this model results from the stationary distribution of the system. The second definition uses the fluctuation-dissipation theorem (FDT). The third definition is given by the Arrhenius dependence of the model system. It is shown numerically that the effective temperature according to the first definition depends very strongly on the curvature of the potential minia of the double well potential and not on the exact shape of the meta stable potential. The second central statement in this thesis is that the effective temperature according to the first definition and the effective temperature defined via the FDT do not coincide for the model system. Further, it can be shown numerically that the second definition and the third definition of the effective temperature are identical for many system settings, but not for all.

Zusammenfassung

Glasige Systeme werden oft als unterkühlte Flüssigkeiten beschrieben bei denen die mikroskopische ungeordnete Struktur einer Flüssigkeit durch schnelles abkühlen 'eingefroren' wird. Dadurch befinden sich glasige Systeme weit entfernt vom thermischen Gleichgewicht. Ein vielversprechendes Konzept um glasige Systeme zu beschreiben sind effektive Temperaturen. In dieser Arbeit werden an einem Modellsystem, welches von Ilg und Barrat entwickelt wurde [J. Phys.: Conf. Ser. **40**, 76 (2006)], drei mögliche effektive Temperaturen untersucht. Das Modellsystem modelliert das thermische Nichtgleichgewicht eines Glases über zwei Wärmebäder die auf unterschiedlichen Temperaturen gehalten werden. Der metastabile Charakter eines Glassystems wird durch ein Doppelmulden-Potenzial modelliert. Die erste Definition einer effektiven Temperatur in diesem Modell ergibt sich aus der stationären Verteilung des Systems. Die zweite Definition verwendet das Fluktuations-Dissipations-Theorem (FDT). Die dritte Definition ergibt sich über die Arrhenius Abhängigkeit des Systems. Es wird nummerisch gezeigt, dass die effektive Temperatur nach der ersten Definition sehr stark von der Krümmung der Potenzialminima des Doppelmulden-Potenzials abhängt und nicht von der genauen Form des metastabilen Potenzials. Die zweite zentrale Aussage in dieser Arbeit ist, dass die effektive Temperatur nach der ersten Definition und die effektive Temperatur die über das FDT definiert ist, für das Modellsystem nicht übereinstimmen. Weiter kann nummerisch gezeigt werden, dass die zweite Definition und die dritte Definition der effektiven Temperatur für viele Systemeinstellungen, aber nicht für alle, identisch sind.

Contents

1. Introduction

Solids can be roughly divided into crystals and amorphous solids. In amorphous solids, which are also called glassy systems, the microscopic structure of the matter is disordered. In contrast, crystals always have a strictly periodic structure [1].

Glassy systems are less well understood than their closest relatives liquids and crystals [1]. Amorphous solids are usually produced by engineering processes in which a viscous liquid is rapidly cooled so that the system cannot change from the disordered structure of a liquid to an ordered crystal structure [2]. A very illustrative example is the production of a wine glass. For this, quartz sand is heated in a melting furnace to such an extent that it becomes a viscous liquid. This viscous molten glass is then brought into a wine glass mould by a glassblower with a glassmaker's pipe by skilful turning and blowing. Due to the extreme temperature difference between the molten glass and room temperature, the viscous molten glass cools down very quickly and vitrifies. The technical processes for the production of glass thus suggest a physical description in which glassy systems are modelled as a supercooled viscous liquid [2,3].

A very powerful approach to the description of glassy systems is provided by thermodynamics [3,4]. Historically, thermodynamics was developed to understand the optimal efficiency of steam engines. Important people in the field of early thermodynamics are Carnot and Clausius. In the mid to late 19th century, Boltzmann and Gibbs developed statistical mechanics in equilibrium through microscopic reasoning which can derive many of the phenomenological statements of early thermodynamics. Since Boltzmann and Gibbs, thermodynamic systems have been studied and described using the methods of statistical mechanics. In the middle of the last century, the development of non-equilibrium thermodynamics, which is close to equilibrium, was also completed. Important contributions were made by Donder, Prigogine, de Groot, and Mazur [4].

Due to the rapid cooling of a viscous liquid, the system does not have the possibility to relax into thermal equilibrium. The thermal equilibrium in this case would correspond to an ordered crystal structure. The system is therefore 'frozen' in its liquid disordered state and vitrified [2]. Typical values for the cooling rate in the laboratory are $0.1 - 100\,\mathrm{K/min}$ [3]. Glassy systems are characterised by the fact that they are far from thermal equilibrium. Therefore, systems are generally called glassy if their relaxation to equilibrium occurs on time scales much larger than the observation time [4]. Above the melting temperature T_m, the relaxation time τ_α of density fluctuations can be estimated by $\tau_\alpha = \sqrt{ma^2/(k_B T)}$, where m is the mass of the molecules, a is a characteristic length distance between molecules and $k_B T$ is the thermal energy. τ_α in this case is in the pico-second range. In the glass state below the glass transition temperature T_g, the relaxation time τ_α is of the order of 100 s, i.e. 14 orders of magnitude larger. This extreme change in relaxation time is very impressive since typical temperatures at which a glass phase occurs are in the range of $T_m/3$. A relatively small temperature decrease leads to a very large increase of the relaxation time τ_α in the region of the gas transition [3].

Glassy systems and supercooled liquids can be classified well by an Angell diagram. An Angell diagram shows the logarithm of the relaxation time as a function of the inverse system temperature. Such a diagram is shown in Figure 1.1. The normalised relaxation time τ_α/τ_0 is plotted as a function of the normalised inverse temperature T_g/T of the system. Note that τ_α/τ_0 is plotted logarithmically in Figure 1.1. If a supercooled liquid has a straight curve in the Angell diagram, it is called 'strong'. In the other case, the liquid is called 'fragile'. Strong glasses

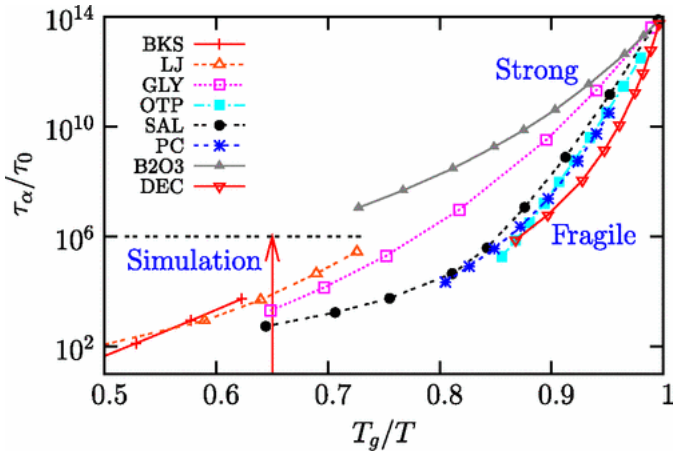

Figure 1.1: An Angell diagram is shown in which the increase in relaxation time is plotted as the glass transition temperature T_g is approached for different liquids. A time scale is also given, which is accessible for numerical simulations. Glass-forming liquids can now be divided into 'strong' and 'fragile'. For 'strong' fluids, $\log(\tau_\alpha)$ is a straight line. For 'fragile' fluids, the curves are curved. The figure is taken from [3].

therefore have an Arrhenius dependence which is written by

$$\tau_\alpha = \tau_0 \exp\left(\frac{E_b}{k_B T}\right) \tag{1.1}$$

where E_b denotes the activation energy. The terms 'strong' and 'fragile' fluid do not refer to mechanical properties. Strong fluids have a strong short-range order. A typical example of 'strong' liquids is window glass in which the silicon atoms and the oxygen atoms both above and below T_g locally have a tetrahedral short-range order [3]. This thesis focuses on 'strong' liquids where Arrhenius dependence occurs. Therefore, 'fragile' fluids will not be discussed further in the following.

Since Arrhenius dependence occurs for 'strong' fluids, it is natural to describe these systems with activated rate theory, which explains the Arrhenius factor through a model. The basic problem in activated rate theory is called the barrier crossing or Kramer's problem, where a single degree of freedom is coupled to a heat bath and moves in a double well potential. The quantity of interest in this process is the average time it takes for the system to change state and move from one potential well to the other well under the influence of the coupled heat bath. The single degree of freedom is often called the reaction coordinate. The assumption is that the state of a glass system can be summarised in a single reaction coordinate. The other degrees of freedom of the glass system are combined into a heat bath and thus influence the reaction coordinate [5]. As described at the beginning, glassy systems are characterised by the fact that they are far from thermal equilibrium. Ilg and Barrat have therefore proposed a model in which the reaction coordinate is coupled to two heat baths with different temperatures T_1 and T_2 . This is a conceptually simple but elegant way to generate a thermal non-equilibrium system. The first heat bath with temperature T_1 combines the fast fluctuating degrees of freedom of the glass system. The second heat bath with temperature T_2 combines the slow long-range correlated degrees of freedom [6].

An important physical question, also in experimental terms, is how to define a temperature in a many-body system which is far from equilibrium and its relaxation to equilibrium is characterised by several different time scales [3]. In the model [6], two different relaxation timescales are considered by the temperatures T_1 and T_2, where the first heat bath has a very small relaxation timescale and the second heat bath has a very large relaxation timescale. An answer to this question could be given by the concept of effective temperatures. A first definition of an

effective temperature uses the fluctuation-dissipation theorem (FDT) where the temperature of the equilibrium system is replaced by the effective temperature. However, there are other ways to define an effective temperature in a non-equilibrium system [3].

The aim of this thesis is to investigate three possible definitions of effective temperatures for the model system [6] and to discuss them analytically and numerically. The first definition of an effective temperature is given by the stationary canonical probability distribution of the system. The second definition uses the (FDT) in an integrated form. The third definition follows from the Arrhenius dependence of the system. Finally, the three definitions are examined in terms of their similarities and differences.

This thesis is divided into 6 chapters. Chapter 2 summarises the most important stochastic concepts for statistical mechanics in non-equilibrium, which are needed for this thesis.

In Chapter 3, the model of Ilg and Barrat [6] is first presented and discussed in detail. Here, the model is most easily defined via a generalised non-Markovian Langevin equation. By introducing an auxiliary variable, the generalised non-Markovian Langevin equation can be transformed into a set of Markovian equations for this particular model. The transformation distinguishes the case for general friction and the case for strong friction. The Markovian equations can be solved exactly for a quadratic potential. The correlation function and the susceptibility are then calculated with the analytically exact solution.

Chapter 4 is dedicated to the activated rate theory. For this purpose, the derivation of the Fokker Planck equation is outlined first. The Fokker Planck equation is then used to derive the mean escape rate for a double trough potential. Subsequently, a possibility is discussed how to determine the mean escape rate numerically from a two-level correlation function. The chapter ends with the derivation of the probability distribution function for the reaction coordinate of the model of Ilg and Barrat for the Ornstein-Uhlenbeck process.

In the chapter 5 the concept of effective temperature is discussed on the model of Ilg and Barrat for the overdamped case. Three different definitions of an effective temperature are presented. The first definition uses a stationary canonical distribution. The second definition of an effective temperature uses the fluctuation dissipation theorem (FDT). The last definition is realised via the Arrhenius factor.

In chapter 6 the numerical methods in this thesis are presented in detail. Central to this chapter is the numerical solution of the model for the double well potential. Further, the numerical solutions of the correlation function and the susceptibility for the reaction coordinate are presented.

Chapter 7 presents the numerical results and compares them with analytical considerations. In this chapter, the numerical implementation is first tested using the Ornstein-Uhlenbeck process, since the analytical solution is known for this process. Then the time t_{st} at which the system assumes a stationary distribution is determined. The time t_{st} is important in the calculation of effective temperatures. Subsequently, the friction strength is determined at which the model changes to the overdamped case. In the last part of the chapter, the effective temperatures, which were defined in chapter 5, are calculated numerically and compared with analytical approximations.

2. Basic concepts of stochastics

In this section, the important concepts in stochastics are briefly presented. These concepts will become especially important for the derivation of the Fokker Planck equation. The presentation and definitions are already tailored to the later application. The aim is not to make more generalisations than are absolutely necessary.

2.1 Random variables and probability distribution functions

Statistical mechanics deals with systems that normally contain $\sim 10^{23}$ particles. Given this large number of degrees of freedom, it is practically impossible and also not meaningful to characterise the system by its individual degrees of freedom. The basic approach in statistical mechanics is to simplify the system with its many microscopic degrees of freedom to a few macroscopic variables that characterise the macroscopic state of the system. Typical macroscopic variables are the total energy E, the temperature T or the total volume V [7, pp. 3–4]. Depending on the choice of ensemble, individual macroscopic variables can fluctuate. For example, in the canonical ensemble, the system is locked to a heat bath, so the energy E of the system can fluctuate [7, pp. 50–53].

This concept of statistical mechanics in equilibrium is now to be generalised a little. We assume that a system with many degrees of freedom can be described by a few reaction coordinates $x_1, x_2, ...x_n$. The reaction coordinates do not necessarily have to be macroscopic quantities. For example, a reaction coordinate could also be an electron position in a solid and thus a microscopic quantity [5]. It is only important that the problem can be described with a few reaction coordinates. In the case of the electron, the macroscopic solid can be reduced to an effective one-particle problem in a potential. The remaining degrees of freedom form a heat bath and cause the reaction coordinates to fluctuate. Because the reaction coordinates fluctuate, the state of the system can be well characterised by a probability distribution function.

Let $\boldsymbol{x}$ be a vector that uniquely determines the state of the system for any time $t \geq 0$. In our case, the vector $\boldsymbol{x}$ summarises all reaction coordinates. Let $E \subset \mathbb{R}^n$ be the set of states that $\boldsymbol{x}$ can assume, $\boldsymbol{x} \in E$. In stochastics, E is called the event set [7, p. 4].

Now the term 'random variable' must be introduced. Let $\boldsymbol{X}$ be a random variable. $\boldsymbol{X}$ has no predetermined value, but can take on different values $\boldsymbol{x} \in E$. The probability that $\boldsymbol{X}$ takes values in the n-dimensional cube $[\boldsymbol{x}, \boldsymbol{x} + d\boldsymbol{x}] \subset E$ is given by $p(\boldsymbol{x})d^n x$. The function $p(\boldsymbol{x})$ is the probability distribution function which satisfies the properties

$$p(\boldsymbol{x}) \geq 0 \quad \text{for all} \quad \boldsymbol{x} \in E \tag{2.1}$$

$$\int_E p(\boldsymbol{x}) d^n x = 1. \tag{2.2}$$

The first property expresses that the probability $p(\boldsymbol{x})dx$ that the reaction coordinate takes a value in the cube $[\boldsymbol{x}, \boldsymbol{x} + d\boldsymbol{x}]$ must always be greater than or equal to zero. The second property states that the total probability of being in any state $\boldsymbol{x} \in E$ is 1. The probability distribution function $p(\boldsymbol{x})$ can also depend on time. This is noted as $p(\boldsymbol{x}, t)$. In this case, the random variable

$\boldsymbol{X}(t)$ also depends on the time. The time-dependent probability density $p(\boldsymbol{x}, t)$ must also satisfy the properties in equations (2.1) and (2.2) for all times t [7, pp. 4–7].

The average of the random variable $\boldsymbol{X}$ is defined by

$$\langle \boldsymbol{X} \rangle = \int_E \boldsymbol{x} p(\boldsymbol{x}, t) d^n x \tag{2.3}$$

[7, pp. 4–7]. Let X_i be the i-th component of the vector $\boldsymbol{X}$. Thus, the variance of the random variable $\boldsymbol{X}$ can be defined in the same way by

$$\langle (X_i - \langle X_i \rangle)^2 \rangle = \int_E (x_i - \langle X_i \rangle)^2 p(\boldsymbol{x}, t) d^n x \tag{2.4}$$

[7, pp. 4–7]. An important generalisation of the variance, which also plays an important role in this thesis, is the correlation function. $X_i(t_2)$ and $X_j(t_1)$ are two components of the random variable $\boldsymbol{X}$ at the times t_2 and t_1. Let $\boldsymbol{f}$ be a function with $X_i \mapsto f_i(X_i)$ for all $i \in \{1, ..., n\}$. Then the correlation function is defined by [8, pp. 63–64]

$$\begin{aligned} \mathrm{Cor}_f(t_2, t_1) &= \langle [f_i(x_i(t_2)) - \langle f_i(X_i(t_2)) \rangle] [f_j(x_j(t_1)) - \langle f_j(X_j(t_1)) \rangle] \rangle \\ &= \int_E [f_i(x_i(t_2)) - \langle f_i(X_i(t_2)) \rangle] [f_j(x_j(t_1)) - \langle f_j(X_j(t_1)) \rangle] \\ &\qquad \times p(\boldsymbol{x}(t_2), t_2; \boldsymbol{x}(t_1), t_1) d^n x. \end{aligned} \tag{2.5}$$

2.2 Conditional probability and Markov processes

The concept of conditional probability is needed for the characterisation of Markov processes. Markov processes are an important model process in non-equilibrium statistical mechanics as they are conceptually relatively simple. Therefore, concept of conditional probability is briefly presented in the following. This entire section is strongly oriented towards the presentations in J. Honerkamp [8, pp. 65–69].

Let $\boldsymbol{x}_n \in \mathbb{R}^m$ be the reaction coordinates at time t_n. Then the probability

$$p_2(\boldsymbol{x}_n, t_n | \boldsymbol{x}_{n-1}, t_{n-1}) d^m x \tag{2.6}$$

denotes the probability that the reaction coordinates are in the cube $\boldsymbol{X}_n \in [\boldsymbol{x}_n, \boldsymbol{x}_n + d\boldsymbol{x}]$ at time t_n under the condition that the reaction coordinates had the values $\boldsymbol{x}_{n-1}$ at time t_{n-1}. The function $p_2(\boldsymbol{x}_n, t_n | \boldsymbol{x}_{n-1}, t_{n-1})$ as a function of $(\boldsymbol{x}_{n-1}, t_{n-1}) \in \mathbb{R}^{m+1}$ is again a probability distribution function with the properties $p_2(\boldsymbol{x}_n, t_n | \boldsymbol{x}_{n-1}, t_{n-1}) \geq 0$ for all $(\boldsymbol{x}_n, t_n) \in \mathbb{R}^{m+1}$ and

$$\int_{\mathbb{R}^m} p_2(\boldsymbol{x}_n, t_n | \boldsymbol{x}_{n-1}, t_{n-1}) d^m x_n = 1.$$

The second property states that the reaction coordinates that possessed the state $\boldsymbol{x}_{n-1}$ at time t_{n-1} must certainly be in some state at time t_n. Let $p_2(\boldsymbol{x}_n, t_n; \boldsymbol{x}_{n-1}, t_{n-1})$ be the joint probability density that the reaction coordinates have the values $\boldsymbol{x}_n$ at time t_n and at time t_{n-1} the reaction coordinates had the values $\boldsymbol{x}_{n-1}$. For the conditional probability, the multiplication theorem

$$p_1(\boldsymbol{x}_n, t_n; \boldsymbol{x}_{n-1}, t_{n-1}) = p_2(\boldsymbol{x}_n, t_n | \boldsymbol{x}_{n-1}, t_{n-1}) p_2(\boldsymbol{x}_{n-1}, t_{n-1}) \tag{2.7}$$

applies where the marginal density $p_2(\boldsymbol{x}_{n-1}, t_{n-1})$ is calculated by

$$p_2(\boldsymbol{x}_{n-1}, t_{n-1}) = \int_{\mathbb{R}^m} p_2(\boldsymbol{x}_n, t_n; \boldsymbol{x}_{n-1}, t_{n-1}) d^m x_n. \tag{2.8}$$

The conditional probability can now be generalised to $n-1$ conditions. Then the probability

$$p_n(\boldsymbol{x}_n, t_n | \boldsymbol{x}_{n-1}, t_{n-1}; \boldsymbol{x}_{n-2}, t_{n-2}; ...; \boldsymbol{x}_1, t_1) d^m x \tag{2.9}$$

denotes the probability that the reaction coordinates are in the cube $\boldsymbol{X}_n = [\boldsymbol{x}_n, \boldsymbol{x} + d\boldsymbol{x}]$ at time t_n under the condition that the reaction coordinates had the values $\boldsymbol{x}_{n-1}$ at time t_{n-1}, at time t_{n-2} the values $\boldsymbol{x}_{n-2}$, ... and finally at time t_1 the values $\boldsymbol{x}_1$.

Handling Markov processes is usually much easier than handling non-Markov processes. Markov processes are characterised by the property

$$p_n(x_n, t_n | x_{n-1}, t_{n-1}; ...; x_1 t_1) = p_2(x_n, t_n | x_{n-1} t_{n-1}). \tag{2.10}$$

The Markov condition thus means that the transition from $\boldsymbol{x}_{n-1}$ to $\boldsymbol{x}_n$ in the time from $t_n - 1$ to t_n is independent of the history of how the system arrived at the state $\boldsymbol{x}_{n-1}$. The temporal development of a Markov process thus depends only on the present. One can therefore say that a Markov process is a stochastic process without memory.

Now the proof of the Chapamn-Kolmogorov equation will be briefly sketched. For this purpose, the joint probability distribution function $p_3(\boldsymbol{x}_3, t_3; \boldsymbol{x}_2, t_2; \boldsymbol{x}_1, t_1)$ is considered. The multiplication theorem applied twice to the probability density yields

$$p_3(\boldsymbol{x}_3, t_3; \boldsymbol{x}_2, t_2, \boldsymbol{x}_1, t_1) = p_3(\boldsymbol{x}_3, t_3 | \boldsymbol{x}_2, t_2, \boldsymbol{x}_1, t_1) p_2(\boldsymbol{x}_2, t_2 | \boldsymbol{x}_1, t_1) p_1(\boldsymbol{x}_1, t_1). \tag{2.11}$$

For a Markov process the first conditional probability yields

$$p_3(\boldsymbol{x}_3, t_3 | \boldsymbol{x}_2, t_2, \boldsymbol{x}_1, t_1) = p_2(\boldsymbol{x}_3, t_3 | \boldsymbol{x}_2, t_2) \tag{2.12}$$

This follows directly from equation (2.10). Now equation (2.11) is inserted into the marginal distribution $p_2(\boldsymbol{x}_3, t_3; \boldsymbol{x}_1, t_1)$. This yields

$$\begin{aligned} p_2(\boldsymbol{x}_3, t_3; \boldsymbol{x}_1, t_1) &= \int_{\mathbb{R}^m} p_3(\boldsymbol{x}_3, t_3; \boldsymbol{x}_2, t_2; \boldsymbol{x}_1, t_1) d^m x_2 \\ &= \int_{\mathbb{R}^m} p_3(\boldsymbol{x}_3, t_3 | \boldsymbol{x}_2, t_2) p_2(\boldsymbol{x}_2, t_2 | \boldsymbol{x}_1, t_1) p_1(\boldsymbol{x}_1, t_1) d^m x_2 \end{aligned} \tag{2.13}$$

The last equation is divided by $p_1(\boldsymbol{x}_1, t_1)$ on both sides. Then the Chapman-Kolmogorov equation is given by

$$p_2(\boldsymbol{x}_3, t_3 | \boldsymbol{x}_1, t_1) = \frac{p_2(\boldsymbol{x}_3, t_3; \boldsymbol{x}_1, t_1)}{p_1(\boldsymbol{x}_1, t_1)} = \int_{\mathbb{R}^m} p_2(\boldsymbol{x}_2, t_3 | \boldsymbol{x}_2, t_2) p_2(\boldsymbol{x}_2, t_2 | \boldsymbol{x}_1, t_1) d^m x_2. \tag{2.14}$$

The Chapman-Kolmogorov equation will become important for the derivation of the Fokker Planck equation. The Fokker Planck equation is discussed in section 4.

3. Langevin dynamics

The Langevin dynamics has proven to be a very rich approach for systems in thermal non-equilibrium. For the problem discussed here, a phenomenological approach to the Langevin equations will be chosen, as this is sufficient here. For Langevin dynamics, one starts from a deterministic description and then adds a stochastic force that leads to small fluctuations. These fluctuations correspond to the thermal energy k_BT in thermal equilibrium, where T is the temperature and k_B is the Boltzmann constant [7, pp. 417–420].

In order to set up a concrete Langevin equation, one starts from Newton's equations of motion $m\ddot{x}(t) = F$ for a single particle in one dimension. Here m is the mass of the particle, $x(t)$ is the position of the particle at time t and F is the total deterministic force. The particle is in a potential $V(x)$. In addition, Stokes friction acts on the particle, which is characterised by the term $-\gamma_0\dot{x}$. The total deterministic force is thus $F = -\partial_x V - \gamma_0\dot{x}$ where γ_0 is the coefficient of friction. Now a stochastic force $f(t)$ is added to Newton's equations of motion, yielding $m\ddot{x}(t) = -\partial_x V - \gamma_0\dot{x} + f(t)$. Due to the stochastic character of the force f, the position x and the velocity $v = \dot{x}$ of the particle also become stochastic variables [7, pp. 417–418].

The motivation for the stochastic force will be short discussed here with Brownian molecular motion. A relatively heavy particle is in a solvent. The solvent molecules exert undirected force impacts on the particle. These undirected force impacts of the solvent molecules are modelled with a stochastic force [7, p. 417].

The properties of the stochastic force are defined by its average $\langle f(t)\rangle = \phi_1(t)$ and its autocorrelation function $\langle f(t)f(s)\rangle = \phi_2(t,s)$ where $\phi_1(t)$ and $\phi_2(t,s)$ are concrete functions that depend on time [7, p. 418]. The stochastic force leads to small fluctuations in the movement of the particle. These fluctuations can be interpreted as a temperature. Therefore, a stochastic force can often be assigned to a temperature.

The activated rate theory, which was briefly introduced in the introduction, makes the assumption that the temporal evolution of the reaction coordinates $y_1, y_2, ..., y_n$ can be described by Langevin equations. Thus, the reaction coordinates change on average by the deterministic equation $a\ddot{y}_i(t) = -\partial_{y_i} V - \gamma_0\dot{y}_i$, where a is a system dependent constant. The remaining degrees of freedom, which form a heat bath, influence y_i by small fluctuations. The stochastic force $f_i(t)$ is thus added to the evolution equation so that the reaction coordinates fulfil the equation $a\ddot{y}_i(t) = -\partial_{y_i} V - \gamma_0\dot{y}_i + f_i(t)$. A double well potential is often chosen for the potential V. For a clear understanding it is often easier to understand the abstract reaction coordinates as the position of a mass point. Then $\boldsymbol{y} = (y_1, ..., y_n)^\intercal$ describes the position of a mass point in space $\mathbb{R}^n$ and the constant a can be identified as mass m. In the following sections, the central model in this thesis is presented and discussed.

3.1 Model according to Ilg and Barrat

The model of Ilg and Barrat [6] was developed to investigate essential properties of glassy systems on a simple model. The model considers a particle with mass m at position $x \in \mathbb{R}$ and velocity $v = \dot{x}$ in an external potential $V(x)$. The system is affected by fast fluctuating degrees of freedom that have no history and slow fluctuatingdegrees of freedom that have memory. The

rapidly fluctuating degrees of freedom are counteracted by the frictional force $-\Gamma_0 v$ with the coefficient of friction Γ_0. For the slow fluctuating degrees of freedom with memory, the frictional force

$$-\int_0^t \Gamma(t-s)v(s)ds$$

counteracts [6]. $\Gamma(t-s)$ is the retarded friction coefficient. Through the integral, the friction $\Gamma(t-s)v(s)$ at earlier times $s < t$ is also included. Thus this friction force has a memory. For the simple prototype $m\ddot{x}(t) = \partial_x V - \gamma_0 v + f(t)$ of the Langevin equation, a phenomenological substitution rule yields

$$-\gamma_0 v \quad \longrightarrow \quad -\Gamma_0 v - \int_0^t \Gamma(t-s)v(s)ds \tag{3.1}$$

[9, p. 19]. The rapidly fluctuating degrees of freedom are summarised by the stochastic force $\eta(t)$. The stochastic force $\eta(t)$ is related to the temperature T_1. The slow fluctuating degrees of freedom are summarised by the stochastic force $\xi(t)$. ξ is assigned to the temperature T_2. The model thus has two heat baths with the temperatures T_1 and T_2. Thermal non-equilibrium in glassy systems is achieved by the fact that $T_1 \neq T_2$ applies to the temperatures. With the total stochastic force $f = \eta + \xi$, the equations of motion of the model are given by

$$\dot{x} = v \tag{3.2}$$

$$m\dot{v} = -\frac{\partial V}{\partial x} - \int_0^t \Gamma(t-s)v(s)ds - \Gamma_0 v(t) + \eta(t) + \xi(t) \tag{3.3}$$

[6]. The stochastic force $\eta(t)$ belongs to the fast fluctuating degrees of freedom with the assigned temperature T_1 and is therefore modelled with a Gaussian white noise with

$$\langle \eta(t) \rangle = 0 \tag{3.4}$$

$$\langle \eta(t)\eta(s) \rangle = 2k_B T_1 \Gamma_0 \delta(t-s) \tag{3.5}$$

where k_B is the Boltzmann constant and $\delta(t-s)$ is the Dirac delta. The stochastic force $\xi(t)$ belongs to the slow fluctuating degrees of freedom with the assigned temperature T_2 and is characterised by the correlation [6]

$$\langle \xi(t)\xi(s) \rangle = k_B T_2 \Gamma(t-s). \tag{3.6}$$

3.2 Transformation from a non-Markov to a Markov process

Since the equations (3.2) and (3.3) are not Markovian, their treatment is very difficult. One way to overcome this difficulty is to introduce another auxiliary variable. Through this auxiliary variable, the non-Markov process can be transformed into a Markov process. For this transformation, the shape of the Memoy kernel must be fixed. It makes sense to choose the exponential decay

$$\Gamma(t) = \frac{1}{\alpha} \exp\left(-\frac{t}{\alpha\gamma}\right) \tag{3.7}$$

of the memory function $\Gamma(t)$ [6].

For the transformation from equations (3.2) and 3.3 into a set of Markov equations, it is helpful to represent the stochastic force $\xi(t)$ as a linear combination of white noise. A possible form of the stochastic force $\xi(t)$, which has the correlation denfined in equation (3.6) is given by

$$\xi(t) = \sqrt{\frac{k_B T_2}{\alpha}} e^{-\frac{1}{\alpha\gamma}t} + \int_0^t e^{-\frac{1}{\alpha\gamma}(t-\tau)} \zeta(\tau) d\tau. \tag{3.8}$$

where ζ is a Gaussian white noise with $\langle\zeta\rangle = 0$ and the correlation

$$\langle\zeta(t)\zeta(s)\rangle = \frac{2k_BT_2}{\alpha^2\gamma}\delta(t-s) \tag{3.9}$$

[6]. The assertion in equation (3.8) can be easily proven by showing that the stochastic force ξ satisfies the relation $\langle\xi(t)\xi(s)\rangle = k_BT_2\Gamma(t-s)$. The detailed calculation that $\xi(t)$ defined in equation (3.8) satisfies the relation in equation (3.6) is given in the appendix in *Lemma* 1. Equation (3.8) is now substituted into equation (3.3). This yields

$$m\dot{v} = -\frac{\partial V}{\partial x} + \sqrt{\frac{k_BT_2}{\alpha}}e^{-\frac{1}{\alpha\gamma}t} + \int_0^t e^{-\frac{1}{\alpha\gamma}(t-s)}\left(\zeta(s) - \frac{1}{\alpha}v(s)\right)ds - \Gamma_0 v(t) + \eta(t). \tag{3.10}$$

The limit in which the second heat bath is decoupled from the system is particularly important. For this one considers equation (3.10) and sets $ds\zeta(s) = \sqrt{2k_BT_2/(\alpha^2\gamma)}dW(s)$ where $W(t)$ is the Wiener process defined by $\langle W(t)\rangle = 0$ and $\langle(W(t)-W(s))^2\rangle = t-s$ [10, p. 4–5]. Then equation (3.10) is given by

$$\begin{aligned} m\dot{v} = -\frac{\partial V}{\partial x} + \sqrt{\frac{k_BT_2}{\alpha}}e^{-\frac{1}{\alpha\gamma}t} + \sqrt{\frac{1}{\alpha}}\sqrt{\frac{2k_BT_2}{\gamma\alpha}}\int_0^t e^{-\frac{1}{\alpha\gamma}(t-s)}dW(s) \\ -\frac{1}{\alpha}\int_0^t v(s)e^{-\frac{1}{\alpha\gamma}(t-s)}ds - \Gamma_0 v(t) + \eta(t). \end{aligned} \tag{3.11}$$

Considering the limit $\alpha \to \infty$ while keeping $\alpha\gamma =$ constant, the second heat bath decouples completely from the system and the equation reads

$$m\dot{v} = -\frac{\partial V}{\partial x} - \Gamma_0 v(t) + \eta(t). \tag{3.12}$$

Two cases can now be distinguished. In the first case, $m\dot{v}$ is generally non-zero for all times $t \geq 0$. This case is called *Kramers' case* in this work. The second case is the overdamped case in which $m\dot{v} = 0$ is zero for all times $t \geq 0$. The second case is a special case of the first and is named *Smoluchovski's case* in this work. In the following two subsections, the two cases will now be analysed separately.

3.2.1 Kramers' case

For Kramers' case, the variable $z(t)$ with the definition

$$z(t) = \sqrt{\frac{k_BT_2}{\alpha}}e^{-\frac{1}{\alpha\gamma}t} + \int_0^t e^{-\frac{1}{\alpha\gamma}(t-s)}\left(\zeta(s) - \frac{1}{\alpha}v(s)\right)ds \tag{3.13}$$

is chosen as the auxiliary variable [6]. Substituting equation (3.13) into equation (3.10) yields

$$m\dot{v} = -\frac{\partial V}{\partial x} + z(t) - \Gamma_0 v(t) + \eta(t) \tag{3.14}$$

z is a differentiable function. The derivative with respect to the time t yields

$$\begin{aligned} \dot{z} &= -\frac{1}{\alpha}v(t) - \frac{1}{\alpha\gamma}\left[\sqrt{\frac{k_BT_2}{\alpha}}e^{-\frac{1}{\alpha\gamma}t} + \int_0^t e^{-\frac{1}{\alpha\gamma}(t-s)}\left(\zeta(s) - \frac{1}{\alpha}v(s)\right)ds\right] + \zeta(t) \\ &= -\frac{1}{\alpha}v(t) - \frac{1}{\alpha\gamma}z(t) + \zeta(t). \end{aligned} \tag{3.15}$$

With equations (3.2), (3.14) and (3.15), the set of Markovian equations is for Kramers' case [6]

$$\dot{x} = v \tag{3.16}$$

$$m\dot{v} = -\frac{\partial V}{\partial x} + z(t) - \Gamma_0 v(t) + \eta(t) \tag{3.17}$$

$$\dot{z} = -\frac{1}{\alpha} v(t) - \frac{1}{\alpha\gamma} z(t) + \zeta(t) \tag{3.18}$$

3.2.2 Smoluchovski's case

The Smoluchovski case is the overdamped case. In equation (3.3), $m\dot{v}$ is therefore set to zero for all times $t \geq 0$ This yields

$$0 = -\frac{\partial V}{\partial x} - \int_0^t \Gamma(t-s)\dot{x}(s)ds - \Gamma_0 \dot{x}(t) + \xi(t) + \eta(t). \tag{3.19}$$

Integration by parts and convert according to $\dot{x}$ yields

$$\dot{x} = -\frac{1}{\Gamma_0}\frac{\partial}{\partial x}\left[V + \frac{x^2}{2\alpha}\right] - \frac{1}{\Gamma_0}\int_0^t [\partial_t \Gamma(t-s)]x(s)ds + \frac{1}{\Gamma_0}\xi(t) + \frac{1}{\Gamma_0}\eta(t). \tag{3.20}$$

where the boundary term $\Gamma(t)x_0$ was set to zero as in the work of P. Ilg and J.L. Barrat [6]. For the Smoluchovski's case,

$$x_2 = -\int_0^t [\partial_t \Gamma(t-s)]x(s)ds + \xi(t) \tag{3.21}$$

is chosen as the auxiliary variable. Substituting equation (3.21) into equation (3.20) yields

$$\dot{x} = -\frac{1}{\Gamma_0}\frac{\partial U}{\partial x} - \frac{1}{\Gamma_0}x_2 + \frac{1}{\Gamma_0}\eta(t) \tag{3.22}$$

where $U = V(x) + x^2/(2\alpha)$ was set [6]. Analogous to Kramer's case, x_2 is differentiated according to time. This yields the differential equation

$$\begin{aligned} \dot{x}_2(t) &= \frac{d}{dt}\left[\frac{1}{\alpha^2\gamma}e^{-\frac{1}{\alpha\gamma}t}\int_0^t e^{\frac{1}{\alpha\gamma}s}x_1(s)ds\right] + \frac{d}{dt}\xi(t)) \\ &= -\frac{1}{\alpha\gamma}x_2(t) + \frac{1}{\alpha^2\gamma}x + \zeta(t). \end{aligned} \tag{3.23}$$

Now $x = x_1$, $\kappa_2 = \alpha$, $\Gamma_1 = \Gamma_0$, $\Gamma_2 = \alpha^2\gamma$, $\nu_1 = 1/\Gamma_0$ and $\nu_2 = 1/(\alpha^2\gamma)$ is set. Equations (3.22) and (3.23) then yields the set of Markovian equations of motion

$$\dot{x}_1 = -\frac{1}{\Gamma_1}\frac{\partial U}{\partial x_1} + \nu_1 x_2 + \eta_1(t) \tag{3.24}$$

$$\dot{x}_2 = -\frac{\kappa_2}{\Gamma_2}x_2 + \nu_2 x_1 + \eta_2(t) \tag{3.25}$$

for the overdamped case. Where $\eta_1 = \eta/\Gamma_0$ and $\eta_2 = \zeta$ was set. Thus the average is $\langle\eta_1\rangle = \langle\eta_2\rangle = 0$ and the variances are determined by $\langle\eta_i(t)\eta_j(s)\rangle = 2k_B T_i \Gamma_i^{-1}\delta_{ij}\delta(t-s)$. The Kronecker δ_{ij} is necessary because $\eta(t)$ and $\zeta(t)$ are uncorrelated Gaussian white random variables [6].

3.3 Exact solution in the overdamped case with harmonic force

The equations (3.24) and (3.24) are now to be solved analytically for the potential $U(x_1) = \kappa_1 x_1^2/2$. This whole section follows the presentation in [6]. The potential $U(x_1)$ is composed of $U(x_1) = V(x_1) + x_1^2/(2\alpha)$. The potential $V(x_1)$ therefore has the form $V(x_1) = \kappa x_1^2/2$. Let $\boldsymbol{x} = (x_1, x_2)^\intercal$ and $\boldsymbol{\eta} = (\eta_1, \eta_2)^\intercal$. Then the two equations can be compactly represented by the matrix equation

$$\dot{\boldsymbol{x}} = -\Lambda \boldsymbol{x} + \boldsymbol{\eta} \tag{3.26}$$

where the matrix Λ has the form

$$\Lambda = \begin{pmatrix} \frac{\kappa_1}{\Gamma_1} & -\nu_1 \\ -\nu_2 & \frac{\kappa_2}{\Gamma_2} \end{pmatrix} \tag{3.27}$$

The eigenvalues of the matrix Λ are

$$\lambda_{1,2} = \frac{1}{2}\left(\frac{\kappa_1}{\Gamma_1} + \frac{\kappa_2}{\Gamma_2}\right) \pm \frac{1}{2}\sqrt{\left(\frac{\kappa_1}{\Gamma_1} - \frac{\kappa_2}{\Gamma_2}\right)^2 + 4\nu_1\nu_2} = \frac{1}{2}\left(\frac{\kappa_1}{\Gamma_1} + \frac{\kappa_2}{\Gamma_2}\right) \pm \frac{1}{2}\sqrt{D}. \tag{3.28}$$

It is $\lambda_1 > \lambda_2 > 0$ exactly when $D > 0$ and $\kappa_1\kappa_2/(\Gamma_1\Gamma_2) > \nu_1\nu_2$, where the last condition in the old parameters is $\alpha\kappa + 1 > 1$. Since $\alpha, \gamma, \Gamma_0 > 0$ is given by the model, $D > 0$ and $\alpha\kappa + 1 > 1$ are always satisfied if $\kappa > 0$. Set $a = \kappa_1/\Gamma_1 - \kappa_2/\Gamma_2$. A possible set of eigenvectors is then given by

$$\boldsymbol{v}_1 = \begin{pmatrix} -\frac{a+\sqrt{D}}{2\nu_2} \\ 1 \end{pmatrix} \qquad \boldsymbol{v}_2 = \begin{pmatrix} \frac{-a+\sqrt{D}}{2\nu_2} \\ 1 \end{pmatrix} \tag{3.29}$$

where the eigenvector $\boldsymbol{v}_1$ belongs to the eigenvalue λ_1 and the eigenvector $\boldsymbol{v}_2$ belongs to the eigenvalue λ_2. The two linearly independent solutions of the homogeneous DGL $\dot{\boldsymbol{x}} = -\Lambda\boldsymbol{x}$ are combined in the matrix $Y(t) = (e^{-\lambda_1 t}\boldsymbol{v}_1, e^{-\lambda_2 t}\boldsymbol{v}_2)$. Then the general solution of the inhomogeneous equation (3.26) is given by

$$\boldsymbol{x}(t) = \boldsymbol{x}_{hom} + \boldsymbol{x}_{part} = Y(t)Y(t_0)^{-1}\boldsymbol{x}_0 + \int_{t_0}^{t} Y(t)Y(s)^{-1}\boldsymbol{\eta} ds. \tag{3.30}$$

Set $t_0 = 0$ and $\boldsymbol{x}_0 = (x_1^0, x_2^0)^\intercal$ where the exponent notes the time $t_0 = 0$. Then

$$\boldsymbol{x}_{hom} = Y(t)Y(0)^{-1}\boldsymbol{x}_0 = \begin{pmatrix} b_{11}(x_1^0 + a_1 x_2^0)e^{-\lambda_1 t} + b_{12}(x_1^0 + a_2 x_2^0)e^{-\lambda_2 t} \\ b_{21}(x_1^0 + a_1 x_2^0)e^{-\lambda_1 t} + b_{22}(x_1^0 + a_2 x_2^0)e^{-\lambda_2 t} \end{pmatrix} \tag{3.31}$$

and

$$\begin{aligned} \boldsymbol{x}_{part} &= \int_0^t Y(t)Y(s)^{-1}\boldsymbol{\eta} ds \\ &= \int_0^t \begin{pmatrix} b_{11}(\eta_1 + a_1\eta_2)e^{-\lambda_1(t-s)} + b_{12}(\eta_1 + a_2\eta_2)e^{-\lambda_2(t-s)} \\ b_{21}(\eta_1 + a_1\eta_2)e^{-\lambda_1(t-s)} + b_{22}(\eta_1 + a_2\eta_2)e^{-\lambda_2(t-s)} \end{pmatrix} ds \end{aligned} \tag{3.32}$$

where a_i is given by the vector

$$\begin{pmatrix} a_1 \\ a_2 \end{pmatrix} = \begin{pmatrix} \frac{a-\sqrt{D}}{2\nu_2} \\ \frac{a+\sqrt{D}}{2\nu_2} \end{pmatrix} \tag{3.33}$$

and b_{ij} by the matrix

$$\begin{pmatrix} b_{11} & b_{12} \\ b_{21} & b_{22} \end{pmatrix} = \begin{pmatrix} \frac{a+\sqrt{D}}{2\sqrt{D}} & -\frac{a-\sqrt{D}}{2\sqrt{D}} \\ -\frac{\nu_2}{\sqrt{D}} & \frac{\nu_2}{\sqrt{D}} \end{pmatrix}. \tag{3.34}$$

For a single component $x_i(t)$ we get

$$x_i(t) = \sum_{\alpha=1}^{2} b_{i\alpha}(x_1^0 + a_\alpha x_2^0)e^{-\lambda_\alpha t} + \sum_{\alpha=1}^{2}\int_0^t b_{i\alpha}(\eta_1(\tau_1) + a_\alpha\eta_2(\tau_1))e^{-\lambda_\alpha(t-\tau_1)}d\tau_1. \tag{3.35}$$

3.3.1 Correlation function

A general form of a corrlation function is given in equation (2.5). With the function $f_i(\boldsymbol{x}) = x_i$ we get the correlation function

$$\mathrm{Cor}_{ij}(t,s) = \langle x_i(t)x_j(s)\rangle - \langle x_i(t)\rangle\langle x_j(s)\rangle \tag{3.36}$$

[6]. In section 3.3 the random variables $x_1(t)$ and $x_2(t)$ were determined concretely for a harmonic external force. With the solutions for $x_1(t)$ and $x_2(t)$ given by equation (3.35) we get

$$\begin{aligned}\langle x_i(t)x_j(s)\rangle = &\sum_{\alpha,\beta=1}^{2} b_{i\alpha}b_{j\beta}(x_1^0 + a_\alpha x_2^0)(x_1^0 + a_\beta x_2^0)e^{-\lambda_\alpha t - \lambda_\beta s} \\ &+ \sum_{\alpha,\beta=1}^{2} 2\frac{b_{i\alpha}b_{j\beta}}{\lambda_\alpha + \lambda_\beta}\left(\frac{k_B T_1}{\Gamma_1} + a_\alpha a_\beta \frac{k_B T_2}{\Gamma_2}\right)\left(e^{-\lambda_\alpha(t-s)} - e^{-(t\lambda_\alpha + s\lambda_\beta)}\right)\end{aligned} \tag{3.37}$$

and

$$\langle x_i(t)\rangle\langle x_j(s)\rangle = \sum_{\alpha,\beta=1}^{2} b_{i\alpha}b_{j\beta}(x_1^0 + a_\alpha x_2^0)(x_1^0 + a_\beta x_2^0)e^{-\lambda_\alpha t - \lambda_\beta s} \tag{3.38}$$

where $\langle \eta_i(t)\rangle = 0$ and $\langle \eta_i(t)\eta_j(s)\rangle = 2k_B T_i \Gamma_i^{-1}\delta_{ij}\delta(t-s)$ was used. For $t\lambda_\alpha + s\lambda_\beta \gg 1$ the correlation function results in

$$\mathrm{Cor}_{ij}(t,s) = \sum_{\alpha,\beta=1}^{2} 2\frac{b_{i\alpha}b_{j\beta}}{\lambda_\alpha + \lambda_\beta}\left(\frac{k_B T_1}{\Gamma_1} + a_\alpha a_\beta \frac{k_B T_2}{\Gamma_2}\right)e^{-\lambda_\alpha(t-s)} \tag{3.39}$$

where it is obvious that for long times t and s the correlation function is translationally invariant in time, i.e. $\mathrm{Cor}_{ij}(t,s) = \mathrm{Cor}_{ij}(t-s)$ [6].

3.3.2 Susceptibility or linear response

Next, the linear response in the overdamped case is determined. For this, a small disturbance force $f(t)$ is added to equation (3.19) [6]. The result is

$$0 = -\frac{\partial V}{\partial x} - \int_0^t \Gamma(t-s)\dot{x}(s)ds - \Gamma_0\dot{x}(t) + \xi(t) + \eta(t) + f(t). \tag{3.40}$$

Using the same calculation as in section 3.2.2, we obtain the differential equations

$$\dot{x}_1 = -\frac{1}{\Gamma_1}\frac{\partial U}{\partial x_1} + \nu_1 x_2 + \frac{1}{\Gamma_1}f(t) + \eta_1(t) \tag{3.41}$$

$$\dot{x}_2 = -\frac{\kappa_2}{\Gamma_2}x_2 + \nu_2 x_1 + \eta_2(t). \tag{3.42}$$

With the substitution $\eta_1(t) \to \eta_1(t) + f(t)/\Gamma_1$, the solution of the perturbed differential equation system is given by equation (3.35). The linear response of the system is generally given by

$$\chi_i(t,s) := \frac{\delta}{\delta f(s)}\langle x_i(t)\rangle\Big|_{f=0} \tag{3.43}$$

where $\delta/\delta f(s)$ notates the functional derivative [6]. With the concrete solution for $x_i(t)$ we get

$$\chi_i(t,s) = \frac{1}{\Gamma_1}\sum_{\alpha=1}^{2} b_{i\alpha}e^{-\lambda_\alpha(t-s)}\Theta(t-s) \tag{3.44}$$

where $\Theta(t)$ notes the step function. The linear response $\chi_i(t,s)$ of the system is also called susceptibility. With the correlation function $\mathrm{Cor}_{ij}(t,s)$ and the susceptibility $\chi_i(t,s)$, a time-dependent effective temperature can be defined using the fluctuation-dissipation theorem [6]. The concrete calculation is carried out in chapter 5. When calculating susceptibilities numerically, it is often easier to calculate the integrated susceptibility. The integrated version of the susceptibility in equation (3.44) is given by

$$\chi_i'(t-s) = \int_0^{t-s} \chi_i(\tau)d\tau = \frac{1}{\Gamma_1}\sum_{\alpha=1}^{2}\frac{b_{i\alpha}}{\lambda_\alpha}\left(1-e^{-(t-s)\lambda_\alpha}\right) \tag{3.45}$$

where $t-s \geq 0$ [6].

4. Fokker Planck equation

For some physical questions it is necessary to know the probability distribution $p(\boldsymbol{x})$ of a random variable $\boldsymbol{X}$. An important formula for calculating such a probability density is the Fokker Planck equation. The equation will be derived in subsection 4.1. In the subsection 4.2 an important application of the Fokker-Planck equation is discussed. The application is to solve the basic problem of activated rate theory for a simple model system. Then a way to numerically determine the escape rate for a double trough potential from a two level correlation function is discussed. The chapter ends with the calculation of the probability distribution function for the particle position x_1.

4.1 Derivation of the Fokker Planck equation

Let $\boldsymbol{x}_1 = (\boldsymbol{r}_1, \boldsymbol{v}_1)^\intercal \in \mathbb{R}^{2m}$ be the position $\boldsymbol{r}_1$ and the velocity $\boldsymbol{v}_1$ of a single particle at time t_1 and, analogously, let the vector $\boldsymbol{x}_2 = (\boldsymbol{r}_2, \boldsymbol{v}_2)^\intercal \in \mathbb{R}^{2m}$ be the position $\boldsymbol{r}_2$ and the velocity $\boldsymbol{v}_2$ of the same particle at time t_2. The conditional probability $p(\boldsymbol{x}_2, t+\tau|\boldsymbol{x}_1, t)$ is the probability that $\boldsymbol{X}_2$ is in state $\boldsymbol{X}_2 \in [\boldsymbol{x}_2, \boldsymbol{x}_2 + d\boldsymbol{x}_2]$ at time $t_2 = t+\tau$ under the condition that the particle was in state $\boldsymbol{x}_1$ at time t_1. With the probability $p_2(\boldsymbol{x}_2, t+\tau|\boldsymbol{x}_1, t)$, the first two moments of $(\boldsymbol{x}_2 - \boldsymbol{x}_1)_i$ can now be determined, where $(\boldsymbol{x}_2 - \boldsymbol{x}_1)_i$ denotes the i-th component of the vector $\boldsymbol{x}_2 - \boldsymbol{x}_1$. For the first two moments, it is now required that they depend linearly on time. This is expressed with

$$\int_{\mathbb{R}^m} (\boldsymbol{x}_2 - \boldsymbol{x}_1)_i \; p_2(\boldsymbol{x}_2, t+\tau|\boldsymbol{x}_1, t) d^{2m}x_2 = A_i(\boldsymbol{x}_1, t)\tau + o(\tau) \tag{4.1}$$

$$\int_{\mathbb{R}^m} (\boldsymbol{x}_2 - \boldsymbol{x}_1)_i \; (\boldsymbol{x}_2 - \boldsymbol{x}_1)_j \; p_2(\boldsymbol{x}_2, t+\tau|\boldsymbol{x}_1, t) d^{2m}x_2 = D_{ij}(\boldsymbol{x}_1, t)\tau + o(\tau) \tag{4.2}$$

where $o(\tau)$ is the Landau symbol. For higher moments $k > 2$,

$$\int_{\mathbb{R}^m} (\boldsymbol{x}_2 - \boldsymbol{x}_1)_{i_1} ... (\boldsymbol{x}_2 - \boldsymbol{x}_1)_{i_k} \; p_2(\boldsymbol{x}_2, t+\tau|\boldsymbol{x}_1, t) d^{2m}x_2 = o(\tau) \quad \text{for} \quad k > 2 \tag{4.3}$$

shall always be valid. Processes characterised by equations (4.1)−(4.3) are called diffusion processes. The functions $A_i(\boldsymbol{x}_1, t)$ and $D_{ij}(\boldsymbol{x}_1, t)$ are unique, deterministic functions [8, pp. 74–75]. For Markov processes, a partial differential equation for the conditional probability $p_2(\boldsymbol{x}_2, t+\tau|\boldsymbol{x}_1, t)$ can now be derived quite easily. The following derivation of the Fokker-Planck equation is taken from [8, pp. 74–75].

Let $R(\boldsymbol{x}_2) \in \mathbb{R}$ be any test function with compact support [10, p. 50]. Further, let $R(\boldsymbol{x}_2)$ be two times continuously differentiable and both $R(\boldsymbol{x}_2)$ and the derivative $\nabla_{\boldsymbol{x}_2} R(\boldsymbol{x}_2)$ be zero for $\|\boldsymbol{x}_2\| \to \infty$. Then the definition of the derivative yields

$$\begin{aligned} &\int_{\mathbb{R}^{2m}} R(\boldsymbol{x}_2) \partial_t p_2(\boldsymbol{x}_2, t|\boldsymbol{x}_1, t_1) d^{2m}x_2 \\ &\quad = \lim_{\tau \to 0} \frac{1}{\tau} \int_{\mathbb{R}^{2m}} R(\boldsymbol{x}_2)[p_2(\boldsymbol{x}_2, t+\tau|\boldsymbol{x}_1, t_1) - p_2(\boldsymbol{x}_2, t|\boldsymbol{x}_1, t_1] d^{2m}x_2. \end{aligned} \tag{4.4}$$

The conditional probability $p_2(\boldsymbol{x}_2, t+\tau|\boldsymbol{x}_1, t_1)$ will be rewritten with the Chapman-Kolmogorov equation defined in equation (2.14). Then, using Taylor's theorem, the test function $R(\boldsymbol{x}_2)$ is expanded around the point $\boldsymbol{x}$ to the second order, where $\|\boldsymbol{x}_2 - \boldsymbol{x}\| \ll 1$. Further, let x_i be the i-th component of the vector $\boldsymbol{x}$. For the right-hand side of the last equation, the following thus applies

$$\begin{aligned}
&\lim_{\tau\to 0}\frac{1}{\tau}\int_{\mathbb{R}^{2m}} R(\boldsymbol{x}_2)[p_2(\boldsymbol{x}_2, t+\tau|\boldsymbol{x}_1, t_1) - p_2(\boldsymbol{x}_2, t|\boldsymbol{x}_1, t_1]d^{2m}x_2 \\
&= \lim_{\tau\to 0}\frac{1}{\tau}\int_{\mathbb{R}^{2m}} R(\boldsymbol{x}_2)\left[\int_{\mathbb{R}^{2m}} p_2(\boldsymbol{x}_2, t+\tau|\boldsymbol{x}, t)p_2(\boldsymbol{x}, t|\boldsymbol{x}_1, t_1)d^{2m}x - p_2(\boldsymbol{x}_2, t|\boldsymbol{x}_1, t_1)\right] d^{2m}x_2 \\
&= \lim_{\tau\to 0}\frac{1}{\tau}\Bigg\{\int_{\mathbb{R}^{2m}}\int_{\mathbb{R}^{2m}}\left[R(\boldsymbol{x}) + (\boldsymbol{x}_2 - \boldsymbol{x})_i\frac{\partial R(\boldsymbol{x})}{\partial x_i} + \frac{1}{2}(\boldsymbol{x}_2 - \boldsymbol{x})_i(\boldsymbol{x}_2 - \boldsymbol{x})_j\frac{\partial^2 R(\boldsymbol{x})}{\partial x_i \partial x_j} + ...\right] \\
&\qquad \times p_2(\boldsymbol{x}_2, t+\tau|\boldsymbol{x}, t)p_2(\boldsymbol{x}, t|\boldsymbol{x}_1, t_1)d^{2m}x\, d^{2m}x_2 - \int_{\mathbb{R}^{2m}} R(\boldsymbol{x}_2)p_2(\boldsymbol{x}_2, t|\boldsymbol{x}_1, t_1)d^{2m}x_2\Bigg\}
\end{aligned} \tag{4.5}$$

whereby Einstein's summation convention is used here. For the first summand in the penultimate line, with the order of integration reversed, the following applies

$$\begin{aligned}
\int_{\mathbb{R}^{2m}} R(\boldsymbol{x})p_2(\boldsymbol{x}, t|\boldsymbol{x}_1, t_1)\underbrace{\int_{\mathbb{R}^{2m}} p_2(\boldsymbol{x}_2, t+\tau|\boldsymbol{x}, t)d^{2m}x_2}_{=1}\, d^{2m}x \\
= \int_{\mathbb{R}^{2m}} R(\boldsymbol{x})p_2(\boldsymbol{x}, t|\boldsymbol{x}_1, t_1)d^{2m}x
\end{aligned} \tag{4.6}$$

Since the value of the integral is independent of the name of the integration variable, the first summand in the penultimate line matches the last summand in the last line except for the sign. Thus these terms cancel each other out. Using the definitions of A_i and D_{ij} yields in the limes $\tau \to 0$ the result

$$\begin{aligned}
\int_{\mathbb{R}^{2m}} R(\boldsymbol{x}_2)\partial_t p_2(\boldsymbol{x}_2, t|\boldsymbol{x}_1, t_1)d^{2m}x_2 &= \int_{\mathbb{R}^{2m}} R(\boldsymbol{x})\partial_t p_2(\boldsymbol{x}, t|\boldsymbol{x}_1, t_1)d^{2m}x \\
&= \int_{\mathbb{R}^{2m}}\left[A_i(\boldsymbol{x}, t)\frac{\partial R(\boldsymbol{x})}{\partial x_i} + D_{ij}(\boldsymbol{x}, t)\frac{\partial^2 R(\boldsymbol{x})}{\partial x_i \partial x_j}\right] p_2(\boldsymbol{x}, t|\boldsymbol{x}_1, t_1)d^{2m}x.
\end{aligned} \tag{4.7}$$

Integration by parts of the last integral yields

$$\int_{\mathbb{R}^{2m}} R(\boldsymbol{x})\left[\partial_t p_2(\boldsymbol{x}, t|\boldsymbol{x}_1, t_1) + \left\{\frac{\partial}{\partial x_i}A_i(\boldsymbol{x}, t) - \frac{1}{2}\frac{\partial^2}{\partial x_i \partial x_j}D_{ij}(\boldsymbol{x}, t)\right\}p_2(\boldsymbol{x}, t|\boldsymbol{x}_1, t_1)\right]d^{2m}x = 0 \tag{4.8}$$

using that $R(\boldsymbol{x}_2)$ and the derivative $\nabla_{\boldsymbol{x}_2} R(\boldsymbol{x}_2)$ be zero for $\|\boldsymbol{x}_2\| \to \infty$. Using the fundamental lemma of the calculus of variations yields the Fokker Planck equation

$$\partial_t p_2(\boldsymbol{x}, t|\boldsymbol{x}_1, t_1) = \left\{-\frac{\partial}{\partial x_i}A_i(\boldsymbol{x}, t) + \frac{1}{2}\frac{\partial^2}{\partial x_i \partial x_j}D_{ij}(\boldsymbol{x}, t)\right\}p_2(\boldsymbol{x}, t|\boldsymbol{x}_1, t_1) \tag{4.9}$$

[10, p. 50]. Integration of the last equation over the initial distribution $p_1(\boldsymbol{x}_1, t_1)$ yields the widely used variant of the FokkerPlanck equation

$$\partial_t p(\boldsymbol{x}, t) = \left\{-\frac{\partial}{\partial x_i}A_i(\boldsymbol{x}, t) + \frac{1}{2}\frac{\partial^2}{\partial x_i \partial x_j}D_{ij}(\boldsymbol{x}, t)\right\}p(\boldsymbol{x}, t) \tag{4.10}$$

where the relation

$$p(\boldsymbol{x}, t) = \int_{\mathbb{R}^{2m}} p_2(\boldsymbol{x}, t|\boldsymbol{x}_1, t_1)p_1(\boldsymbol{x}_1, t_1)d^{2m}x_1 \tag{4.11}$$

was used.

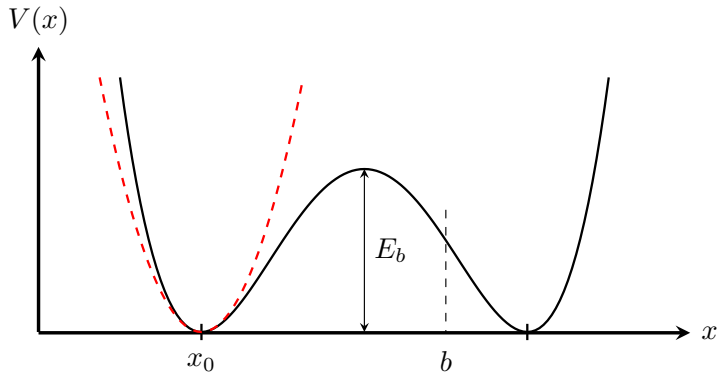

Figure 4.1: Sketch of the double well potential. A particle in this potential will spend most of its time in the vicinity of one of the two potential wells. Since a stochastic force also acts on the particle, it can jump from one potential minimum to the other minimum, although its average energy is not sufficient to overcome the energy barrier E_b. For the left potential well, the quadratic approximation for the minimum at $x = x_0$ is shown as a red dashed line. The illustration is inspired by the illustration in [8, p. 172].

4.2 Escape across a potential barrier in the overdamped case

The initial situation can best be formulated using a Langevin equation. Consider a particle with mass m at the position $x(t)$ at time t. The particle is in a double well potential. Such a potential is shown in Figure 4.1. The particle is additionally affected by the frictional force $-G\dot{x}$ with the friction coefficient G. Then the Langevin equation is $m\ddot{x}(t) = -\partial_x V - G\dot{x} + f(t)$ where the stochastic force $f(t)$ satisfies the first two moments $\langle f(t)\rangle = 0$ and $\langle f(t)f(s)\rangle = 2Gk_BT\delta(t-s)$ [7, p. 422–423].

Without the stochastic force $f(t)$, the particle would come to rest in one of the two potential wells due to friction. With the stochastic force, the particle can pass the energy barrier E_b if the realisation of the stochastic force is favourable enough. Most of the time, however, the particle moves in the vicinity of one of the two potential wells. The decisive question is now at what rate the particle jumps from one potential well to the other. This rate is also called the mean escape rate in the following.

This section is divided into two subsections. In the first subsection, the mean escape rate for an overdamped motion is derived with the corresponding Fokker Planck equation. In the second subsection, an important relation is derived with which the mean escape rate can be determined numerically.

4.2.1 Derivation of the reaction rate with the Fokker Planck equation

In this subsection, an analytical expression is derived for the mean escape rate in the case of large friction. In the overdamped case, the acceleration term in the Langevin equation ist $m\ddot{x} = 0$. This Langevin equation is called the Smoluchowski equation and has the form

$$\dot{x}(t) = -\frac{1}{G}\partial_x V + \frac{1}{G}f(t) \tag{4.12}$$

[7, pp. 422–423]. To calculate the mean escape rate, one needs the probability $p(x,t|x_0,t_0)$ of the random variable x, where x_0 is the starting point at time t_0 of the particle. The probability $p(x,t|x_0,t_0)$ can be calculated with a Fokker Planck equation, which is now derived from the Langevin equation (4.12). For this, the functions A_i and D_{ij} of the Fokker Planck equation (4.9) must be determined. To determine the functions A_i and D_{ij}, use the definitions in equation

(4.1) and equation (4.2). If the Langevin equation (4.12) is integrated over the interval $[t, t+\tau]$, where τ is very small, the following results for the function A_1

$$\begin{aligned} A_1(t,x) &= \lim_{\tau\to 0}\frac{1}{\tau}\langle[x(t+\tau)-x(t)]\rangle = \lim_{\tau\to 0}\frac{1}{\tau}\left\langle\int_t^{t+\tau}\dot{x}(s)ds\right\rangle \\ &= \lim_{\tau\to 0}\frac{1}{\tau}\left\langle\int_t^{t+\tau}\left(-\frac{1}{G}\partial_x V+\frac{1}{G}f(s)\right)ds\right\rangle = -\frac{1}{G}\partial_x V \end{aligned} \tag{4.13}$$

using that $\langle f(s)\rangle = 0$. In the same way for $s \geq s'$ yields further,

$$\begin{aligned} D_{11}(x,t) &= \lim_{\tau\to 0}\frac{1}{\tau}\langle[x(t+\tau)-x(t)]^2\rangle = \lim_{\tau\to 0}\frac{1}{\tau}\left\langle\left(\int_t^{t+\tau}\dot{x}(s)ds\right)\left(\int_t^{t+\tau}\dot{x}(s')ds'\right)\right\rangle \\ &= \lim_{\tau\to 0}\frac{1}{\tau}\left[\left(\frac{\tau}{G}\partial_x V\right)^2 - 2\frac{\tau\partial_x V}{G^2}\int_t^{t+\tau}\langle f(s)\rangle ds\right. \\ &\qquad\left. +\frac{1}{G^2}\int_t^{t+\tau}\int_t^{t+\tau}f(s)f(s')dsds'\right] \\ &= \lim_{\tau\to 0}\frac{1}{\tau}\frac{1}{G^2}2Gk_BT\int_t^{t+\tau}\int_t^{t+\tau}\delta(s-s')dsds' = 2\frac{k_BT}{G} \end{aligned} \tag{4.14}$$

where $\langle f(s)f(s')\rangle = 2Gk_BT\delta(s-s')$ was used [11, p. 78]. For the Langevin equation (4.12), the corresponding Fokker Planck equation is thus given by

$$\partial_t p(x,t|x_0,t_0) = \partial_x\left[\frac{\partial_x V(x)}{G}+\frac{k_BT}{G}\partial_x\right]p(x,t|x_0,t_0) \tag{4.15}$$

For the following discussion the Fokker Planck operator is needed which is defined by

$$\Omega(x) = \partial_x\left[\frac{\partial_x V(x)}{G}+\frac{k_BT}{G}\partial_x\right]. \tag{4.16}$$

The formal solution of the Fokker Planck equation is then given by

$$p(x,t|x_0,t_0) = \exp(\Omega(t-t_0))p(x,t_0|x_0,t_0) \tag{4.17}$$

where $p(x,t_0|x_0,t_0)$ is the initial distribution given by $p(x,t_0|x_0,t_0) = \delta(x-x_0)$ [9, p. 74]. The average $\langle A(x)\rangle$ of any phase space variable $A(x)$ can be written as the scalar product $\langle A(x), p(x,t|x_0,t_0)\rangle$ with the definition

$$\langle A(x), p(x,t|x_0,t_0)\rangle = \int_{\mathbb{R}} A(x)p(x,t|x_0,t_0)dx. \tag{4.18}$$

With this scalar product the adjoint Fokker Planck operator $\Omega^\dagger$ can be defined by $\langle A(x), \Omega B(x)\rangle = \langle \Omega^\dagger A(x), B(x)\rangle$, where $A(x)$ and $B(x)$ are any two phase space variables [12, p. 29]. With two successive partial integrations, the adjoint Fokker Planck operator $\Omega^\dagger$ is given by

$$\Omega^\dagger = -\frac{\partial_x V}{G}\partial_x + \frac{k_BT}{G}\partial_x^2 \tag{4.19}$$

using that the phase space variables $A(x)$ and $B(x)$ vanish at the boundaries of the integration interval. The adjoint Fokker Planck operator in equation (4.19) can be put into a more clever form. For this purpose, a twice-differentiable test function $\psi(x)$ is considered for which the following applies

$$\begin{aligned} \Omega^\dagger\psi(x) &= \left[-\frac{\partial_x V}{G}\partial_x+\frac{k_BT}{G}\partial_x^2\right]\psi(x) = \frac{k_BT}{G}e^{\beta V}\left(-\frac{\partial_x V}{k_BT}e^{-\beta V}\partial_x\psi(x)+e^{-\beta V}\partial_x^2\psi(x)\right) \\ &= \frac{k_BT}{G}e^{\beta V}\partial_x e^{-\beta V}\partial_x\psi(x). \end{aligned} \tag{4.20}$$

Thus the adjoint Fokker Planck operator $\Omega^\dagger$ can also be written by

$$\Omega^\dagger(x) = \frac{k_B T}{G} e^{\beta V} \partial_x e^{-\beta V} \partial_x \tag{4.21}$$

[9, p. 75]. To derive a formula for the mean escape rate, consider the potential in Figure 4.1. A particle is placed at the location x_0 at the starting time $t_0 =$. The particle is supposed to be able to move on the interval $(-\infty, b]$. The boundary point $x = -\infty$ is selected as reflective, whereby the condition

$$\frac{\partial}{\partial x_0} p(x, t|x_0, t_0)\bigg|_{x_0=-\infty} = 0 \tag{4.22}$$

is placed on the probability density. The boundary point $x = b$ is chosen to be absorbing, so the probability density must satisfy the relation

$$p(x, t|x_0, t_0)\big|_{x_0=b} = 0 \tag{4.23}$$

[8, p. 167]. The function

$$S(t, x_0) = \int_{-\infty}^{b} p(x, t|x_0, t_0) dx = \int_{-\infty}^{b} e^{\Omega(t-t_0)} \delta(x - x_0) dx \tag{4.24}$$

gives the probability that the particle is still in the interval $(-\infty, b]$ in time t. Since the right boundary point at $x = b$ is absorbing, the probability $S(t, x_0)$ becomes smaller and smaller for increasing times t and for $t \to \infty$ $S(t = \infty, x_0) = 0$ holds. The probability $p(x, t|x_0, t_0)$ can also be understood as particle density. All particles start at the point x_0. Then $S(t, x_0)$ is the proportion of the particles that is still in the interval $(-\infty, b]$ at time t and has not already been absorbed at the right edge. The difference $S(t, x_0) - S(t + dt, x_0) = \rho(t, x_0)dt$ is the proportion of particles which have not yet left the interval $(-\infty, b]$ before time t, but which leave the interval $(-\infty, b]$ during the time interval dt. The probability stream $\rho(t, x_0)$ that a particle passes the edge b for the first time in the time interval dt is thus given by

$$\rho(t, x_0) = -\frac{dS(t, x_0)}{dt} \tag{4.25}$$

[8, pp. 166–167]. The distribution $\rho(t, x_0)$ is also called the first passing time distribution. The first moment of t is then the mean passing time $\tau_m(x_0)$ which is given by

$$\tau_m(x_0) = \int_0^\infty t \rho(t, x_0) dt. \tag{4.26}$$

If in equation (4.26) the relation according to equation (4.25) is inserted, integrating by parts yields

$$\tau_m(x_0) = -\int_0^\infty t \frac{dS(t, x_0)}{dt} = \int_0^\infty S(t, x_0) dt \tag{4.27}$$

assuming that $S(t, x_0)$ decreases faster than t increases. With the equation (4.22) we get for the left edge $\partial_x \tau_m(x)|_{x=-\infty} = 0$. In the same way, the condition $\tau_m(x)|_{x=b} = 0$ is obtained for the right edge with equation (4.23). On both sides of equation (4.27) the adjoint operator $\Omega^\dagger$ is applied [9, p. 75]. Then, with the definition of the scalar product in equation (4.18), we get the

relation

$$\begin{aligned}
\Omega^\dagger(x_0)\tau_m(x_0) &= \Omega^\dagger(x_0)\int_0^\infty S(t,x_0)dt = \int_0^\infty \Omega^\dagger(x_0)\int_{-\infty}^b e^{\Omega(x)(t-t_0)}\delta(x-x_0)dx\,dt \\
&= \int_0^\infty \Omega^\dagger(x_0)\int_{-\infty}^\infty \left(e^{\Omega(x)(t-t_0)}\delta(x-x_0)\right)\Theta(b-x)dx\,dt \\
&= \int_0^\infty \Omega^\dagger(x_0)\langle e^{\Omega(x)(t-t_0)}\delta(x-x_0),\Theta(b-x)\rangle dt \\
&= \int_0^\infty \Omega^\dagger(x_0)\langle \delta(x-x_0), e^{\Omega^\dagger(x)(t-t_0)}\Theta(b-x)\rangle dt \\
&= \int_0^\infty \Omega^\dagger(x_0)e^{\Omega^\dagger(x_0)(t-t_0)}\Theta(b-x_0)dt = \int_0^\infty \partial_t e^{\Omega^\dagger(x_0)(t-t_0)}\Theta(b-x_0)dt \\
&= e^{\Omega^\dagger(x_0)(t-t_0)}\Theta(b-x_0)\big|_{t=t_0}^{t=\infty} = -\Theta(b-x_0)
\end{aligned} \tag{4.28}$$

In the last line it was used that according to the scalar product defined in equation (4.18), the time evolution of a phase space function $A(x,t)$ is generally given by $A(x,t) = \exp(\Omega^\dagger(t-t_0))A(x,t_0)$. If one sets $A(x,t) = \Theta(b-x(t))$ then the time evolution is given by $\Theta(x-x(t)) = \exp(\Omega^\dagger(t-t_0))\Theta(b-x_0))$. But since $x(t)$ for $t \to \infty$ has almost certainly reached the absorbed edge $\lim_{t\to\infty}\Theta(b-x(t)) = 0$ holds and the upper integral limit vanishes. For the mean escape time τ_m, the concise relation thus results

$$\Omega^\dagger(x_0)\tau_m(x_0) = \left[\frac{k_BT}{G}e^{\beta V}\partial_{x_0}e^{-\beta V}\partial_{x_0}\right]\tau_m(x_0) = -1. \tag{4.29}$$

since for the initial value $x_0 < b$ sensibly holds [13, pp. 153–154]. On both sides of the equation (4.29), multiply on the left side by $G\beta e^{-\beta V}$, then integrate from $-\infty$ to x_0, yielding

$$\begin{aligned}
\int_{-\infty}^{x_0}\partial_y e^{-\beta V}\partial_y\tau_m(y)dy &= e^{-\beta V(x_0)}\partial_{x_0}\tau_m(x_0) - \lim_{x\to-\infty}e^{-\beta V(x)}\partial_x\tau_m(x) = e^{-\beta V(x_0)}\partial_{x_0}\tau_m(x_0) \\
&= \int_{-\infty}^{x_0} -\frac{G}{k_BT}e^{-\beta V(z)}dz
\end{aligned} \tag{4.30}$$

where the reflective boundary condition $\partial_x\tau_m(x)|_{x=-\infty} = 0$ was used. A further integration from x_0 to b yields

$$\int_{x_0}^b \partial_y\tau_m(y)dy = \tau_m(b) - \tau_m(x_0) = -\frac{G}{k_BT}\int_{x_0}^b e^{\beta V(y)}dy\int_{-\infty}^y e^{-\beta V(z)}dz. \tag{4.31}$$

With the absorbing boundary condition $\tau_m(b) = 0$, the analytical expression for the mean escape time $\tau_m(x_0)$ is given by

$$\tau_m(x_0) = \frac{G}{k_BT}\int_{x_0}^b e^{\beta V(y)}dy\int_{-\infty}^y e^{-\beta V(z)}dz. \tag{4.32}$$

The mean recurrence rate is then given by $1/\tau_m(x_0)$. The absorbing boundary point is now set to the local maximum of the double trough potential. Thus $b = 0$ is valid. At the maximum $b = 0$, the probability is $1/2$ that the particle jumps from one potential minimum to the other minimum. The reaction rate Υ is then given by

$$\Upsilon_e = \frac{1}{2}\frac{1}{\tau_m(x_0)} = \frac{k_BT}{2G}\left(\int_{x_0}^0 e^{\beta V(y)}dy\int_{-\infty}^y e^{-\beta V(z)}dz\right)^{-1} \tag{4.33}$$

[9, pp. 76–78]. The subscript 'e' for the reaction rate in equation (4.33) is to express that this result is the exact solution in the overdamped case. The starting position x_0 of the particle is

set to the left minimum as shown in Figure 4.1. The exact solution Υ_e of the reaction rate has the disadvantage that the relation between the reaction rate and the temperature $\beta^{-1} = k_B T$ is not immediately obvious. Equation (4.33) is therefore to be approximated in a suitable way. For this purpose, the potential $V(x)$ at the extreme points $x = x_0$ and $x = 0$ is determined by the series expansions

$$V(z)\big|_{z=x_0} \approx V(x_0) + \frac{\omega_0^2}{2}(z - x_a)^2 \tag{4.34}$$

$$V(y)\big|_{y=0} \approx V(0) - \frac{\omega_1^2}{2}y^2 \tag{4.35}$$

where the approximation becomes better and better if $E_b = V(x_0) - V(0) \gg k_B T$ holds for the energy barier. The second integral in equation (4.33) is dominated by the potential minimum at $x = x_0$. Therefore, approximately infinity can be set for the upper integral limit. For the integral over z the approximation then results

$$\int_{-\infty}^{y} e^{-\beta V(z)} dz \approx \int_{-\infty}^{\infty} e^{-\beta\left((V(x_0) + \frac{\omega_0^2}{2}(z-x_0)^2\right)} dz = \sqrt{\frac{2\pi}{\beta}} \frac{e^{-\beta V(x_0)}}{\omega_0} \tag{4.36}$$

In the same way, the second integral in equation (4.33) is approximated by

$$\int_{x_0}^{0} e^{\beta V(y)} dy \approx \int_{-\infty}^{0} e^{\beta\left(V(0) - \frac{\omega_1^2}{2}y^2\right)} dy = \sqrt{\frac{2\pi}{\beta}} \frac{e^{\beta V(0)}}{\omega_1} \tag{4.37}$$

For equation (4.33) we get the approximation

$$\Upsilon_a = \frac{\omega_0 \omega_1}{2\pi G} e^{-\beta E_b} \tag{4.38}$$

[9, pp. 77–78] where the subscript 'a' stands for approximation. The temperature dependence of the reaction rate is thus given by $\Upsilon = g \exp[-E_b/(k_B T)]$. This law is also called the Arrhenius formula in the theory of chemical reactions and is very well confirmed experimentally [8, pp. 173]. For strong friction, the proportionality constant g according to equation (4.39) is given by $g = \omega_0\omega_1/(2\pi G)$. For mean friction this relation is not correct.

Kramers was able to give an analytical approximate formula for medium to strong friction using a different approach. Karmers' approximate solution for the reaction rate is given by

$$\Upsilon_k = g e^{-\beta E_b} = \frac{\omega_0}{2\pi\omega_1}\left(\sqrt{\frac{G^2}{4} + \omega_1^2} - \frac{G}{2}\right) e^{-\beta E_b} \tag{4.39}$$

where the subscript 'k' is meant to recall Kramers' approximation. The derivation of equation (4.39) is discussed in detail in [14, pp. 110–116] and will not be presented in this thesis. That equation (4.39) contains the case for large friction can be seen by expand the prefactor g into a Laurent series

$$g|_{G=\infty} = \frac{\omega_0}{2\pi\omega_1}\left(\sqrt{\frac{G^2}{4} + \omega_1^2} - \frac{G}{2}\right)\Big|_{G=\infty} = \frac{\omega_0}{2\pi\omega_1}\left(\frac{\omega_1^2}{G} - \frac{\omega_1^4}{G^3} + ...\right). \tag{4.40}$$

For large friction G the same proportionality factor g as in equation (4.38) is then obtained [14, p. 144].

In the model of Ilg and Barrat according to section 3.1, the reaction rate can be determined analytically only for the case in which the second heat bath decouples, i.e. $\alpha \to \infty$. In this case, equation (3.12) results. For the additional case of large friction, we then get $\dot{x}_1 = -\partial_{x_1} V/\Gamma_1 + \eta_1(t)/\Gamma_1$. The corresponding Fokker Planck equation is then given by equation (4.12), where $G = \Gamma_1$. In the case of large damping where $\alpha \to \infty$ also holds, the reaction rate for the model in section 3.1 can thus be calculated exactly with equation (4.33). For $E_b \gg k_B T$, equation (4.38) is a good approximation. Kramers' approximation (4.39) is additionally valid for mean friction.

4.2.2 Calculation of the reaction rate with the two-level correlation function

In this subsection, a way to determine the reaction rate Υ using a correlation function is discussed. A double-well potential is again considered, which is shown in Figure 4.1. A particle can assume two states in this potential. x again denotes the position of the particle. If the particle is in the first state, it is to the left of the origin and $x < 0$ holds. The value '0' is assigned to the first state. If the particle is in the second state, it is located to the right of the origin and $x \geq 0$ applies. The value '1' is assigned to the second state. The state of the particle can be written compactly with the step function $\Theta(x)$ [9, p. 67]. The correlation of the state $\Theta(x)$ is now given by [15, p .20]

$$\mathrm{Cor}_\Theta(t-s) = \frac{\langle \Theta(x(t))\Theta(x(s))\rangle - \langle \Theta(x(t))\rangle\langle \Theta(x(s))\rangle}{\langle \Theta(x(s))^2\rangle - \langle \Theta(x(s))\rangle^2}. \tag{4.41}$$

The rest of this subsection follows the presentation in [9, p. 14–15]. The following argumentation becomes much clearer if one considers a whole ensemble of particles instead of a single particle and interprets the probability of encountering a single particle at the location x as particle density. Then $\langle \Theta(x(t))\rangle$ can be interpreted as the proportion of particles that are in the second state at time t. Let N_0 be the number of particles in state '0' and N_1 the number of particles in state '1'. Let k_0 be the rate at which the particles change from state '0' to state '1'. The rate at which the particles change from the state '1' to the state '0' is k_1. The rate equations are thus

$$\frac{N_0}{dt} = -k_0 N_0 + k_1 N_1 \tag{4.42}$$

$$\frac{N_1}{dt} = -k_1 N_1 + k_0 N_0. \tag{4.43}$$

The total number of particles in the system should be constant, so that $N_0 + N_1 = \text{const}$ applies. For a long time, a stationary solution is established, which is denoted by N_0^{st} and N_1^{st}. Now δN is the deviation from the stationary solution N_0^{st}. Then, because of the particle number conservation $N_0 = N_0^{st} + \delta N$ and $N_1 = N_1^{st} - \delta N$ holds. With the condition $k_0 N_0^{st} = k_1 N_1^{st}$ for a stationary system, the equations (4.42) and (4.43) can be summarised by

$$\frac{d}{dt}\delta N = -(k_0 + k_1)\delta N \tag{4.44}$$

where the solution is given by $\delta N(t) = Ce^{-(k_0+k_1)t}$. C is the integration constant. The macroscopic deviation δN thus decays exponentially. Now the 'Onsager Regression Hypothesis' is used. This states that small fluctuations in the mean decay in the same way as macroscopic deviations from equilibrium. Thus $\mathrm{Cor}_\Theta(t,s) = \delta N(t-s)$. For the symmetric double trough potential, the rates k_0 and k_1 are identical. The rates k_0 and k_1 correspond to the reaction rate Υ. If $t - s = 0$ is set, the integration constant is $C = 1$. Thus, the correlation finally results in

$$\mathrm{Cor}_\Theta(t-s) = e^{-(k_1+k_2)|t-s|} = e^{-2\Upsilon|t-s|}. \tag{4.45}$$

Equation (4.45) is the starting point for the numerical calculation of the reaction rate Υ. The correlation function $\mathrm{Cor}_\Theta(t)$ can be determined very well numerically. Then the reaction rate Υ can be determined via a fit function of the form $f(t) = A\exp(-2\Upsilon t)$.

4.3 Two dimensional Ornstein Uhlenbeck Process

For the overdamped model, which is characterised by equations (3.24) and (3.25), the marginal stationary probability density $p^{st}(x_1)$ is to be calculated. An analytical solution can still be given relatively easily for the potential $V(x_1) = \kappa x_1^2/2$, since an Ornstein Ulenbeck process exists for

this choice. The definition $U(x_1) = V(x_1) + \kappa_1 x_1^2/2 = \kappa_1 x_1^2/2$ with $\kappa_1 = \kappa + 1/\alpha$ is chosen as in chapter 3.3. The Langevin equations (3.24) and (3.25) can be assigned an equivalent Fokker Planck equation. For the equivalent Fokker Planck equation, the drift and diffusion coefficients must be determined after the equations (4.1) and (4.2). This is done as in section 4.2. For the drift coefficients A_i, we obtain

$$A_1(x_1, x_2) = -\frac{\kappa_1}{\Gamma_1} x_1 + \nu_1 x_2 \tag{4.46}$$

$$A_2(x_1, x_2) = -\frac{\kappa_2}{\Gamma_2} x_2 + \nu_2 x_1. \tag{4.47}$$

In the same way, the diffusion coefficients are

$$D_{11} = 2\frac{k_B T_1}{\Gamma_1} \tag{4.48}$$

$$D_{22} = 2\frac{k_B T_2}{\Gamma_2} \tag{4.49}$$

$$D_{12} = D_{21} = 0. \tag{4.50}$$

As initial value $\boldsymbol{x}_0 = (x_1^0, x_2^0)^\intercal$ is chosen at time $t_0 = 0$. Then, using the general Fokker Planck equation (4.9), the concrete Fokker Planck equation for the overdamped model $\boldsymbol{x} = (x_1, x_2)^\intercal$ is given by

$$\begin{aligned} \partial_t p(\boldsymbol{x}, t|\boldsymbol{x}_0, t_0) = \Bigg[&\frac{\partial}{\partial x_1}\left(\frac{\kappa_1}{\Gamma_1} x_1 - \nu_1 x_2\right) + \frac{\partial}{\partial x_2}\left(\frac{\kappa_2}{\Gamma_2} x_2 - \nu_2 x_1\right) \\ &+ \frac{k_B T_1}{\Gamma_1}\frac{\partial^2}{\partial x_1^2} + \frac{k_B T_2}{\Gamma_2}\frac{\partial^2}{\partial x_2^2}\Bigg] p(\boldsymbol{x}, t|\boldsymbol{x}_0, t_0). \end{aligned} \tag{4.51}$$

where for the conditional probability $p(\boldsymbol{x}, t|\boldsymbol{x}_0, t_0)$ the initial condition $p(\boldsymbol{x}, t_0|\boldsymbol{x}_0, t_0) = \delta(\boldsymbol{x} - \boldsymbol{x}_0)$ must be satisfied. The Fokker Planck equation can be written even more compactly by [13, p. 129]

$$\partial_t p(\boldsymbol{x}, t|\boldsymbol{x}_0, t_0) = [\nabla_{\boldsymbol{x}} \cdot \mathsf{G}\boldsymbol{x} + \nabla_{\boldsymbol{x}} \cdot (\mathsf{D}\nabla_{\boldsymbol{x}})] p(\boldsymbol{x}, t|\boldsymbol{x}_0, t_0) \tag{4.52}$$

with the matrices

$$\mathsf{G} = \begin{pmatrix} \frac{\kappa_1}{\Gamma_1} & -\nu_1 \\ -\nu_2 & \frac{\kappa_2}{\Gamma_2} \end{pmatrix} \qquad \text{and} \qquad \mathsf{D} = \begin{pmatrix} \frac{k_B T_1}{\Gamma_1} & 0 \\ 0 & \frac{k_B T_2}{\Gamma_2} \end{pmatrix} \tag{4.53}$$

The Fokker Planck equation (4.51) can be solved by Fourier transformation. For this the transformed conditional probability is given by

$$\hat{p}(\boldsymbol{k}, t|\boldsymbol{x}_0, t_0) = \int_{\mathbb{R}^2} dx^2 \exp(-i\boldsymbol{k} \cdot \boldsymbol{x}) p(\boldsymbol{x}, t|\boldsymbol{x}_0, t_0). \tag{4.54}$$

With the initial condition $p(\boldsymbol{x}, t_0|\boldsymbol{x}_0, t_0) = \delta(\boldsymbol{x} - \boldsymbol{x}_0)$, the initial condition in $\boldsymbol{k}$-space is given by $\hat{p}(\boldsymbol{k}, t_0|\boldsymbol{x}_0, t_0) = \exp(-i\boldsymbol{k} \cdot \boldsymbol{x}_0)$. The matrices G and D are componentwise $(\mathsf{G})_{ij} = g_{ij}$ and $\mathsf{D}_{ij} = d_{ij}$. Now equation (4.51) is Fourier transformed on both sides. This gives

$$\partial_t \hat{p}(\boldsymbol{k}, t|\boldsymbol{x}_0, t_0) = -g_{ij} k_i \frac{\partial}{\partial k_j} \hat{p}(\boldsymbol{k}, t|\boldsymbol{x}_0, t_0) - d_{ij} k_i k_j \hat{p}(\boldsymbol{k}, t|\boldsymbol{x}_0, t_0) \tag{4.55}$$

where Einstein's sum convension is used here [13, p. 130]. To solve the partial differential equation (4.55) the approach

$$\hat{p}(\boldsymbol{k}, t|\boldsymbol{x}_0, t_0) = \exp\left(-ik_i M_i (t - t_0) - \frac{1}{2} k_i k_j \sigma_{ij} (t - t_0)\right) \tag{4.56}$$

is chosen, where $\sigma_{ij} = \sigma_{ji}$ is symmetric. $\boldsymbol{M}$ resp. $\boldsymbol{\sigma}$ is a continuously differentiable vector resp. a continuously differentiable matrix. Substituting the approach into equation (4.55) yields

$$\begin{aligned}&\left[\partial_t + g_{ij}k_i\frac{\partial}{\partial k_j} + d_{ij}k_ik_j\right]\hat{p}(\boldsymbol{k},t|\boldsymbol{x}_0,t_0)\\ &\quad= \left(-ik_i\dot{M}_i - \frac{1}{2}k_ik_j\dot{\sigma}_{ij} - ig_{ij}k_iM_j - g_{ij}k_i\sigma_{jl}k_l + d_{ij}k_ik_j\right)\hat{p}(\boldsymbol{k},t|\boldsymbol{x}_0,t_0) = 0\end{aligned} \tag{4.57}$$

Since the last equation must hold for any $k_i \in \mathbb{R}$, the equation can be divided into powers of k_i. In linear order, $\dot{\boldsymbol{M}}(t-t_0) = -\mathsf{G}\boldsymbol{M}(t-t_0)$ is obtained immediately. For the quadratic order we get $k_ik_j\dot{\sigma}_{ij} = 2k_ik_jd_{ij} - 2k_i(\mathsf{G}\boldsymbol{\sigma})_{ij}k_j$ [13, p. 130]. For the further calculation an argument is necessary, which will be briefly presented in the following.

Let $\boldsymbol{A} \in \mathbb{R}^{2\times 2}$ be an arbitrary but fixed matrix. $\boldsymbol{A}$ can be represented as a linear combination of a symmetric and an asymmetric matrix. This can be expressed by the relation

$$\begin{pmatrix} a_{11} & a_{12}\\ a_{21} & a_{22}\end{pmatrix} = \begin{pmatrix} a_{11} & \frac{a_{11}+a_{21}}{2}\\ \frac{a_{11}+a_{21}}{2} & a_{22}\end{pmatrix} + \begin{pmatrix} 0 & \frac{a_{12}-a_{21}}{2}\\ -\frac{a_{12}-a_{21}}{2} & 0\end{pmatrix} \tag{4.58}$$

On the right side of the equation the arbitrary matrix $\boldsymbol{A}$ is shown. On the left side of the equation, the first matrix is symmetric, while the second matrix is antisymmetric.

Now set $\boldsymbol{A} = \mathsf{G}\boldsymbol{\sigma}$. With $k_iA_{ij}k_j$ only the symmetric part remains for the matrix $\boldsymbol{A}$. The matrix $\boldsymbol{A} = \mathsf{G}\boldsymbol{\sigma}$ is symmetric, so it has the property $\boldsymbol{A}^\intercal = \boldsymbol{A}$. Therefore it can be further written $\dot{\boldsymbol{\sigma}} = 2\mathsf{D} - \mathsf{G}\boldsymbol{\sigma} - \mathsf{G}\boldsymbol{\sigma} = 2\mathsf{D} - \mathsf{G}\boldsymbol{\sigma} - \boldsymbol{\sigma}\mathsf{G}^\intercal$ [13, p. 130].

With the initial condition $\hat{p}(\boldsymbol{k},t_0|\boldsymbol{x}_0,t_0) = \exp(-i\boldsymbol{k}\cdot\boldsymbol{x}_0)$ it is necessarily that $\boldsymbol{M}(0) = \boldsymbol{x}_0$ and $\boldsymbol{\sigma}(0) = 0$ must hold. The differential equation for $\dot{\boldsymbol{M}}$ can be solved with the matrix exponential function $\boldsymbol{W} = \exp(-\mathsf{G}(t-t_0))$. This gives the solution

$$\boldsymbol{M}(t-t_0) = \boldsymbol{W}\boldsymbol{x}_0 = \exp(-\mathsf{G}(t-t_0))\boldsymbol{x}_0 \tag{4.59}$$

where the initial condition $\boldsymbol{M}(0) = \boldsymbol{x}_0$ is obviously satisfied. The solution of the differential equation for $\dot{\boldsymbol{\sigma}}$ is given by

$$\boldsymbol{\sigma}(t-t_0) = 2\int_0^{t-t_0}\boldsymbol{W}(\tau)\mathsf{D}\boldsymbol{W}^\intercal(\tau)d\tau. \tag{4.60}$$

[13, p. 130]. To prove that the given solution for $\boldsymbol{\sigma}$ is indeed a solution of the differential equation $\dot{\boldsymbol{\sigma}} = 2\mathsf{D} - \mathsf{G} - \boldsymbol{\sigma}\mathsf{G}^\intercal$, consider equivalently the differential equation $\ddot{\boldsymbol{\sigma}} = -\mathsf{G}\dot{\boldsymbol{\sigma}} - \dot{\boldsymbol{\sigma}}\mathsf{G}^\intercal$. This differential equation is solved by the solution (4.60). This can be easily shown by differentiating twice using $\dot{\boldsymbol{W}} = -\mathsf{G}\boldsymbol{W}$

$$\begin{aligned}\dot{\boldsymbol{\sigma}} &= 2\boldsymbol{W}(t-t_0)\mathsf{D}\boldsymbol{W}^\intercal(t-t_0)\\ \ddot{\boldsymbol{\sigma}} &= 2\dot{\boldsymbol{W}}(t-t_0)\mathsf{D}\boldsymbol{W}^\intercal(t-t_0) + 2\boldsymbol{W}(t-t_0)\mathsf{D}\dot{\boldsymbol{W}}^\intercal(t-t_0)\\ &= -2\mathsf{G}\boldsymbol{W}\mathsf{D}\boldsymbol{W}^\intercal - 2\boldsymbol{W}\mathsf{D}\boldsymbol{W}^\intercal\mathsf{G}^\intercal = -\mathsf{G}\dot{\boldsymbol{\sigma}} - \boldsymbol{\sigma}\mathsf{G}^\intercal.\end{aligned} \tag{4.61}$$

Using the solutions for $\boldsymbol{M}(t-t_0)$ and $\boldsymbol{\sigma}(t-t_0)$, the solution for $p(\boldsymbol{x},t|\boldsymbol{x}_0,t_0)$ is obtained by back transformation [13, p. 130]

$$\begin{aligned}p(\boldsymbol{x},t|\boldsymbol{x}_0,t_0) &= \int_{\mathbb{R}^2}\frac{d^2k}{(2\pi)^2}\exp(i\boldsymbol{k}\cdot\boldsymbol{x})\exp\left[-\boldsymbol{k}\cdot\boldsymbol{M}(t-t_0) - \frac{1}{2}\boldsymbol{k}^\intercal\boldsymbol{\sigma}(t-t_0)\boldsymbol{k}\right]\\ &= \frac{1}{2\pi\sqrt{\det\boldsymbol{\sigma}(t-t_0)}}\\ &\qquad\times\exp\left[-\frac{1}{2}(\boldsymbol{x}-\boldsymbol{M}(t-t_0))^\intercal\boldsymbol{\sigma}^{-1}(t-t_0)(\boldsymbol{x}-\boldsymbol{M}(t-t_0))\right].\end{aligned} \tag{4.62}$$

The marginal probability distribution function $p(x_1, t|\boldsymbol{x}_0, t_0))$ is then given by

$$p(x_1, t|\boldsymbol{x}_0, t_0) = \int_{\mathbb{R}} p(\boldsymbol{x}, t|\boldsymbol{x}_0, t_0) dx_2 = \frac{1}{\sqrt{2\pi\sigma_{11}(t-t_0)}} \exp\left[-\frac{1}{2}\frac{(x_1 - M_1(t-t_0))^2}{\sigma_{11}(t-t_0)}\right]. \quad (4.63)$$

The proof of this statement can be found in the appendix in lemma 2 .

The matrix G, defined in equation (4.53), coincides with the matrix Λ, defined in equation (3.27). Thus $\Lambda = \mathsf{G}$ holds. The matrix G is diagonalised in the same way as the matrix Λ. Then the result is

$$\boldsymbol{W}(t-t_0) = \sum_{n=0}^{\infty} \frac{1}{n!}(-\mathsf{G}(t-t_0))^n = \boldsymbol{S}\begin{pmatrix} e^{-\lambda_1(t-t_0)} & 0 \\ 0 & e^{-\lambda_2(t-t_0)} \end{pmatrix}\boldsymbol{S}^{-1} \quad (4.64)$$

where the eigenvalues λ_i are given in equation (3.28). For the matrix $\boldsymbol{S}$ holds $\boldsymbol{S} = (\boldsymbol{v}_1, \boldsymbol{v}_2)$ where the column vectors $\boldsymbol{v}_i$ are the eigenvectors of the matrix G already calculated in equation (3.29). The matrix $\boldsymbol{S}^{-1}$ notes the inverse matrix to $\boldsymbol{S}$. If one writes the matrix $\boldsymbol{S}^{-1}$ as

$$\boldsymbol{S}^{-1} = \begin{pmatrix} \boldsymbol{w}_1^\intercal \\ \boldsymbol{w}_2^\intercal \end{pmatrix} \quad (4.65)$$

where the vectors $\boldsymbol{w}_1^\intercal$ and $\boldsymbol{w}_2^\intercal$ are the row vectors of the matrix $\boldsymbol{S}^{-1}$, the solution of $\boldsymbol{M}$ is [16, pp. 155–156]

$$\boldsymbol{M} = \boldsymbol{W}\boldsymbol{x}_0 = e^{-\lambda_1 t}(\boldsymbol{v}_1\boldsymbol{w}_1^\intercal)\boldsymbol{x}_0 + e^{-\lambda_2 t}(\boldsymbol{v}_2\boldsymbol{w}_2^\intercal)\boldsymbol{x}_0 \quad (4.66)$$

where $t_0 = 0$ was set. The matrices $\boldsymbol{v}_1\boldsymbol{w}_1^\intercal$ and $\boldsymbol{v}_2\boldsymbol{w}_2^\intercal$ are

$$\boldsymbol{v}_1\boldsymbol{w}_1^\intercal = \boldsymbol{A}_1 = \frac{1}{\det(\boldsymbol{S})}\begin{pmatrix} -\frac{a+\sqrt{D}}{2\nu_2} & \frac{\nu_1}{\nu_2} \\ 1 & \frac{a-\sqrt{D}}{2\nu_2} \end{pmatrix} \qquad \boldsymbol{v}_2\boldsymbol{w}_2^\intercal = \boldsymbol{A}_2 = \frac{1}{\det(\boldsymbol{S})}\begin{pmatrix} \frac{a-\sqrt{D}}{2\nu_2} & -\frac{\nu_1}{\nu_2} \\ -1 & -\frac{a+\sqrt{D}}{2\nu_2} \end{pmatrix} \quad (4.67)$$

For the matrix $\boldsymbol{\sigma}(t)$ we get [16, pp. 155–156]

$$\begin{aligned} \boldsymbol{\sigma}(t) &= 2\int_0^t \left(\sum_{i=1}^{2} \boldsymbol{A}_i e^{-\lambda_i t}\right) \mathsf{D} \left(\sum_{j=1}^{2} \boldsymbol{A}_j^\intercal e^{-\lambda_j t}\right) \\ &= 2\sum_{i,j=1}^{2} \boldsymbol{A}_i \mathsf{D} \boldsymbol{A}_j^\intercal \frac{1}{\lambda_i + \lambda_j}\left(1 - e^{-(\lambda_i+\lambda_j)t}\right) \end{aligned} \quad (4.68)$$

For the marginal probability density $p(x_1, t|\boldsymbol{x}_0, t_0 = 0)$ defined in equation (4.63), the functions $M_1(t)$ and $\sigma_{11}(t)$ are given by

$$M_1(t) = -\frac{\nu_2}{\sqrt{D}}\left[e^{-\lambda_1 t}\left(-\frac{a+\sqrt{D}}{2\nu_2}x_1^0 + \frac{\nu_1}{\nu_2}x_2^0\right) + e^{-\lambda_2 t}\left(\frac{a-\sqrt{D}}{2\nu_2}x_1^0 - \frac{\nu_1}{\nu_2}x_2^0\right)\right] \quad (4.69)$$

where the initial condition $\boldsymbol{x}_0 = (x_1^0, x_2^0)^\intercal$ was used and

$$\begin{aligned} \sigma_{11}(t) = \frac{2\nu_2^2}{D}\Bigg[&\frac{1}{2\lambda_1}\left(\frac{k_B T_1}{\Gamma_1}\frac{(a+\sqrt{D})^2}{4\nu_2^2} + \frac{k_B T_2 \nu_1^2}{\nu_2}\right)\left(1 - e^{-2\lambda_1 t}\right) \\ &+ \frac{2}{\lambda_1 + \lambda_2}\left(\frac{k_B T_1 \nu_1}{\Gamma_1 \nu_2} - \frac{\nu_1^2 k_B T_2}{\nu_2}\right)\left(1 - e^{-(\lambda_1+\lambda_2)t}\right) \\ &+ \frac{1}{2\lambda_2}\left(\frac{k_B T_1}{\Gamma_1}\frac{(a-\sqrt{D})^2}{4\nu_2^2} + \frac{k_B T_2 \nu_1^2}{\nu_2}\right)\left(1 - e^{-2\lambda_2 t}\right)\Bigg]. \end{aligned} \quad (4.70)$$

If $\alpha, \gamma, \Gamma_0 > 0$ holds, the eigenvalues λ_i are always greater than zero. This has already been discussed in section 3.3. For the stationary probability density $p^{st}(x_1) = p(x_1, t = \infty | \boldsymbol{x}_0, t_0 = 0)$ the results are $M_1(t = \infty) = 0$ and

$$\begin{aligned}\sigma_{11}(t=\infty) = \sigma_{11}^{st} = \frac{2\nu_2^2}{D}\Bigg[\frac{1}{2\lambda_1}\left(\frac{k_B T_1}{\Gamma_1}\frac{(a+\sqrt{D})^2}{4\nu_2^2} + \frac{k_B T_2 \nu_1^2}{\nu_2}\right) \\ + \frac{2}{\lambda_1+\lambda_2}\left(\frac{k_B T_1 \nu_1}{\Gamma_1 \nu_2} - \frac{\nu_1^2 k_B T_2}{\nu_2}\right) \\ + \frac{1}{2\lambda_2}\left(\frac{k_B T_1}{\Gamma_1}\frac{(a-\sqrt{D})^2}{4\nu_2^2} + \frac{k_B T_2 \nu_1^2}{\nu_2}\right)\Bigg].\end{aligned} \tag{4.71}$$

5. Different effective temperatures

Ilg and Barrat suggest in [6] that a key role in understanding glassy systems could be the concept of effective temperatures. A first definition of effective temperatures starts from the fluctuation-dissipation relation, which holds at equilibrium, and generalises it by introducing an effective temperature. In the last two decades, further definitions of effective temperatures have been developed which are now briefly presented and discussed in the following three subchapters. The discussion is carried out on the overdamped model of Ilg and Barrat [6] which is described in section 3.1.

5.1 Definition of an effective temperature using the canonical distribution

The overdamped case is described by the equations (3.24) and (3.25). For the case of a quadratic potential $V(x_1) = \kappa x_1^2/2$ the Ornstein Uhlenbeck process is present which can be solved analytically exactly. According to section 4.3 the probability distribution function of the random variable x_1 can be calculated with equation (4.63). In the stationary case, the probability distribution function $p^{st}(x_1)$ is given by

$$p^{st}(x_1) = \frac{1}{\sqrt{2\pi\sigma_{11}^{st}}} \exp\left(-\frac{1}{2}\frac{x_1^2}{\sigma_{11}^{st}}\right) \tag{5.1}$$

where σ_{11}^{st} is calculated by equation (4.71). It is obvious to extend the quadratic x_1^2 term in the exponential function to a potential. In principle, there are two possibilities. In the first variant, the fraction in the exponential function is expanded with the constant κ. Then the stationary distribution is given by $p^{st}(x_1) \propto \exp(-V(x_1)/(k_B T_{\text{eff},1})$. The effective temperature is then given by

$$k_B T_{\text{eff},1} = \kappa\sigma_{11}^{st}. \tag{5.2}$$

In the second variant, the fraction in the exponential function is expanded with $\kappa_1 = \kappa + 1/\alpha$. Then the stationary probability distribution function is given by $p^{st}(x_1) \propto \exp(-U(x_1)/(k_B T_{\text{eff},2})$ and the associated effective temperature is defined by

$$k_B T_{\text{eff},2} = \kappa_1\sigma_{11}^{st} = \left(\kappa + \frac{1}{\alpha}\right)\sigma_{11}^{st}. \tag{5.3}$$

The idea of determining an effective temperature from the stationary canonical distribution is taken from the paper of Ilg and Barrat [6]. The effective temperatures in equation (5.2) and (5.3) have different behaviour depending on α. Therefore, in the following section, the similarities and differences of $T_{\text{eff},1}$ and $T_{\text{eff},2}$ are discussed in detail.

In Figure 5.1 (a), as a function of the coefficient α, the effective temperature $T_{\text{eff},1}$ is shown, where the effective temperature is given in units of the fast heat bath with temperature T_1. The second slow long-range heat bath with temperature T_2 is set to $T_2 = 2T_1$. The spring constant is $\kappa = 2$ and the friction coefficient is $\Gamma_1 = 4$. Three temperature curves are given for the decay

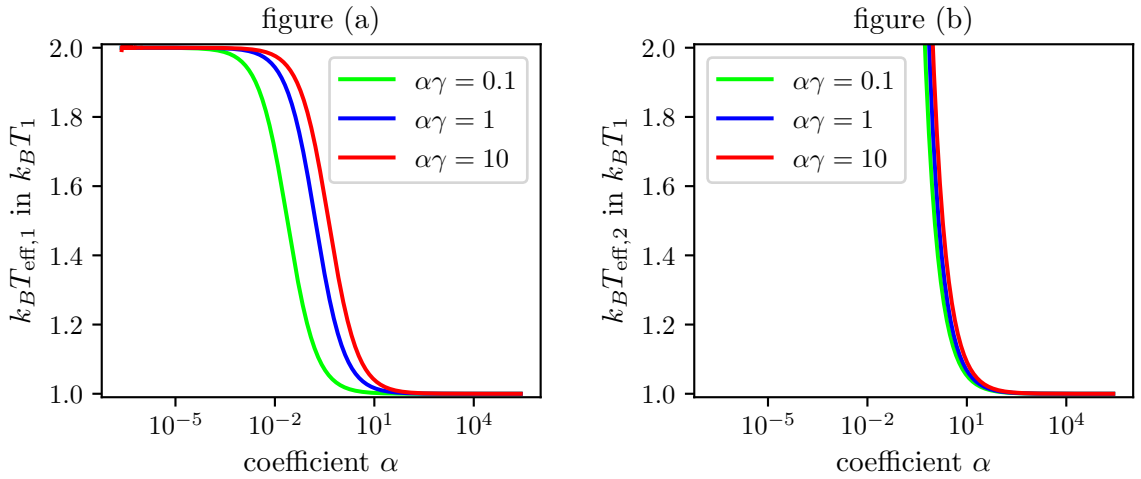

Figure 5.1: In both figures, three effective temperature curves for the three decay constants $\alpha\gamma \in \{0.1, 1, 10\}$ are shown depending on the parameter α. Figure (a) shows the effective temperature $T_{\text{eff},1}$ which is calculated according to equation (5.2). Figure (b) shows the effective temperature $T_{\text{eff},2}$ which is determined by equation (5.3).

constants $\alpha\gamma \in \{0.1, 1, 10\}$. The units of κ, Γ_1, α and $\alpha\gamma$ are not given for clarity. The decay constant $\alpha\gamma$ in equation (3.19) indicates how long-lasting the memory effects are. For large decay constants, the memory effect is large, whereas for small decay constants, the memory effect is small. Figure (a) clearly shows that for increasing $\alpha\gamma$ the effective temperature increases. This was to be expected, since for increasing $\alpha\gamma$ the influence of the temperature T_2 on the system keeps increasing. For increasing parameters α the second heat bath is increasingly decoupled from the system and for $\alpha \to \infty$ the second heat bath is decoupled from the system which means that the system must have the temperature T_1 of the first heat bath. The fact that for $\alpha \to \infty$, the system must have the temperature T_1 can be easily seen from equation 3.12. For $\alpha \to 0$ the second heat bath dominates and $T_{\text{eff},1} = T_2$ holds. It should also be noted that if $T_1 = T_2$ is chosen, the effective temperature is $T_{\text{eff},1} = T_1$.

Figure 5.1 (b) shows the effective temperature $T_{\text{eff},2}$ as a function of the parameter α. For $\alpha \to \infty$ the same discussion applies as in figure (a). For the case $\alpha \to 0$ the effective temperature $T_{\text{eff},2}$ diverges. From a value $\alpha \approx 1$ all temperature curves lie outside the temperature range $[T_1, T_2]$. However, according to the model in section 3.1, one would expect the effective temperature to be in the temperature range $[T_1, T_2]$. This is a first problematic property of the effective temperature $T_{\text{eff},2}$. In simulations it can be observed that there can also be diverging effective temperatures [3]. In this case, this property would not be directly problematic. But if $T_1 = T_2$ is chosen for the two heat baths, the effective temperature has the dependence $T_{\text{eff},2} = (1 + 1/(\alpha\kappa))T_1$ which means that for $\alpha \to 0$ the effective temperature diverges. The model is constructed in such a way that for $T_1 \neq T_2$ the system is in non-equilibrium. For the case $T_1 = T_2$, however, the system is in equilibrium for long times and according to the FDT $T_{\text{eff},2} = T_1$ must apply for all α, which is obviously not fulfilled. The definition of the effective temperature in equation 5.3 thus seems to be problematic, which is why this definition is not discussed further. The definition in equation (5.2), on the other hand, has two more advantages which are discussed in sections 5.2 and 7.4.1.

The previous considerations are only valid for the harmonic potential $V(x_1) = \kappa x_1^2/2$. In this thesis, however, meta-stable systems are to be investigated which can be modelled by a double well potential of the form

$$V_4(x_1) = \frac{\omega_b^4}{16 E_b} x_1^4 - \frac{\omega_b^2}{2} x_1^2 + E_b \tag{5.4}$$

The parameter ω_b gives the curvature of the potential and E_b is the energy barrier between the

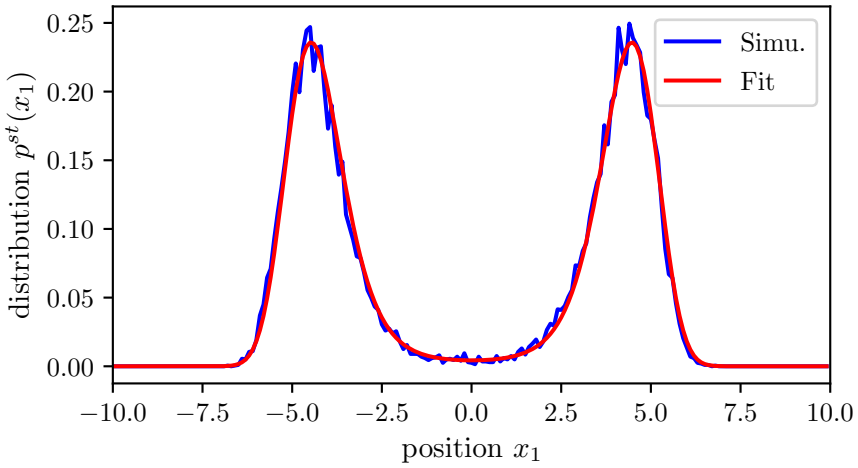

Figure 5.2: The blue curve shows the numerically determined stationary distribution $p^{st}(x_1)$ as a function of the position x_1. The red curve shows the fit function $f(x_1)$ which was fitted to the blue curve. The exact parameters for the numerical solution are not given, as this figure is only intended to explain the basic procedure for determining the effective temperature numerically.

two potential wells. A sketch of the potential $V_4(x_1)$ is given in Figure 4.1 [15]

A criterion for the significance of the effective temperature $T_{\text{eff},1}$ could be that this definition can also be applied to other potentials such as the double well potential. For this, the potential $V_4(x_1)$ is expand into a Taylor series around a potential minimum. The potential minima of $V_4(x_1)$ lies at $x_{min} \in \{\pm 2\sqrt{E_b}/\omega_b\}$. Thus the Taylor series around the left minimum is given by

$$V(x_1) = \omega_b^2 \left(x_1 + 2\frac{\sqrt{Eb}}{\omega_b} \right)^2 + \mathcal{O}(x_1^3) \tag{5.5}$$

The effective temperature $T_{\text{eff},3}$ for the double well potential can be approximated with equation (5.2) by reading the spring constant $\kappa = 2\omega_b^2$ from the expansion in equation (5.5). The analytical approximation for the effective temperature in the double well potential is then given by

$$T_{\text{eff},3} \approx T_{\text{eff},3a} = 2\omega_b^2 \sigma_{11}^{st} \tag{5.6}$$

where also in the function σ_{11}^{st} the spring constant $\kappa = 2\omega_b^2$ is inserted. The subscript 'a' means approximation. This is a quite intuitive procedure to find an analytical approximation of the effective temperature for the double well potential.

To check this analytical approximation, the equations of motion (3.24) and (3.25) are solved numerically for the double well potential. If one generates numerically many paths of the stochastic equations of motion, the stationary distribution can be determined via them. An example of a numerically determined stationary probability distribution is shown as a blue line in Figure 5.2. The function $f(x) = a\exp(-V_4(x)/b)$ is chosen as the fit function. The function $f(x)$ can now be fitted to the blue curve in Figure 5.2 with the parameters a and b. The result for $f(x)$ is shown as a red line in Figure 5.2. The fit parameter b gives the effective temperature for the double well potential. In section 7.4.1, the analytical approximation in equation (5.6) is compared with the numerical solution of the effective temperature for the double well potential.

5.2 Definition of an effective temperature using the FDT

Another definition of effective temperatures in non-equilibrium systems was developed by L. Cugliandolo, J. Kurchan, and L. Peliti [6]. The definition is based on the fluctuation-dissipation

theorem (FDT) which can be derived in equilibrium under very general assumptions. In non-equilibrium systems, the fluctuation-dissipation theorem does not generally hold. It is assumed that a meaningful effective temperature can be defined with the FDT by

$$\frac{d}{dt}\tilde{\mathrm{C}}_{ij}(t) = -k_B(T_{\mathrm{eff}})_{ij}\,\tilde{\chi}_{ij}(t). \tag{5.7}$$

where $\tilde{\mathrm{C}}_{ij}(t)$ denotes a general correlation function and $\tilde{\chi}_{ij}$ a general susceptibility [6]. In general, the effective temperature can depend on the observables. This is notated as $(T_{\mathrm{eff}})_{ij}$. In this thesis, for the general correlation function $\tilde{\mathrm{C}}_{ij} = \mathrm{Cor}_{ij}(t)$ is set, where $\mathrm{Cor}_{ij}(t)$ is defined in equation (3.36). The general susceptibility is set to $\tilde{\chi}_{i1} = \chi_i$, where $\chi_i(t)$ is calculated by equation (3.43). For the overdamped case of the model, the effective temperature is then determined by the expression [6]

$$(T_{\mathrm{eff}})_{i1} = \frac{1}{\chi_i(t)}\frac{d}{dt}\mathrm{Cor}_{i1}(t) \tag{5.8}$$

The definition of the effective temperature in equation (5.8) has a decisive disadvantage, since it cannot be determined numerically in a meaningful way. The reason is that the correlation function $\mathrm{Cor}_{i1}(t)$ and the integrated susceptibility $\chi'_{i1}(t)$ are determined numerically and therefore have a statistical noise. Both calculated functions are therefore not smooth enough that they can be differentiated in a numerically way. The effective temperature $(T_{\mathrm{eff}})_{i1}$ is therefore not numerically accessible. Since in this thesis mainly the double well potential is used where one has to rely on numerical solutions, the effective temperature in equation (5.8) is not considered further.

However, there is another possibility to define an effective temperature via the FDT. For this, the FDT is considered in its integrated version. Then the effective temperature is defined by

$$(k_B T_{\mathrm{eff}})_{i1}(t) = \frac{\mathrm{Cor}_{i1}(0) - \mathrm{Cor}_{i1}(t)}{\chi'_i(t)} \tag{5.9}$$

In the static case, the effective temperature is then given by

$$k_B T_{\mathrm{eff},4} = \mathrm{Cor}_{11}(0)/\chi'_1(t=\infty) \tag{5.10}$$

since the correlation function vanish for $t \to \infty$ [6]. Also for the definition of the effective temperature via the integrated FDT it is obvious to discuss essential features at the Ornstein Uhlenbeck process. In the static case, equation (5.10) yields the interesting relationship

$$\begin{aligned} k_B T_{\mathrm{eff},5} &= \frac{\Gamma_1}{\frac{b_{11}}{\lambda_1} + \frac{b_{12}}{\lambda_2}} \sum_{\alpha,\beta=1}^{2} \frac{2 b_{i\alpha} b_{1\beta}}{\lambda_\alpha + \lambda_\beta} \left(\frac{k_B T_1}{\Gamma_1} + a_\alpha a_\beta \frac{k_B T_2}{\Gamma_2} \right) \\ &= \frac{\Gamma_1}{\frac{b_{11}}{\lambda_1} + \frac{b_{12}}{\lambda_2}} \sigma_{11}^{st} = \kappa \sigma_{11}^{st} \end{aligned} \tag{5.11}$$

where $k_B T_{\mathrm{eff},5}$ is identical to the effective temperature $k_B T_{\mathrm{eff},3a}$ in equation (5.2). Note that this relation is only valid for the Ornstein Uhlenbeck process. In the case $i = 2$, on the other hand, equation (5.9) does not give a meaningful definition of an effective temperature. Figure 5.3 shows the static effective temperature $(T_{\mathrm{eff}})_{21}$ as a function of the parameter α for different decay constants $\alpha\gamma$. For small α all curves lie above the heat bath $T_2 = 2T_1$. Also for the limit $\alpha \to \infty$, the cures do not take the temperature T_1. Thus, the effective temperature $(T_{\mathrm{eff}})_{21}$ does not seem to be a meaningful observable.

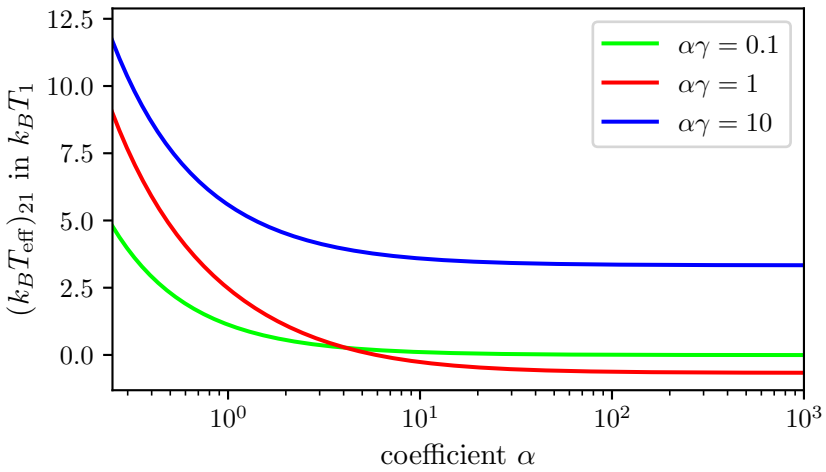

Figure 5.3: Depending on the parameter α, the effective temperature $(T_{\text{eff}})_{21}$, which is calculated with equation (5.9), is shown for different decay constants $\alpha\gamma$. The second heat bath was set at temperature $T_2 = 2T_1$. The definition of $(T_{\text{eff}})_{21}$ does not seem to make sense, since $(T_{\text{eff}})_{21}$ should always lie in the temperature interval $[T_1, T_2]$.

5.3 Definition of the effective temperature using the Arrhenius factor

As discussed in section 4.2, activated processes are characterised by Arrhenius dependence. For the double well potential according to equation (5.4), the reaction rate Υ can be determined numerically very well. A possible numerical procedure is presented in section 4.2.2. If one varies the energy barier E_b, one obtains

$$\Upsilon(E_b) = g \exp\left(\frac{E_b}{k_B T_{\text{eff},6}}\right). \tag{5.12}$$

For a plot with the energy barier E_b on the x axis and the reaction rate $\Upsilon(E_b)$ on the y axis, the effective temperature $T_{\text{eff},6}$ can then be determined as a fit parameter. The same procedure has already been used in [5].

6. Numerical methods

For the model of P. Ilg and J.L. Barrat, presented in section 3.1, an exact analytical solution can only be given for the potential $U(x_1) = V(x_1) + x_1^2/(2\alpha)$. For the double well potential, one generally has to rely on numerical solutions. This chapter therefore discusses in detail how the stochastic equations of motion can be discretised. Then it is shown how the correlation functions in equations (3.36) and (4.41) and the integrated susceptibility in equation (3.43) can be calculated numerically.

6.1 Dimensionless equations of motion

The model can be characterised by the equations (3.2) and (3.3). Numerically, the integro-differential equation (3.3) is quite difficult to solve. In section 3.2.1 and 3.2.2 it was shown that the integro-differential equation can be transformed into a set of ordinary differential equations. In section 3.2.1, the case for arbitrary friction is discussed, and this case is also referred to as Kramers' case in this thesis. In section 3.2.2, the overdamped case is discussed, which is also referred to here as the Smoluchovski's case.

For the numerical treatment, the exact form of the potential $V(x_1)$ must fixed. For this, the double well potential $V_4(x_1)$ in equation (5.4) is chosen. For dimensional reasons, a possible characteristic time scalar is given by $\tau_c = \sqrt{m}/\omega_b$, where m is the mass of the particle. The energy of the system will be measured in units of $k_B T_1$. With these determinations, the characteristic length of the system is $\xi_c = \sqrt{k_B T_1}/\omega_b$. Since the energy of the system is measured in units of $k_B T_1$, the thermal energy of the slow heat bath is determined by $k_B T_2 = \epsilon k_B T_1$. The dimensionless parameter ϵ is thus the constant of proportionality between the thermal energies of the two heat baths. All physical observables can be measured by the dimensions length ξ_c, time τ_c and mass m. The mass m, the curvature of the potential ω_b and the thermal energy $k_B T_1$ are chosen as basic units. From this, the dimensions length ξ_c and time τ_c can be calculated.

All physical observables can now be de-dimensioned by the characteristic dimensions ξ_c, τ_c and m. For example, for the position $x = \xi_c \tilde{x}$, where $\tilde{x}$ denotes the dimensionless position. The other observables are then

$$\begin{array}{llll} t = \tau_c \tilde{t} & x_1 = \xi_c \tilde{x}_1 & v = \frac{\xi_c}{\tau_c}\tilde{v} & z = \frac{\xi_c m}{\tau_c^2}\tilde{z} \\ \alpha = \frac{\tau_c^2}{m}\tilde{\alpha} & E_b = k_B T_1 \tilde{E}_b & \Gamma_0 = \frac{m}{\tau_c}\tilde{\Gamma}_0 & \gamma = \frac{m}{\tau_c}\tilde{\gamma}. \end{array} \tag{6.1}$$

In the following two subchapters, the Kramers' case and the Smoluchovski's case are discussed separately. For both cases, the equations of motion are discretised and de-dimensioned for a numerical solution.

6.1.1 Numerical equation for Kramers' case

For the case of arbitrary friction, the equations (3.16) – (3.18) result. For the numerical treatment, the three equations of motion are rewritten in a differential form. The reformulation is done with no mathematical rigour. The equations (3.16)-(3.18) are integrated in the interval

$[t, t+dt]$. The result is

$$dx = x(t+dt) - x(t) = vdt \tag{6.2}$$

$$mdv = mv(t+dt) - mv(t) = \left(-\frac{\partial V}{\partial x} + z - \Gamma_0 v\right) dt + \int_t^{t+dt} \eta(s) ds \tag{6.3}$$

$$dz = z(t+dt) - z(t) = \left(-\frac{1}{\alpha} v - \frac{1}{\alpha\gamma} z\right) dt + \int_t^{t+dt} \zeta(s) ds \tag{6.4}$$

[8, p. 81]. The stochastic forces η and ζ are gaussian white noise. Therefore, the Mean values are $\langle\eta\rangle = \langle\zeta\rangle = 0$ and the variances are $\langle\eta(s_1)\eta(s_2)\rangle = \sigma_\eta^2 \delta(s_1 - s_2)$ and $\langle\zeta(s_1)\zeta(s_2)\rangle = \sigma_\zeta^2 \delta(s_1 - s_2)$. The integrals for the stochastic forces

$$\sigma_\eta dW_\eta = \int_t^{t+dt} \eta(s) ds \qquad\qquad \sigma_\zeta dW_\zeta = \int_t^{t+dt} \zeta(s) ds \tag{6.5}$$

are again gaussian distributed since the sum of gaussian random variables is gaussian distributed. Motivated by the relations

$$\begin{aligned} \langle(\sigma_\eta dW_\eta)^2\rangle &= \int_t^{t+dt} \int_t^{t+dt} \langle\eta(s_1)\eta(s_2)\rangle ds_1 ds_2 = \sigma_\eta^2 dt \\ \langle(\sigma_\zeta dW_\zeta)^2\rangle &= \int_t^{t+dt} \int_t^{t+dt} \langle\zeta(s_1)\zeta(s_2)\rangle ds_1 ds_2 = \sigma_\zeta^2 dt \end{aligned} \tag{6.6}$$

symbolically $\sigma_\eta dW_\eta = \sigma_\eta \sqrt{dt}\, \tilde{\eta}$ and $\sigma_\zeta dW_\zeta = \sigma_\zeta \sqrt{dt}\, \tilde{\zeta}$ is written, where $\tilde{\eta}$ and $\tilde{\zeta}$ are two independent normally distributed random variables with mean $\mu = 0$ and variance $\sigma^2 = 1$. The stochastic processes dW_η and dW_ζ are thus not of order dt but only of order $\sqrt{dt}$. The normally distributed processes dW_η and dW_ζ each have mean $\mu = 0$ and variance $\sigma^2 = dt$. This is noted by $dW_\eta \sim N(0, dt)$ and $dW_\zeta \sim N(0, dt)$. The nomenclature $\psi \sim N(\mu, \sigma^2)$ expresses that the random variable ψ is normally distributed with mean μ and variance σ^2 [8, p. 81]. For the equations (3.17) and (3.18) the concrete values $\sigma_\eta = \sqrt{2k_B T_1 \Gamma_0}$ and $\sigma_\zeta = \sqrt{2k_B T_2/(\alpha^2\gamma)}$ are obtained. The equations (6.2), (6.3) and (6.4) thus write symbolically through

$$dx = vdt \tag{6.7}$$

$$mdv = \left(-\frac{\partial V}{\partial x} + z - \Gamma_0 v\right) dt + \sqrt{2k_B T_1 \Gamma_0}\sqrt{dt}\tilde{\eta} \tag{6.8}$$

$$dz = \left(-\frac{1}{\alpha} v - \frac{1}{\alpha\gamma} z\right) dt + \sqrt{\frac{2k_B T_2}{\alpha^2\gamma}}\sqrt{dt}\tilde{\zeta} \tag{6.9}$$

where $\tilde{\eta} \sim N(0,1)$ and $\tilde{\zeta} \sim N(0,1)$. For the numerical equations of motion, the time t is divided into discrete equidistant time steps $t_0 = 0 < t_1 = h < ... < t_i = hi < ..., t_N = hN$, where $h > 0$ is a small time step. For the numerical solution, $dt \approx h$ is now set. Further, $dx(t_i) \approx x(t_i+h) - x(t_i) = x_{i+1} - x_i$, $dv(t_i) \approx v(t_i+h) - v(t_i) = v_{i+1} - v_i$ and $dz \approx z(t_i+h) - z(t_i) = z_{i+1} - z_i$. If the numerical approximations for the equations (6.7)−(6.9) are applied and, in addition, the physical quantities are de-dimensioned by equation (6.1), the discrete Euler method is automatically obtained. The discrete Euler method is thus [8, p. 178]

$$\tilde{x}_{i+1} = \tilde{x}_i + \tilde{v}_i \tilde{h} \tag{6.10}$$

$$\tilde{v}_{i+1} = \tilde{v}_i + \left(-\frac{1}{4\tilde{E}_b}\tilde{x}_i^3 + \tilde{x}_i + \tilde{z}_i - \tilde{\Gamma}_0 \tilde{v}_i\right) \tilde{h} + \sqrt{2\tilde{\Gamma}_0}\, \sqrt{\tilde{h}}\tilde{\eta} \tag{6.11}$$

$$\tilde{z}_{i+1} = \tilde{z}_i - \left(\frac{\tilde{v}_i}{\tilde{\alpha}} + \frac{\tilde{z}_i}{\tilde{\alpha}\tilde{\gamma}}\right) \tilde{h} + \sqrt{\frac{2\epsilon}{\tilde{\gamma}\tilde{\alpha}^2}}\, \sqrt{\tilde{h}}\tilde{\zeta} \tag{6.12}$$

with the dimensionless positions $\tilde{x}(t_i)$, the dimensionless velocities $\tilde{v}(t_i)$ and the dimensionless auxiliary variable $\tilde{z}(t_i)$. Importantly, for each new iteration, the gaussian random variables $\tilde{\eta}$ and $\tilde{\zeta}$ are always regenerated. With the initial values $\tilde{x}_0$, $\tilde{v}_0$ and $\tilde{z}_0$ and the equations (6.10)−(6.12) a complete numerical simulation can be generated. The discrete equations are implemented in `C++`. For the generation of the gaussian random variables, the library `# include <random>` is used with the functions `random_device rd {};` and `mt19937 gen{rd()};` for the generation of equally distributed random variables and `normal_distribution<double> d{0,1};` for the generation of the gaussian random variables. The initial values of the dimensionless position $\tilde{x}_0$ and the dimensionless velocity $\tilde{v}_0$ can be chosen freely. For $z(t)$, the equation (3.13) yields $z(0) = (k_B T_2/\alpha)^{\frac{1}{2}}$. The dimensionless quantity is then $\tilde{z} = (\epsilon/\tilde{\alpha})^{\frac{1}{2}}$ thus depends on the parameters ϵ and $\tilde{\alpha}$.

Another popular numerical method for stochastic differential equations is the Heun method. For a more compact notation, set $F_2(\tilde{x}, \tilde{v}, \tilde{z}) = -\tilde{x}_i^3/(4\tilde{E}_b) + \tilde{x}_i + \tilde{z}_i - \tilde{\Gamma}_0 \tilde{v}_i$ and $F_3(\tilde{v}, \tilde{z}) = \tilde{v}_i/\tilde{\alpha} + \tilde{z}_i/(\tilde{\alpha}\tilde{\gamma})$. The solution of the differential equation system (3.16)−(3.18) in the Heun method is given by

$$\tilde{x}_{i+1} = \tilde{x}_i + \frac{\tilde{h}}{2}[\tilde{v}_i + \hat{v}_{i+1}] \tag{6.13}$$

$$\tilde{v}_{i+1} = \tilde{v}_i + \frac{\tilde{h}}{2}\left[F_2(\tilde{x}_i, \tilde{v}_i, \tilde{z}_i) + F_2(\hat{x}_{i+1}, \hat{v}_{i+1}, \hat{z}_{i+1})\right] + \sqrt{2_1\tilde{\Gamma}_0}\,\sqrt{\tilde{h}}\tilde{\eta} \tag{6.14}$$

$$\tilde{z}_{i+1} = \tilde{z}_i + \frac{\tilde{h}}{2}\left[F_3(\tilde{v}_i, \tilde{z}_i) + F_3(\hat{v}_{i+1}, \hat{z}_{i+1})\right] + \sqrt{\frac{2\epsilon}{\tilde{\gamma}\tilde{\alpha}^2}}\,\sqrt{\tilde{h}}\tilde{\zeta} \tag{6.15}$$

where the interpolation points $\hat{x}_{i+1}$, $\hat{v}_{i+1}$ and $\hat{z}_{i+1}$ at the endpoint of the interval $[t_i, t_{i+1}]$ are given by

$$\hat{x}_{i+1} = \tilde{x}_i + \tilde{h}\tilde{v}_i \tag{6.16}$$

$$\hat{v}_{i+1} = \tilde{v}_i + \tilde{h}F_2(\tilde{x}_i, \tilde{v}_i, \tilde{z}_i) + \sqrt{2\tilde{\Gamma}_0}\,\sqrt{\tilde{h}}\tilde{\eta} \tag{6.17}$$

$$\hat{z}_{i+1} = \tilde{z} + \tilde{h}F_3(\tilde{v}_i, \tilde{z}_i) + \sqrt{\frac{2\varepsilon}{\tilde{\gamma}\tilde{\alpha}^2}}\,\sqrt{\tilde{h}}\tilde{\zeta} \tag{6.18}$$

[8, p. 179]. In the equations (6.13)−(6.15) and (6.16)−(6.18) the same random numbers $\tilde{\eta}$ and $\tilde{\zeta}$ are used respectively. For the Heun method, the initial conditions $\tilde{x}_0$, $\tilde{v}_0$ and $\tilde{z}_0$ are chosen the same as for the Euler method.

6.1.2 Numerical equation for Smoluchovski's case

In the Smoluchovski's case, i.e. in the case of large friction, the differential equations (3.24) and (3.25) result. In the same way as in section 6.1.1, the equations are rewritten in differential form. The result is

$$dx_1 = \left(-\frac{1}{\Gamma_1}\frac{\partial U}{\partial x_1} + \nu_1 x_2\right)dt + \sqrt{\frac{2k_B T_1}{\Gamma_1}}\sqrt{dt}\tilde{\eta}_1 \tag{6.19}$$

$$dx_2 = \left(-\frac{\kappa_2}{\Gamma_2}x_2 + \nu_2 x_1\right)dt + \sqrt{\frac{2k_B T_2}{\Gamma_2}}\sqrt{dt}\tilde{\eta}_2 \tag{6.20}$$

where $\tilde{\eta}_1$ and $\tilde{\eta}_2$ are Gaussian random variables with mean $\mu = 0$ and variance $\sigma^2 = 1$. For the potential $U(x_1) = V(x_1) + x_1^2/(2\alpha)$ holds. Further, the potential V is given by equation (5.4). The physical quantities are de-dimensioned by equation (6.1). Finally, $x_1(t_i) = X_i$ and $x_2(t_i) = Y_i$ are set for easier notation and for a more compact representation $f_1(\tilde{X}_i, \tilde{Y}_i) = (-\tilde{X}_i^3/(4\tilde{E}_b) + (1 - 1/\tilde{\alpha})\tilde{X}_i + \tilde{Y}_i)/\tilde{\Gamma}_0$ and $f_2(\tilde{X}_i, \tilde{Y}_i) = \tilde{X}_i/(\tilde{\gamma}\tilde{\alpha}^2) - \tilde{Y}_i/(\tilde{\alpha}\tilde{\gamma})$. In the same way as

already discussed in section 6.1.1, the discrete Euler method is immediately obtained

$$\tilde{X}_{i+1} = f_1(\tilde{X}_i, \tilde{Y}_i)\tilde{h} + \sqrt{\frac{2}{\tilde{\Gamma}_0}}\sqrt{\tilde{h}}\tilde{\eta}_1 \tag{6.21}$$

$$\tilde{Y}_{i+1} = f_2(\tilde{X}_i, \tilde{Y}_i)\tilde{h} + \sqrt{\frac{2\epsilon}{\tilde{\gamma}\tilde{\alpha}^2}}\sqrt{\tilde{h}}\tilde{\eta}_2 \tag{6.22}$$

The initial value $\tilde{X}_0$ is freely selectable. For the auxiliary variable $x_2(t)$ $x_2(0) = (k_B T_2/\alpha)^{\frac{1}{2}}$ holds. Thus the initial value of the dimensionless auxiliary variable is given by $\tilde{Y}_0 = (\epsilon/\tilde{\alpha})^{\frac{1}{2}}$.

For comparison, the differential equations (3.24) and (3.25) shall also be solved using the Heun method. In dimensionless form, the Heun method is given by

$$\tilde{X}_{i+1} = \tilde{X}_i + \frac{\tilde{h}}{2}[f_1(\tilde{X}_i, \tilde{Y}_i) + f_1(\hat{X}_{i+1}, \hat{Y}_{i+1})] + \sqrt{\frac{2}{\tilde{\Gamma}_0}}\sqrt{\tilde{h}}\tilde{\eta}_1 \tag{6.23}$$

$$\tilde{Y}_{i+1} = \tilde{Y}_i + \frac{\tilde{h}}{2}[f_2(\tilde{X}_i, \tilde{Y}_i) + f_2(\hat{X}_{i+1}, \hat{Y}_{i+1})] + \sqrt{\frac{2\epsilon}{\tilde{\gamma}\tilde{\alpha}^2}}\sqrt{\tilde{h}}\tilde{\eta}_2 \tag{6.24}$$

where the interpolation points $\hat{X}_{i+1}$ and $\hat{Y}_{i+1}$ are calculated by

$$\hat{X}_{i+1} = \tilde{X}_i + \tilde{h} f_1(\tilde{X}_i, \tilde{Y}_i) + \sqrt{\frac{2}{\tilde{\Gamma}_0}}\sqrt{\tilde{h}}\tilde{\eta}_1 \tag{6.25}$$

$$\hat{Y}_{i+1} = \tilde{Y}_i + \tilde{h} f_2(\tilde{X}_i, \tilde{Y}_i) + \sqrt{\frac{2\epsilon}{\tilde{\gamma}\tilde{\alpha}^2}}\sqrt{\tilde{h}}\tilde{\eta}_2 \tag{6.26}$$

Analogous to the Euler method, the initial conditions $\tilde{X}_0$ can be chosen arbitrarily and for the initial condition of the auxiliary variable $\tilde{Y}_i = (\epsilon/\alpha)^{\frac{1}{2}}$ holds.

6.2 Numerical correlation functions

A single numerical solution of a stochastic differential equation alone does not have much significance, since only possible paths are calculated. The many possible paths must therefore be suitably summarised in a set of measured variables. Important measured variables are correlation functions and susceptibilities. In this section, the numerical calculations of the correlation functions $\mathrm{Cor}_{ij}(t,s)$ and $\mathrm{Cor}_{\Theta}(t,s)$ are presented. In the next section, the numerical calculation of the susceptibility is presented.

The correlation functions are determined in a stationary state. In the following we will always assume that a stationary distribution exists. The exact procedure will be briefly illustrated using the example of the correlation function $\mathrm{Cor}_{ij}(t,s)$ which is defined in equation (3.36). The fixed initial conditions $\tilde{X}_0$ and $\tilde{Y}_0 = (\epsilon/\alpha)^{\frac{1}{2}}$ are chosen. For the numerical calculation, the Heun method is used. Then the equations (6.23)−(6.26) are used to generate R paths for the random variables $\tilde{X}_i$ and $\tilde{Y}_i$. The index i indicates the current time t_i and therefore runs from 0 to N. If t_e is the total running time of a single path, N is given by $N = t_e/h$ where h is the discrete step size. If t_e is chosen only sufficiently large, there is an index n with $0 < n < N$ from which the random variables $\tilde{X}_i$ and $\tilde{Y}_i$ assume a stationary distribution. For times $t_i > t_n$, the system has a stationary distribution. The index n can be estimated by the following procedure: For two time points t_n and t_{n+m} which are far enough apart, i.e. $m \gg 1$, R realisations of the random variables $\tilde{X}_n$ and $\tilde{X}_{n+m}$ are generated. The realisations of the random variables $\tilde{X}_n$ and $\tilde{X}_{n+m}$ are plotted separately in a histogram. If the histograms are identical, the system is already in a stationary state at time t_n. Let $\tilde{X}_i^r$ be the r-th realisation of the random variable $\tilde{X}_i$ at time

t_i. Similarly, $\tilde{Y}_i^r$ denotes the r-th realisation of the random variable $\tilde{Y}_i$ at time t_i. Then the correlation function Cor_{11} can be numerically approximated by

$$\frac{\mathrm{Cor}_{11}(t_i,t_n)}{\xi_1^2} \approx K_{11}(t_i,t_n) = \frac{1}{R}\sum_{r=1}^{R}\tilde{X}_i^r\tilde{X}_n^r - \left(\frac{1}{R}\sum_{r=1}^{R}\tilde{X}_i^r\right)\left(\frac{1}{R}\sum_{r=1}^{R}\tilde{X}_n^r h\right) \tag{6.27}$$

where $i \geq n$. ξ_j is the length scalar of the variable x_j. In the case of the position x_1, ξ_1 is given by $\xi_1 = \xi_c$ and in the case of the auxiliary variable x_2, ξ_2 is given by $\xi_2 = m\xi_c\tau_c^{-2}$. The correlation functions Cor_{12}, Cor_{21} and Cor_{22} can be calculated in the same way.

The correlation function $\mathrm{Cor}_\Theta(t,s)$ which is defined in equation (4.41) can be numerically approximated analogous to the correlation function $\mathrm{Cor}_{ij}(t,s)$. With the step function $\Theta(\cdot)$ the numerical approximation yields

$$\mathrm{Cor}_\Theta(t_i - t_n) \approx \frac{\left(\sum_{r=1}^{R}\Theta(\tilde{X}_i^r)\Theta(\tilde{X}_n^r)\right) - \left(\sum_{r=1}^{R}\Theta(\tilde{X}_i^r)\right)\left(\sum_{r=1}^{R}\Theta(\tilde{X}_n^r)\right)}{\left(\sum_{r=1}^{R}\Theta(\tilde{X}_n^r)\right) - \left(\sum_{r=1}^{R}\Theta(\tilde{X}_n^r)\right)^2}. \tag{6.28}$$

6.3 Numerical susceptibilities

Another important parameter is the linear response of the system, i.e. the susceptibility $\chi(t)$. In this thesis we restrict ourselves to the linear response of the overdamped system. For this purpose, the equations of motion of the overdamped system are perturbed with a small external force $f(t)$. The concrete procedure is presented in section 3.3.2. In this work, two ways are used to numerically calculate the linear response of the overdamped system. Both variants are briefly presented in the following, whereby for both types a small constant external force $f = \mathrm{const}$ is assumed as disturbance.

The first possibility, which will always be referred to as the naive variant in the following, uses the definition of the linear response by the functional derivative [1], represented in equation (3.43). Let $\Delta x_i(t)$ be the difference between the perturbed solution and the unperturbed solution. For the susceptibility $\chi_i(t-s)$ with $t \geq s$ the relation is obtained

$$\langle \Delta x_i\rangle(t-s) = \int_0^{t-s}\chi_i(\tau)f(\tau)d\tau = f\int_0^{t-s}\chi_i(\tau)d\tau = f\chi_i'(t-s) \tag{6.29}$$

where the external force f can be pulled in front of the integral, since it is constant. The integrated susceptibility is denoted by χ_i'. The constant of proportionality between $\langle\Delta x_i\rangle$ and the external force f is thus the integrated susceptibility χ_i'. The procedure for the numerical determination of χ_i' is discussed using the Heun method. The Euler method follows analogously. The unperturbed equations of motion are given by (6.23)−(6.26). The perturbed equations of motion result from equations (6.23)−(6.26) by the substitution $f_1(\tilde{X}_i,\tilde{Y}_i) \to f_1(\tilde{X}_i,\tilde{Y}_i,f) = (-\tilde{X}_i^3/(4\tilde{E}_b) + (1-1/\tilde{\alpha})\tilde{X}_i + \tilde{Y}_i + f)/\tilde{\Gamma}_0$ where f in the function $f_1(\tilde{X}_i,\tilde{Y}_i,f)$ denotes the small external disturbance force. Now R paths of the perturbed equations of motion and R paths of the unperturbed equations of motion are generated, using the same sequence of stochastic forces η_1 and η_2 for the perturbed system and the unperturbed system. Let $\tilde{X}_j^r|_f$ be the r-th path of the perturbed system and $\tilde{X}_j^r|_0$ be the r-th path of the unperturbed system. Then the numerical average of $\langle\Delta x_1\rangle$ is calculated by

$$\frac{\langle\Delta x_1\rangle(t_j - t_n)}{\xi_1} \approx \overline{\Delta x_1} = \frac{1}{R}\sum_{r=1}^{R}(\tilde{X}_j^r|_f - \tilde{X}_j^r|_0). \tag{6.30}$$

[1] I am very grateful to Prof. Fuchs for the conversation in which he outlined this method to me.

As in section 6.2, t_n denotes a time at which the system is stationary. The constant force f is only switched on after the time t_n. So before time t_n the paths $\tilde{X}_j|_f$ and $\tilde{X}_j|_0$ are identical. The difference $\langle \Delta x_2 \rangle \approx \overline{\Delta x_2}$ can also be determined with the substitution $\tilde{X} \to \tilde{Y}$ by equation (6.30). For two small external forces f and f' with $f \gg f'$, the differences $\overline{\Delta x_i}|_f$ and $\overline{\Delta x_i}|_{f'}$ are calculated respectively. Applies to both forces

$$\frac{\overline{\Delta x_i}|_f}{f} = \frac{\overline{\Delta x_i}|_{f'}}{f'} = \chi_i' = \text{const.} \tag{6.31}$$

then the system is in the range of linear response and the integrated susceptibility is numerically calculated by

$$\chi_i'(t_j - t_n) = \frac{\xi_i \overline{\Delta x_i}}{f} \tag{6.32}$$

The susceptibility χ_i can be determined from the integrated susceptibility χ_i' by differentiating. However, since the numerical derivative of χ_i' is often very unstable, the susceptibility χ_i can only be determined well in a few cases.

The second variant to determine the linear response of the overdamped system follows the Malliavin Weight Sampling (MWS) method proposed by P. B. Warren and R. J. Allen [17]. The following section follows [18], where in [18] the calculation of the linear response for a general phase space variable A is performed. We restrict ourselves at this point to the position x_1 and the auxiliary variable x_2. For the MWS procedure, the differential form of the overdamped equation of motion (6.19) and (6.20) is used. In the equations (6.19) and (6.20) the substitution $dx_1 = x_1' - x_1$ and $dx_2 = x_2' - x_2$ is performed. Here x_1 denotes the position of the particle at time t and x_1' the position of the particle at time $t' = t + dt$. The same applies to the auxiliary variable x_2. The updating rule is then given by

$$x_1' = x_1 + f_1 dt + g_1 \sqrt{dt} \tilde{\eta}_1 \tag{6.33}$$

$$x_2' = x_2 + f_2 dt + g_2 \sqrt{dt} \tilde{\eta}_2 \tag{6.34}$$

where $f_1 = (-\partial_{x_1} U/\Gamma_0 + \nu_1 x_2 + f/\Gamma_1)$, $f_2 = (-\kappa_2 x_2/\Gamma_2 + \nu_2 x_1)$ and $g_i = (2k_B T_i/\Gamma_i)^{\frac{1}{2}}$ is set as an abbreviation. f in function f_1 denotes again the external small constant disturbance force. Let $p(x_1, x_2, t)$ be the probability that the system is in the state $(x_1, x_2)^\intercal$ at time t. The updated probability $p(x_1', x_2', t + dt)$ is given by

$$p(x_1', x_2', t + dt) = \int_{\mathbb{R}^2} dx_1 dx_2 W(x_1', x_2'|x_1, x_2) p(x_1, x_2, t) \tag{6.35}$$

where $W(x_1', x_2'|x_1, x_2)$ is the transition probability from the state $(x_1, x_2)^\intercal$ to the updated state $(x_1', x_2')^\intercal$. In the equations (6.33) and (6.34), the random variables $\tilde{\eta}_1$ and $\tilde{\eta}_2$ are gaussian distributed with mean $\mu = 0$ and variance $\sigma^2 = 1$. Thus the transition probability $W(x_1', x_2'|x_1, x_2)$ can be immediately given by

$$W(x_1', x_2'|x_1, x_2) = \frac{1}{Z} \exp\left(-\frac{(x_1' - x_1 - f_1 dt)^2}{2g_1^2} - \frac{(x_2' - x_2 - f_2 dt)^2}{2g_2^2} \right) \tag{6.36}$$

where Z is the normalisation. Now the Malliavin weight q is introduced. The infinitesimal change of the Malliavin weight is given by the relation

$$dq = \frac{\partial}{\partial f} \log(W(x_1', x_2'|x_1, x_2)). \tag{6.37}$$

Then, analogous to the equations (6.33) and (6.34), the updating rule of the Malliavin weights is determined by

$$q' = q + \frac{(x_1' - x_1 - f_1 dt)}{g_1^2} \frac{\partial f_1}{\partial f} dt = q + \frac{1}{\sqrt{2k_B T_1 \Gamma_1}} \sqrt{dt} \tilde{\eta}_1 \tag{6.38}$$

[18]. The key result in [17] is that the integrated susceptibility χ_i' can be calculated using the Malliavin weights. The integrated susceptibility is calculated with the MWS method by

$$\chi_i'(t_j - t_n) = \langle x_i q \rangle \tag{6.39}$$

where $x_i(t_j)$ is the solution of the unperturbed system at time t_j and q is the Malliavin weight at time t_j. In the time interval $[0, t_n]$ the solution x_i is is brought into a stationary state. In this time interval the Malliavin weights are kept constant $q = 0$. For times $t_j > t_n$, the Malliavin weights are updated using the prescription in (6.38). For the concrete implementation of the MWS procedure, the updating rule of the Malliavin weights has to be converted into a dimensionless form. The updating rule for the dimensionless Malliavin weight $\tilde{q}_j$ at time t_j is given by

$$\tilde{q}_{j+1} = \tilde{q}_j + \frac{1}{\sqrt{2\tilde{\Gamma}_0}} \sqrt{\tilde{h}} \tilde{\eta}_1 \tag{6.40}$$

For time points $t_j < t_n$, $\tilde{q}_j$ is always kept at zero. For time points $t_j > t_n$, the Malliavin weights $\tilde{q}_{j+1}$ are calculated by equation (6.40). The integrated susceptibility χ_1' is numerically given by

$$\frac{\chi_1'(t_j - t_n)}{\frac{\tau_c^2}{m}} \approx \frac{\overline{x_1 q_f} - (\overline{x_1})(\overline{q_f})}{\frac{\tau_c^2}{m}} = \frac{1}{R} \sum_{r=1}^{R} \tilde{X}_j^r \tilde{q}_j^r - \left(\frac{1}{R} \sum_{r=1}^{R} \tilde{X}_j^r \right) \left(\frac{1}{R} \sum_{r=1}^{R} \tilde{q}_j^r \right). \tag{6.41}$$

The susceptibility $\chi_2'(t_j - t_n)$ can also be calculated with equation (6.41). For this, only the substitutions $\tilde{X}_j \to \tilde{Y}_j$ and $\tau_c^2/m \to 1$ have to be carried out. t_n is a time at which the system is in a steady state. The additional term $(\overline{x_1})(\overline{q_f})$ is added to make the numerical simulation more stable. Since $\tilde{q}_j$ is a random walk, for infinitely long simulation runs $\overline{q} = 0$ and the additional term $(\overline{x_1})(\overline{q_f})$ vanishes. For finite simulation times, the additional term has the effect of attenuating the statistical error. The individual paths $\tilde{X}_j^r$ in equation (6.41) are calculated using the unperturbed equations (6.21) and (6.24). The r-th realisation of the Malliavin weights $\tilde{q}_j^r$ is calculated using equation (6.40). It is important to note that equation (6.21) and equation (6.41) use the same generated random number $\tilde{\eta}_1$. This makes the MWS method numerically very effective [17, 18].

7. Results and discussion

7.1 Numerical approximation for the Ornstein-Uhlenbeck process

The Ornstein-Uhlenbeck process has already been solved analytically for the overdamped case in sections 3.3 and 4.3. The probability distribution function $p(x_1, t|\boldsymbol{x}_0, t_0)$ can be calculated explicitly by equation (4.63). Furthermore, the correlation function and the susceptibility can be calculated for the Ornstein-Uhlenbeck process by equations (3.39) and (3.44).

Therefore, it is advisable to solve the Ornstein-Uhlenbeck process numerically in order to be able to estimate the validity of later numerical results. For this purpose, the potential is defined by $V(x_1) = \omega_b^2 x_1^2/2$. The Ornstein Uhlenbeck process will be solved with the Heun procedure. The relevant equations are (6.23)−(6.26). Because of the quadratic potential $V(x_1)$, the substitution $f_1 \to f_1(\tilde{X}_i, \tilde{Y}_i) = (-(1 + 1/\tilde{\alpha})\tilde{X}_i + \tilde{Y}_i)/\tilde{\Gamma}_0$ must be carried out for equations (6.23)−(6.26).

The dimensionless parameters of the model are set to $\tilde{\alpha} = 1$, $\tilde{\gamma} = \tilde{\Gamma}_0 = 4$, $\tilde{E}_b = 5$ and $\epsilon = 2$. The initial values are set by $\tilde{X}_0 = 0$ and $\tilde{Y}_0 = (\epsilon/\tilde{\alpha})^{\frac{1}{2}}$. The step size is set to $\tilde{h} = 0.01$. The values of the parameters remain fixed for the entire section 7.1. In the following, the analytical probability distribution function $p(x_1, t|\boldsymbol{x}_0, t_0)$ is compared with the numerical one. In the same way, for the corrlation function and the susceptibility, the analytical solution is compared with the numerical one.

First, probability distribution functions are generated numerically for the times $t = 1\,\tau_c$, $t = 10\,\tau_c$ and $t = 100\,\tau_c$. For this, 10^5 paths are generated in the time interval $[0, 100\,\tau_c]$ with equations (6.23)−(6.26). The positions $x_1(t)$ yielded at the time points $t = 1\,\tau_c$, $t = 10\,\tau_c$ and $t = 100\,\tau_c$ are shown as histograms in each case. In Figure 7.1 the generated histograms are shown as dashed curves normalised to 1.

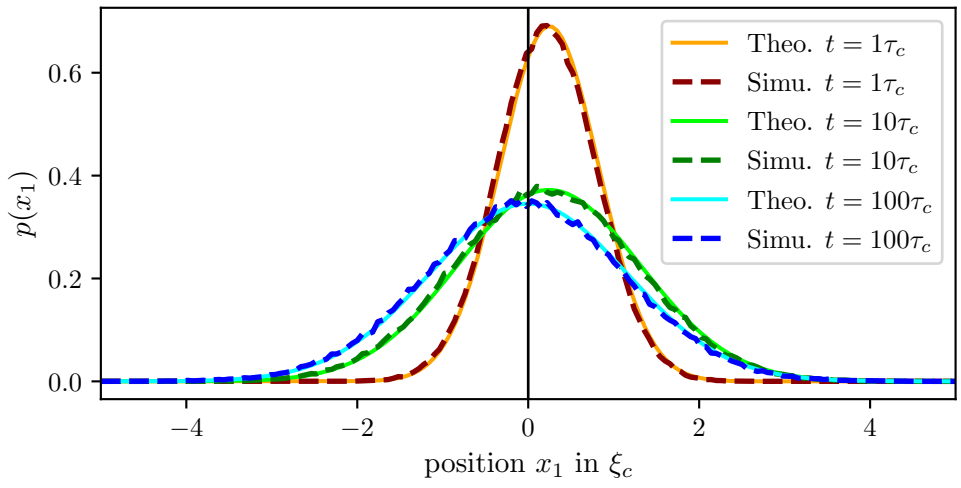

Figure 7.1: The dashed lines are the simulated probability distribution functions $p(x_1, t|\boldsymbol{x}_0, t_0)$ of the Ornstein Uhlenbeck process for times $t = 1\,\tau_c$, $t = 10\,\tau_c$ and $t = 100\,\tau_c$. The solid lines are the analytical solutions calculated by equation (4.63).

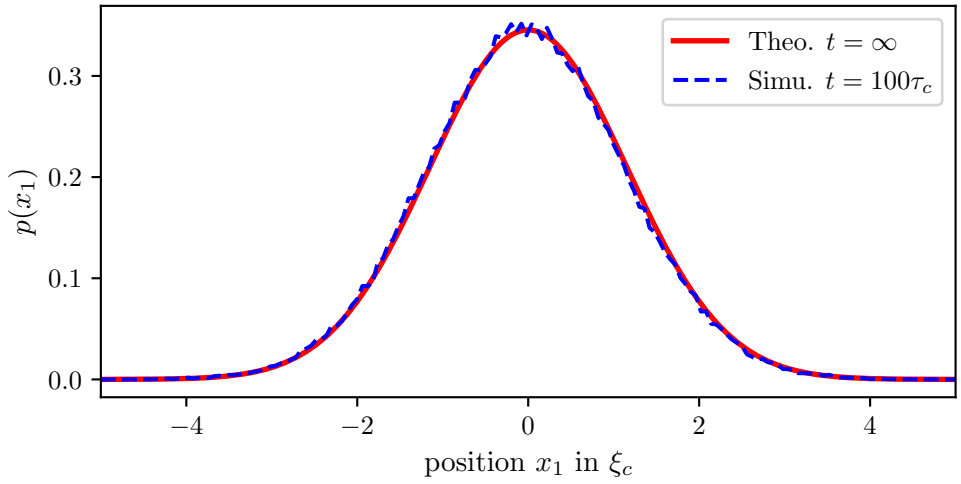

Figure 7.2: Numerical distribution functions $p(x_1, t|\boldsymbol{x}_0, t_0 = 0)$ for time $t = 100\,\tau_c$ and analytical distribution function for $t = \infty$. Since both curves lie on top of each other, the statement is justified that for times $t \geq 100\,\tau_c$ the distribution is stationary.

Figure 7.1 also shows the analytical solutions as solid lines. For all times $t = 1\,\tau_c$, $t = 10\,\tau_c$ and $t = 100\,\tau_c$ the values from the simulation agree very well with the analytical solution.

If the histograms for the times $t = 1\,\tau_c$, $t = 10\,\tau_c$ and $t = 100\,\tau_c$ are compared with each other, it can be clearly seen how the probability distribution function $p(x_1, t|\boldsymbol{x}_0, t_0)$ relaxes into a stationary distribution $p^{st}(x_1)$. The histogram for the time $t = 100\,\tau_c$ is already very close to the stationary distribution. To illustrate this fact, in Figure 7.2 the histogram for $t = 100\,\tau_c$ is shown as a blue dashed line and the analytical distribution function for $t = \infty$ is shown as a red solid line. Since both histograms in Figure 7.2 agree very well, the statement is justified that already for $t = 100\,\tau_c$ the stationary distribution $p^{st}(x_1)$ is assumed in a very good approximation.

Because of the initial conditions $\tilde{X}_0 = 0$ and $\tilde{Y}_0 = (\epsilon/\tilde{\alpha})^{\frac{1}{2}}$, in Figure 7.1 the maximum of the distribution at time $t = 1\tau_c$ is still to the right of the origin $x_1 = 0$. With an increase in time $t \geq 1\,\tau_c$, the position of the maximum relaxes to the origin $x_1 = 0$. The stationary distribution is thus independent of the initial values and since the quadratic potential is symmetrical to the origin, the stationary distribution must also be symmetrical to the origin. The symmetry of the

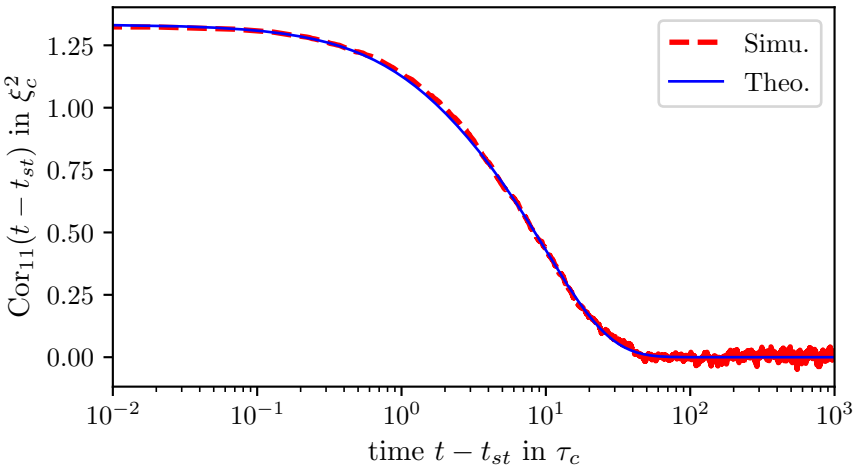

Figure 7.3: The red dashed line shows the numerical solution of the correlation function $\mathrm{Cor}_{11}(t - t_{st})$ for the parameters $\tilde{\alpha} = 1$, $\tilde{\gamma} = \tilde{\Gamma}_0 = 4$, $\tilde{E}_b = 5$ and $\epsilon = 2$. The blue solid line shows the analytical solution given by equation (3.39). The time t_{st} was set to $t_{st} = 100\,\tau_c$.

stationary distribution is an important property that will be used later to evaluate the quality of the stationary distribution for the double well potential.

Second, the correlation function Cor_{11} is calculated numerically. As described in section 6.2, the correlation function is determined in a stationary state. According to Figure 7.2, the system is very close to a stationary state for time $t = 100\,\tau_c$. Therefore, $t_{st} = t_n = 100\,\tau_c$ is chosen as the time at which the system has a stationary distribution. The correlation function $\mathrm{Cor}_{11}(t - t_{st})$ is determined numerically with equation (6.27) where the number of realisations is set to $R = 10^4$. The free initial value is again set to $\tilde{X}_0 = 0$. The numerical correlation function is shown as a red dashed line in Figure 7.3. The analytical solution can be calculated by equation (3.39). In figure 7.3, the analytical solution is shown as a blue solid line. It can be clearly seen that the numerical solution for $\mathrm{Cor}_{11}(t - t_{st})$ agrees well with the analytical solution.

Finally, the integrated susceptibility χ_1' is calculated numerically using the naive method and the MWS method. Both methods are described in detail in section 6.3.

In the naive method, for two small external disturbance forces $f^{(1)}$ and $f^{(2)}$, the integrated susceptibility is calculated according to equation (6.32), respectively. The number R of realisations is set to $R = 10^4$ and the stationary time to $t_{st} = 100\,\tau_c$. The values of the external forces are set to $\tilde{f}^{(1)} = 0.25$ and $\tilde{f}^{(2)} = 0.016$. In figure 7.4 (a), the susceptibility calculated with the perturbing force $\tilde{f}^{(1)}$ is shown as a dark green line, the light green dashed line shows the susceptibility with the perturbing force $\tilde{f}^{(2)}$. Since the integrated susceptibilities lie very well on top of each other for both disturbance forces, the system is in the range of the linear response. Using the naive method, the numerical solution of the integrated susceptibility $\chi'(t - t_{st})$ is given by the dark green and light green curves in Figure 7.4 (a). In figure 7.4 (b) the analytical solution, calculated by equation (3.45), is shown as a blue solid line. For comparison, the susceptibility with the perturbative force $\tilde{f}^{(2)}$ is also shown. For the naive method, the analytical and the numerical solution agree perfectly.

For the MWS method, the integrated susceptibility $\chi_1'(t - t_{st})$ is calculated with equation (6.41). The MWS method gives good results when the number R of realisations is large. Therefore, in Figure 7.5 the integrated susceptibility $\chi_1'(t - t_{st})$ is shown as a light green curve for the number $R = 10^4$, as a blue curve for $R = 16 \cdot 10^4$ and as an orange curve for $R = 64 \cdot 10^4$. In addi-

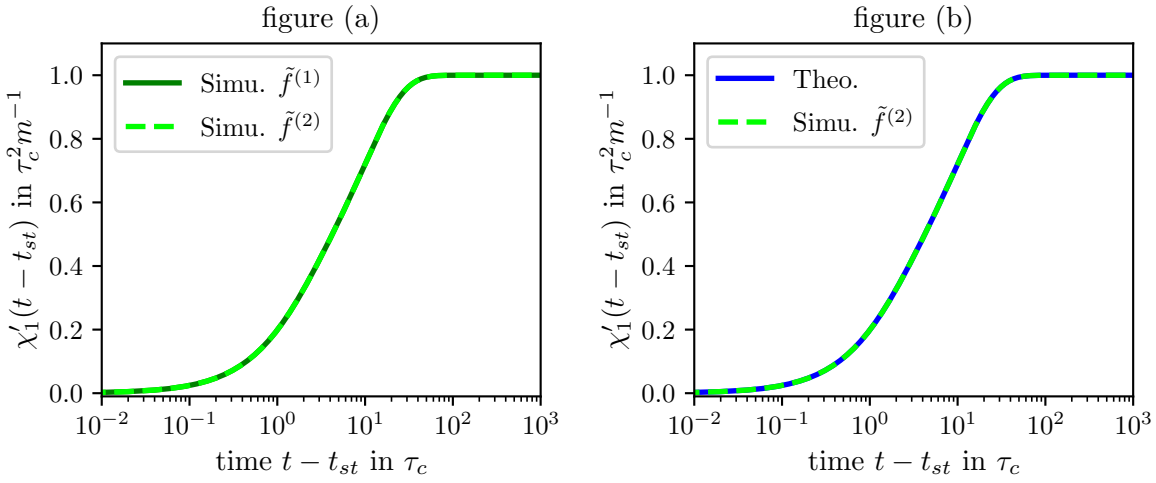

Figure 7.4: In figure (a), the integrated susceptibility calculated with the disturbance force $\tilde{f}^{(1)}$ is shown as a dark green line. The light green dashed line shows the susceptibility with the disturbance force $\tilde{f}^{(2)}$. Since both curves lie on top of each other, the system is in the range of linear response. The numerical solution with the naive method is thus given by the dark green and light green curves. In figure (b) the numerical solution, with the disturbance force $\tilde{f}^{(2)}$, and the analytical solution are shown together for comparison purposes. The analytical solution is calculated with equation (3.45).

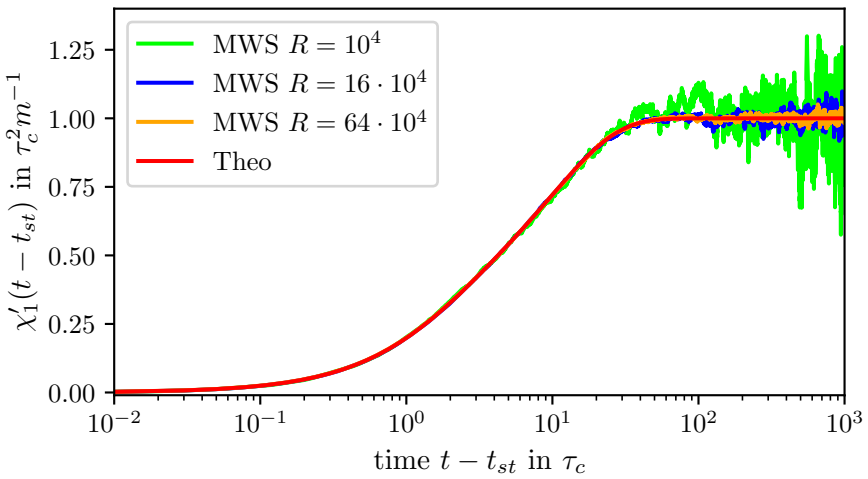

Figure 7.5: The stationary time is set to $t_{st} = 100\,\tau_c$. The light green curve shows the integrated susceptibility $\chi_1'(t - t_{st})$ for number $R = 10^4$, the blue curve shows the susceptibility for $R = 16 \cdot 10^4$ and the orange curve shows $\chi_1'(t - t_{st})$ for the realisations $R = 64 \cdot 10^4$. From a time difference $t - t_{st} \geq 0$ the susceptibility reaches a saturation value. As R increases, the statistical error decreases. For comparison, the analytical solution is shown as a red line.

tion, the analytical solution, which is again calculated by equation (3.45), is shown as a red curve in Figure 7.5. For the number $R = 10^4$, the numerical solution still deviates relatively strongly from the analytical solution. For the time difference $t - t_{st} \geq 200\,\tau_c$ the numerical solution oscillates strongly around the analytical value. However, the oscillations are quite unproblematic since the time average of the oscillations is 0.987, which is very close to the analytical value 1. A somewhat more severe deviation occurs in the time interval $20\tau_c \leq t - t_{st} \leq 100\,\tau_c$. In this time interval, the deviations do not average out. If one needs a better numerical value of $\chi_1'(t - t_{st})$ in this time interval, the number of realisations must be increased. For the number $R = 16 \cdot 10^4$ the statistical error is already very small compared to the number $R = 10^4$. A further improvement can be achieved by the number $R = 64 \cdot 10^4$. For increasing number R, however, longer and longer simulation times result. Therefore, only the values $R = 10^4$ and $R = 10^5$ are chosen for the number R in this thesis. The step size is set to $h = 0,01\,\tau_c$ for all other sections.

7.2 Rectification of the equilibrium

The numerical calculation of correlation functions and susceptibilities is always carried out in a stationary distribution of the system. It is therefore very important to know the time t_{st} at which the system has a stationary distribution. In this section, the stationary time t_{st} for the double well potential is estimated by numerical methods. The energy barrier is set to $\tilde{E}_b = 5$ and $\epsilon = 2$ is chosen for the second heat bath.

The dimensionless friction $\tilde{\Gamma}_0$ is varied in the interval $[1, 10]$ for this entire thesis. The influence of the second heat bath with temperature T_2 is determined by the parameter α. If $\alpha \to 0$, the second heat bath dominates. If, on the other hand, $\alpha \to \infty$ applies, the influence of the second heat bath disappears and the first heat bath dominates. For the entire numerical calculations $\tilde{\alpha}$ is varied in the interval $[0.25, 150]$. The last characteristic quantity of the model of Ilg and Barrat is the decay constant $\alpha\gamma$ of the memory kernel in equation (3.6). The decay constant $\tilde{\alpha}\tilde{\gamma}$ is varied in the interval $[0.1, 10]$.

The determination of the stationary time t_{st} is discussed in detail using the parameters $\tilde{\Gamma}_0 = 1$, $\tilde{\alpha} = 0.25$ and $\tilde{\alpha}\tilde{\gamma} = 0.1$ as examples. Using the equations (6.23)−(6.26), three histograms with waiting times $t = 10^2\,\tau_c$, $t = 10^3\,\tau_c$ and $t = 10^4\,\tau_c$ are generated. The number R of realisations

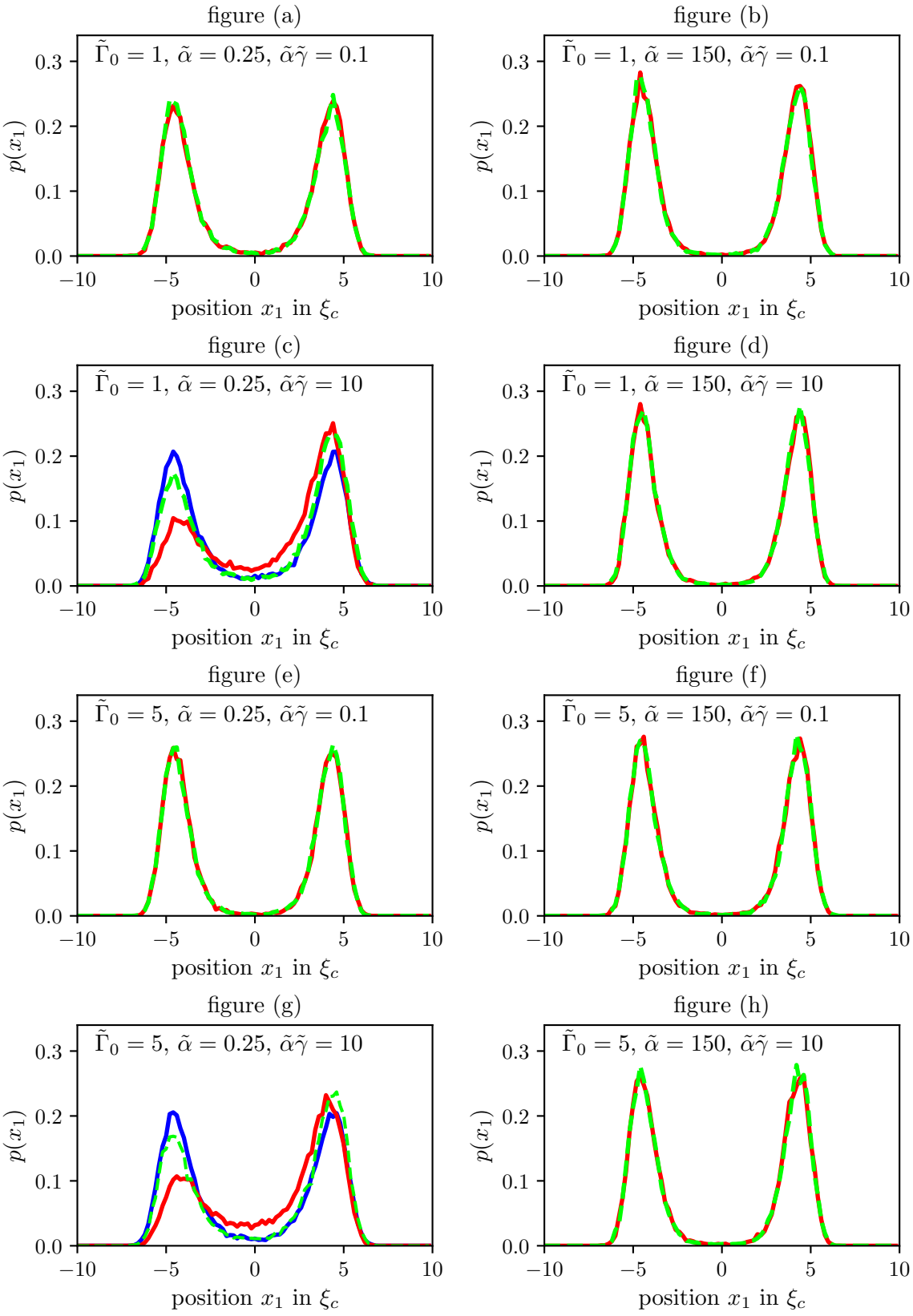

Figure 7.6: In figures (a)−(h), the parameters $\tilde{\Gamma}_0$, $\tilde{\alpha}$ and $\tilde{\alpha}\tilde{\gamma}$ are varied respectively. The light green dashed curves are the histograms for the waiting time $t = 10^2\,\tau_c$, the red solid curves are the histograms for the times $t = 10^3\,\tau_c$ and the blue solid lines show the histograms for $t = 10^4\,\tau_c$.

is set to $R = 10^4$. For the starting position $\tilde{X}_0$ the minima of the double well potential are chosen, which lie at $\pm 2\sqrt{E_b}/\omega_b$. Which minimum is chosen as the starting position is decided randomly with probability 0.5 in each case. As a result, the system relaxes more quickly into into a stationary state. The histogram for the waiting time $t = 10^2 \tau_c$ is shown in Figure 7.6 (a) as a light green dashed line. The histogram for $t = 10^3\,\tau_c$ is shown as a red solid line. The two histograms agree very well. The histogram for the waiting time $t = 10^4\,\tau_c$ is omitted for clarity if the distributions are already identical for $t = 10^2\,\tau_c$ and $t = 10^3\,\tau_c$. Since the system is already relaxed into the stationary distribution at time $t = 10^2\,\tau_c$, the stationary time $t_{st} = 10^2\,\tau_c$ can be chosen for the parameters $\tilde{\Gamma}_0 = 1$, $\tilde{\alpha} = 0.25$ and $\tilde{\alpha}\tilde{\gamma} = 0.1$. Since the double well potential in equation (5.4) is symmetrical to the origin $x_1 = 0$, the stationary distribution must have the same symmetry. The symmetry criterion is quite well satisfied in Figure 7.6 (a).

The same colour code applies to all histograms in the figures 7.6 and 7.7. The green dashed line is always the histogram for the waiting time $t = 10^2\,\tau_c$, the red solid line always denotes the histogram for the time $t = 10^3\,\tau_c$ and the blue solid line corresponds to the waiting time $t = 10^4\,\tau_c$.

Figure 7.6 (b) shows the first two histograms for the parameters $\tilde{\Gamma}_0 = 1$, $\tilde{\alpha} = 150$ and $\tilde{\alpha}\tilde{\gamma} = 0.1$. Also with this choice of parameters, the stationary time can be set to $t_{st} = 10^2\,\tau_c$. If we now fix $\tilde{\Gamma}_0 = 1$ and $\tilde{\alpha}\tilde{\gamma} = 0.1$ and vary $\tilde{\alpha}$ in the interval $[0.25, 150]$, we can reasonably assume that for all values $\tilde{\alpha} \in [0.25, 150]$ the stationary time is $t_{st} = 10^2\,\tau_c$.

Figure 7.6 (c) gives a new behaviour compared to figures (a) and (b). In figure (c) the parameters $\tilde{\Gamma}_0 = 1$, $\tilde{\alpha} = 0.25$ and $\tilde{\alpha}\tilde{\gamma} = 10$ are chosen. For this choice of parameters, even the

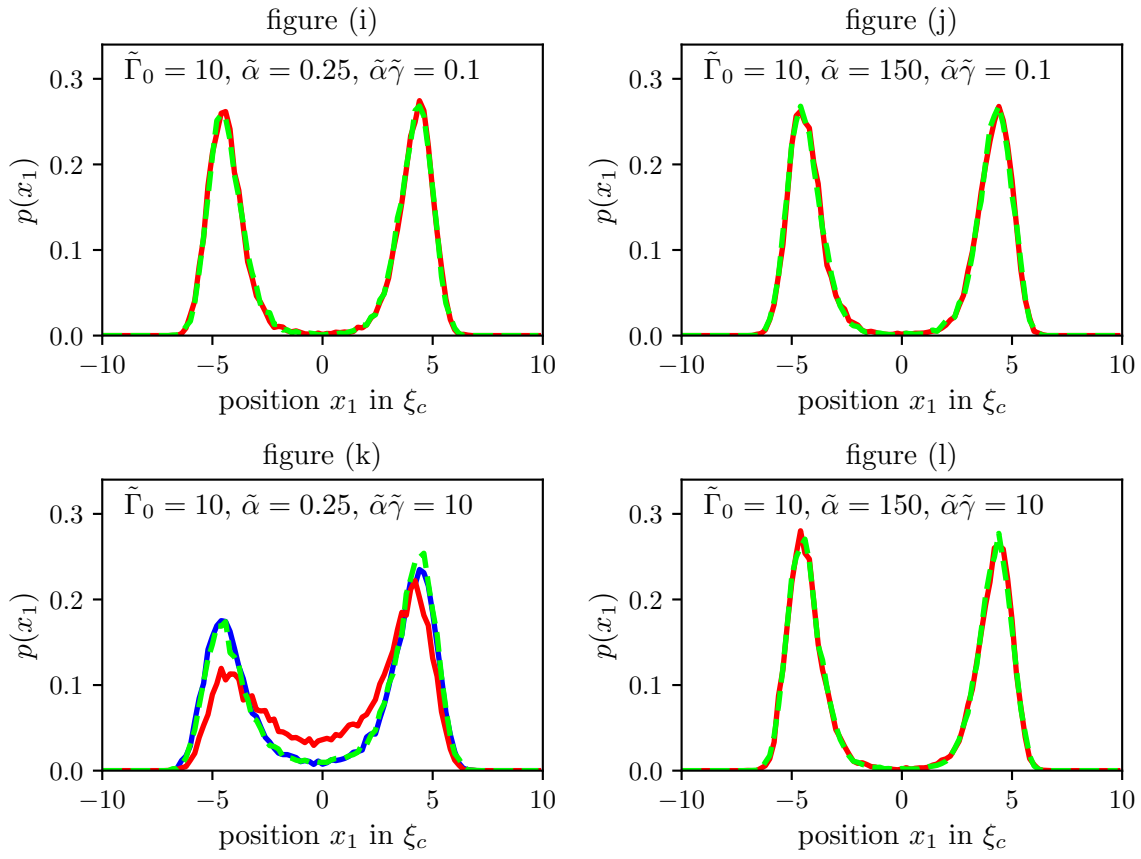

Figure 7.7: In figures (i)−(l), respectively, the parameters $\tilde{\alpha}$ and $\tilde{\alpha}\tilde{\gamma}$ are varied and the coefficient of friction is fixed $\tilde{\Gamma}_0 = 10$. The light green dashed curves are the histograms for the waiting time $t = 10^2\,\tau_c$, the red solid curves are the histograms for the times $t = 10^3\,\tau_c$ and the blue solid lines show the histograms for $t = 10^4\,\tau_c$.

histograms with waiting times $t = 10^3\,\tau_c$ and $t = 10^4\,\tau_c$ are not identical. With large memory effects, the system therefore takes a very long time to become stationary. To save computing time, the symmetry criterion is used. For the waiting times $t = 10^2\,\tau_c$ and $t = 10^3\,\tau_c$ the histograms are not symmetrical to the origin $x_1 = 0$. However, the histograms slowly relax into a symmetrical distribution. The histogram for $t = 10^4\,\tau_c$ then has the symmetry expected for a stationary distribution. Therefore, for figure (c) the stationary time $t_{st} = 10^4\,\tau_c$ is used.

In the figures 7.6 (e)−(h) the same histograms for the friction coefficient $\tilde{\Gamma}_0 = 5$ are shown. The case for the friction coefficient $\tilde{\Gamma}_0 = 1$ differs only very slightly from the case for the friction coefficient $\tilde{\Gamma}_0 = 5$. Thus, for small memory effects, a stationary time of $t_{st} = 10^2\,\tau_c$ is sufficient. Small memory effects correspond to the choice $\tilde{\alpha} \approx 150$ or $\tilde{\alpha}\tilde{\gamma} \approx 0.1$. If $\tilde{\Gamma}_0$ is in the range between 1 and 5 and strong memory effects are investigated, i.e. $\tilde{\alpha}\tilde{\gamma} \approx 10$, the stationary time must be set to $t_{st} = 10^4\,\tau_c$.

A slightly different behaviour results in the figures 7.7 (i)−(l). For these figures, the friction coefficient is set to $\tilde{\Gamma}_0 = 10$. The choice of the other parameters is as in the previous figures. For strong memory effects, i.e. Figure 7.7 (k), all three histograms do not have the necessary symmetry for a stationary distribution. The stationary time is thus presumably at least $t_{st} = 10^5\,\tau_c$. Since the stationary time $t_{eq} = 10^5\,\tau_c$ is extremely high, strong memory effects are only investigated for friction coefficients $\tilde{\Gamma}_0 \in [0, 5]$ in this thesis.

Other works, such as the project practical by M. Gruber, set the stationary time $t_{st} = 0$ and randomly select starting points $\tilde{X}_0$, where the distribution of the starting values is given by a Boltzmann distribution of the form $\exp(-V(x)/(k_B T)$ [15]. This procedure saves enormous computational time, since the entire iteration steps up to the time t_{st} are omitted. However, this procedure is not applicable for the model of Ilg and Barrat with the two heat baths, since the thermal energy $k_B T$ would have to be known a priori.

7.3 Validity range of the overdamped case

The overdamped equations of motion (3.24) and (3.25) are only valid for large damping. The case of large damping is also referred to as Smoluchovski's case in this thesis. The equations (3.24) and (3.25) make no statements about how large Γ_1 and α must be chosen so that the Smoluchovski's case exists. The case for arbitrary friction is also called Kramers' case after section 3.2.1.

In order to be able to compare Kramers' case with Smoluchovski's case, the reaction rate Υ is chosen as the measurand. According to section 4.2.2, the reaction rate Υ can be calculated by equation (4.45). For both cases, the correlation function $\mathrm{Cor}_\Theta(t - t_{st})$ is solved numerically with equation (6.28). The classical case is investigated first, where the influence of the second heat bath disappears. Therefore, the parameters $\tilde{\alpha} = 10^4$ and $\tilde{\alpha}\tilde{\gamma} = 0.1$ are chosen. The step size is again set to $h = 0.01\,\tau_c$ and the number of realisations is $R = 10^4$. The energy barrier is set to $\tilde{E}_b = 5$ and $\epsilon = 1$ is chosen for the second heat bath. For vanishing memory effects, according to section 7.2, it is sufficient to choose a stationary time of $t_{st} = 10^2\,\tau_c$. The numerical solution of Kramers' case is carried out with the Euler method given by the equations (6.10)−(6.12), and the Heun method which is given by the equations (6.13)−(6.18). The numerical solution of Smoluchovski's case is also determined using Euler's method given by the equations (6.21) and (6.22), and Heun's method which is given by the equations (6.23)−(6.26). As described in section 4.2.2, equation (4.45) is used to determine the reaction rate Υ as a fit parameter. Figure 7.8 shows the reaction rate Υ as a function of the friction coefficient Γ_0. The reaction rates calculated with the Euler method are shown in figure 7.8 (a), the reaction rates calculated with the Heun method are shown in figure (b).

For the Smoluchovski's case, the numerically determined reaction rates are shown as blue stars in figures (a) and (b). In this case, the reaction rates in figures (a) and (b) are identical. In the Smoluchovski's case, the reaction rate can be calculated analytically exactly with equation

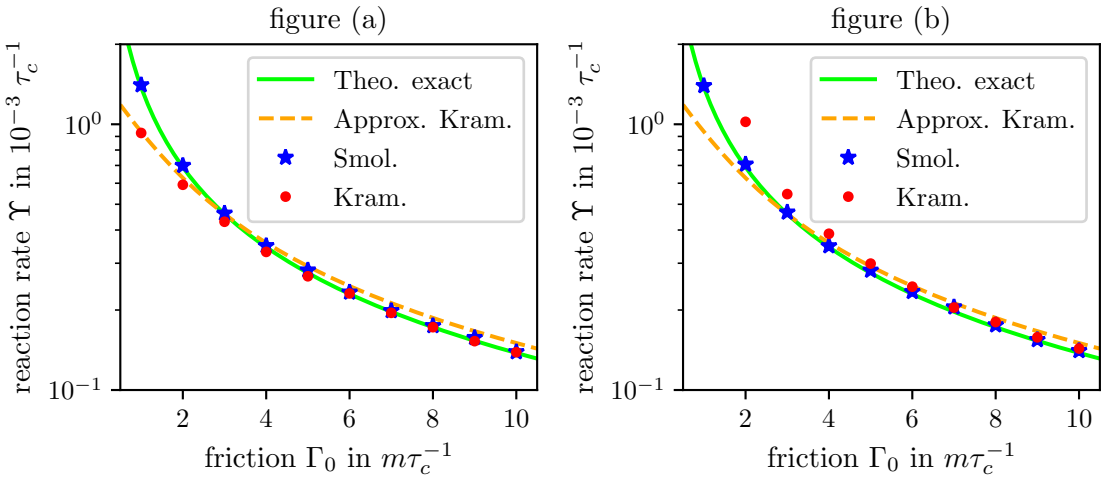

Figure 7.8: Figure (a) shows the numerically calculated reaction rates with the Euler method. Figure (b) shows the numerically calculated reaction rates with the Heun method. The blue stars in both figures show the numerically calculated reaction rates for the Smoluchovski's case. The red dots show the numerical results for the Kramers' case. The light green curve is the exact analytical solution for the Smoluchovski's case which is calculated with equation (4.33). The orange dashed line is the Kramers' analytical approximate solution for medium to strong friction which is calculated with equation (4.39).

(4.33). The exact analytical solution is shown in figures 7.8 (a) and (b) as a light green solid line. In addition, Kramers' analytical approximation, which is given in equation (4.39), is shown as an orange dashed line in both figures. Kramers' approximation is valid for medium to large damping. The exact analytical solution agrees very well with the numerically determined reaction rates for the Smoluchovski case. Kramers' analytical approximation still differs somewhat from the exact solution for large friction. However, Kramers' approximation becomes better and better when the energy barrier $E_b \gg k_B T$ is increased. For friction coefficients $\tilde{\Gamma}_0 \geq 3$, the Smoluchovski's case and the Kramer's case always coincide.

In Kramers' case, the numerically calculated reaction rates are shown as red dots in Figure 7.8. Obviously, in figures (a) and (b) the reaction rates in Kramers' case do not match. For decreasing friction $\Gamma_0 \to 0$, the reaction rate for the Karmers' case falls below the analytically exact curve in the Euler method. With the Heun method, on the other hand, the reaction rate for the Kramers' case rises above the analytically exact curve as the friction $\Gamma_0 \to 0$ decreases. In figure (a), the orange dashed curve agrees very well with the red dots in the region $\tilde{\Gamma}_0 \in [1, 3]$. In figure (b) this is not the case in the range $\tilde{\Gamma}_0 \in [1, 3]$. So the Euler method seems to be better for the Kramers' case. For the Smoluchovski's case, the Euler method and the Heun method work equally well. From Figure 7.8 (a) it can now be read that from a friction coefficient $\tilde{\Gamma}_0 \geq 3$ the Smoluchovski's case is valid.

In figure 7.8 only the classical case is considered where no memory effects occur because $\tilde{\alpha} = 10^4$ and $\tilde{\alpha}\tilde{\gamma} = 0.1$ was set. If the memory kernel $\Gamma(t)$ is added to the motion, it is apriori not clear whether for $\tilde{\Gamma}_0 \geq 3$ the Smoluchovski's case coincides with the Kramers' case. Therefore, in Figure 7.9, for the parameters $\tilde{\alpha} = 0.25$ and $\tilde{\alpha}\tilde{\gamma} = 10.0$, the reaction rate Υ is shown as a function of the friction coefficient Γ_0. The choice of the parameters $\tilde{\alpha} = 0.25$ and $\tilde{\alpha}\tilde{\gamma} = 10.0$ corresponds to the case of large memory effects. Comparing the Kramers' case with the Smoluchovski's case in Figure 7.9, for large memory effects both cases coincide for $\tilde{\Gamma}_0 \geq 1$. Thus, for friction coefficients $G \geq 3$, the Smoluchovski's case agrees reliably with the Kramers' case.

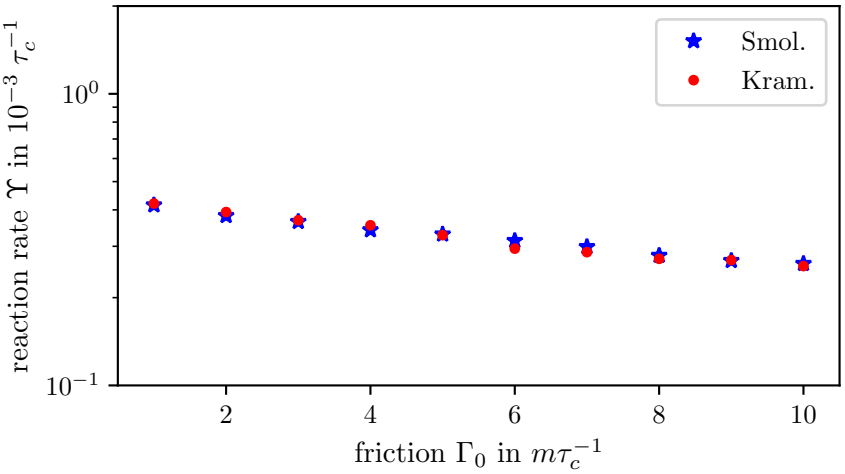

Figure 7.9: Numerically calculated reaction rates depending on the friction coefficient Γ_0 for the parameter choices $\tilde{\alpha} = 0.25$ and $\tilde{\alpha}\tilde{\gamma} = 10.0$. The blue stars are the numerically calculated reaction rates for the Smoluchovski's case. The red dots show the numerical results for the Kramers' case. For the friction coefficient $\Gamma_0 \geq 1$ both cases agree in a good approximation.

7.4 Effective temperatures in simulations

In chapter 5 three possible effective temperatures are defined. These definitions are numerically verified and discussed in this section.

7.4.1 Effective temperature with the canonical distribution

In this subsection, the analytical approximation $T_{\text{eff},3a}$ for the double well potential according to equation (5.6) is numerically verified. The coefficient α takes the values $\tilde{\alpha} \in \{y | y = 0.25 \cdot 2^i, i \in \{0, 1, ..., 9\}\}$. For the decay constant $\alpha\gamma$, $\tilde{\alpha}\tilde{\gamma} \in \{0.1, 1, 10\}$ holds. The friction coefficient is set constant to $\Gamma_1 = 4$, the energy barrier is $\tilde{E}_b = 5$ and the second heat bath is kept at temperature $T_2 = 2\,T_1$. For all combinations of the parameters α and $\alpha\gamma$, stationary distributions are determined as in section 7.2. Since very large memory effects also occur with the combination of all parameters, $t_{st} = 10^4\,\tau_c$ is always chosen as waiting time. According to section 7.2, it can be ensured for the waiting time $t_{st} = 10^4\,\tau_c$ that all calculated distributions are stationary. A typical stationary distribution is shown as a blue line in Figure 5.2. As described in section 5.1, the effective temperature $T_{\text{eff},3}$ can be determined from the numerically determined distributions with a fit function of the form $f(x_1) = a\exp(-V_4(x_1)/b)$ by the fit parameter b.

In figure 7.10 the effective temperature $k_B T_{\text{eff},3}$ in units of $k_B T_1$ is plotted as a function of the coefficient α. The points are the numerically determined effective temperatures for the double well potential. For the decay constant $\tilde{\alpha}\tilde{\gamma} = 0.1$, the effective temperature as a function of α is shown as red dots. The analytical approximate solution from equation (5.6) is drawn as an orange solid line. For the decay constant $\tilde{\alpha}\tilde{\gamma} = 1$, the effective temperature is shown as dark green dots. The analytical approximation is given by the light green solid line. For the decay constant $\tilde{\alpha}\tilde{\gamma} = 10$, the effective temperature is shown as dark blue dots. The analytical solution is given by the light blue solid line. The uncertainties $u[T_{\text{eff},3}]$ for the numerically calculated effective temperatures are $u[T_{\text{eff},3}] \leq 0.01\,k_B T_1$ and can hardly be shown in Figure 7.10. For all three decay constants, it is noticeable that the numerical solution agrees very well with the analytical approximation given by equation (5.6). The effective temperature for the double well potential thus depends mainly on the curvature of the potential minima.

This fact could be an indication of a meaningful definition for an effective temperature, since the double well potential is only a model potential and the exact potential of the system is often

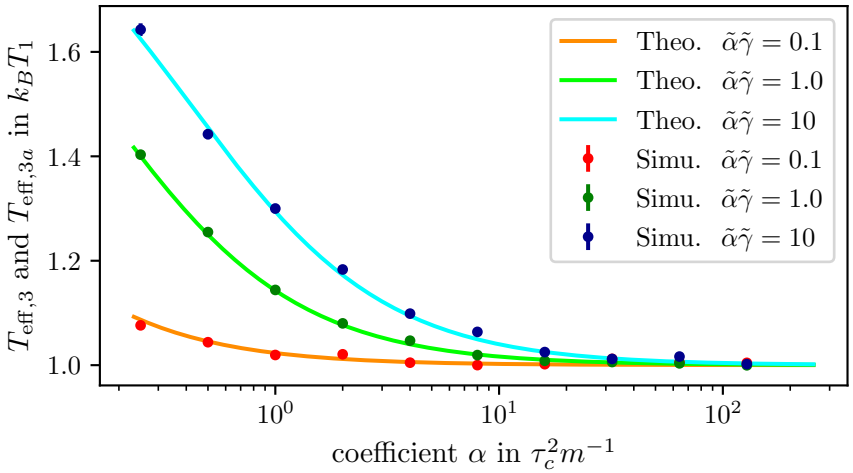

Figure 7.10: For the three decay constants $\tilde{\alpha}\tilde{\gamma} = 0.1$, $\tilde{\alpha}\tilde{\gamma} = 1$ and $\tilde{\alpha}\tilde{\gamma} = 10$ three effective temperature curves are shown depending on the parameter α. The dots denote the numerically determined effective temperatures. The solid lines are the analytical approximate solutions which are calculated with equation (5.6).

not known a priori. However, since the effective temperature depends to a good approximation only on the curvature of the minimum, the exact model form of a meta stable potential does not affect the effective temperature of the system. The effective temperature depends only on the approximate character of the system, i.e. whether it is a meta-stable potential or not, and does not vary too much with the exact potential form. The problem with this argument is that the calculation of the effective temperature for an asymmetric potential is not clear. Since one cannot say a priori how much which minimum contributes to the effective temperature for an asymmetric potential, this argument should be treated with caution.

For $\tilde{\alpha} < 0.25$ it becomes increasingly difficult to numerically generate a stationary probability distribution. For the limit $\alpha \to 0$ one therefore has to rely on analytical approximations. Figure 5.1 (a) shows the same analytical solution as in Figure 7.10 but for the range $\tilde{\alpha} \in [10^{-5}, 10^4]$. For the limit $\alpha \to 0$ the effective temperature is $T_{\text{eff},3} = T_2$ which was also to be expected since the second heat bath dominates for this limit.

7.4.2 Effective temperature with the FDT

In this subsection, the effective temperature defined by the FDT in equation (5.9) is determined numerically for the double well potential. For the dimensionless parameters $\tilde{E}_b = 5$, $\tilde{\Gamma}_0 = 4$ and $\epsilon = 2$ are set. Numerically, the correlation function is determined by equation (6.27), where the number of realisations is set to $R = 10^4$. The integrated susceptibility $\chi_i'(t - t_{st})$ can be determined numerically according to section 6.3 in two ways.

In the naive method, the susceptibility is calculated with equation (6.32), where R is set to $R = 10^4$. For this, the equations of motion are perturbed with the external force $\tilde{f}^{(1)} = 0.01$. To justify that at force $\tilde{f}^{(1)}$ the system is in the range of linear response, the system is also perturbed with the external force $\tilde{f}^{(2)} = 0.002$. The waiting time t_{st} is set to $t_{st} = 10^4\,\tau_c$ as in section 7.4.1. Figure 7.11 (a) shows the integrated susceptibility $\chi_1'(t - t_{st})$ for the double well potential with the parameter choice $\tilde{\alpha} = 0.25 \cdot 2^9 = 128$ and $\tilde{\alpha}\tilde{\gamma} = 0.1$ as a function of time $t - t_{st}$. This parameter choice results in very small memory effects. The red curve shows the integrated susceptibility for the disturbance force $\tilde{f}^{(1)}$ and the light green curve is the integrated susceptibility for the disturbance force $\tilde{f}^{(2)}$. Figure (b) shows the susceptibility $\chi_1'(t - t_{st})$ for the parameters $\tilde{\alpha} = 0.5$ and $\tilde{\alpha}\tilde{\gamma} = 10$. This parameter choice gives large memory effects. Also in figure (b), the red curve gives the susceptibility at perturbation force $\tilde{f}^{(1)}$ and the light green

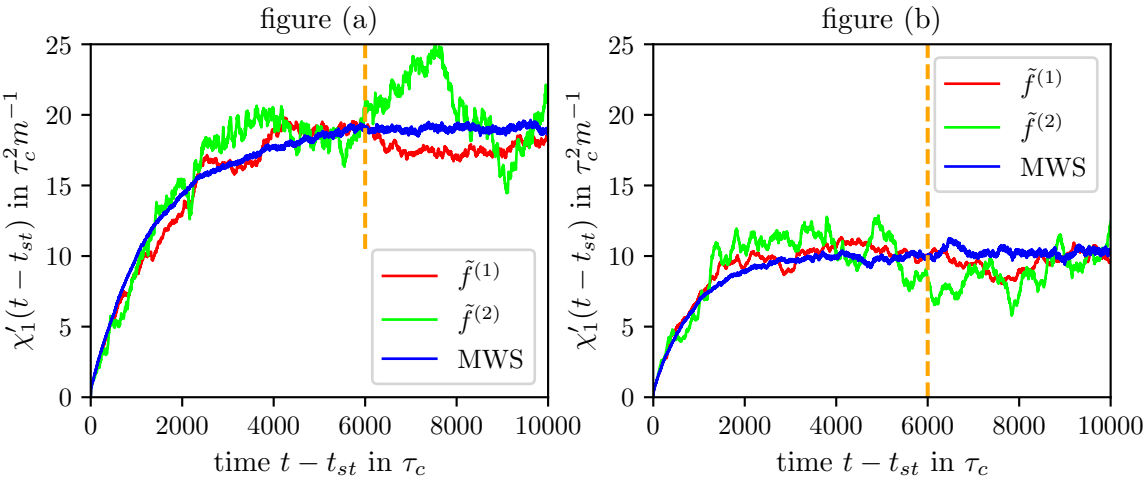

Figure 7.11: In both figures, the integrated susceptibility $\chi_1'(t-t_{st})$ is shown as a function of the time difference $t-t_{st}$. The waiting time is set to $t_{st} = 10^4\,\tau_c$. Figure (a) shows the numerically calculated susceptibility for the parameters $\tilde{\alpha} = 128$ and $\tilde{\alpha}\tilde{\gamma} = 0.1$. Figure (b) shows the numerically calculated susceptibility for the parameters $\tilde{\alpha} = 0.5$ and $\tilde{\alpha}\tilde{\gamma} = 10$. The red curve in both figures shows the susceptibility calculated with the disturbance force $\tilde{f}^{(1)} = 0.01$ according to equation (6.32). The light green curve shows the susceptibility calculated with the disturbance force $\tilde{f}^{(2)} = 0.002$. The blue curve shows the susceptibility calculated with the MWS method according to equation (6.41).

curve gives the susceptibility at perturbation force $\tilde{f}^{(2)}$. In figures (a) and (b), the statistical errors in the naive method of calculating the susceptibilities are very large. The naive method does not seem to be numerically stable for the double well potential.

Therefore, the MWS method is chosen for the calculation of the integrated susceptibility. For a good quality of the linear response function, the number of realisations is set to $R = 10^5$. In figure 7.11 the susceptibility $\chi_1'(t-t_{st})$ which is calculated numerically with the MWS method is shown as a blue curve in figures (a) and (b) respectively. The parameters for $\tilde{\alpha}$ and $\tilde{\alpha}\tilde{\gamma}$ are chosen the same as in the naive method. With the MWS method, the progression of the integrated susceptibility becomes clear. In figure (a), in the time domain $0 \leq t-t_{st} \leq 6000\,\tau_c$

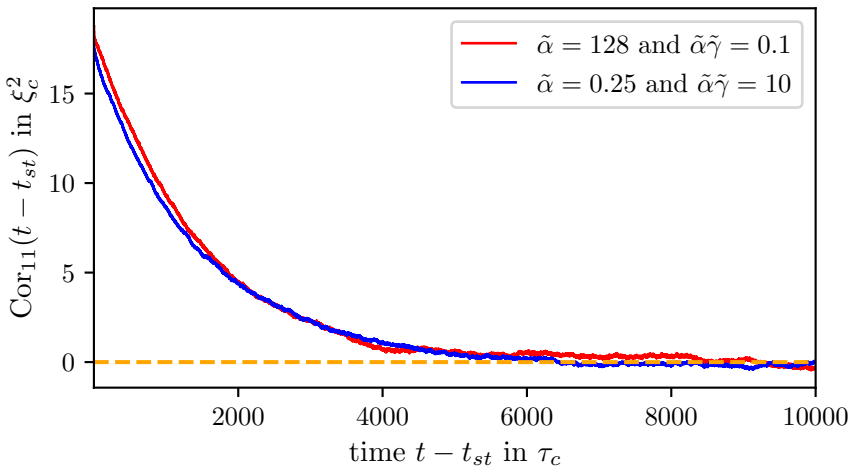

Figure 7.12: The red curve shows the correlation function as a function of time for $\tilde{\alpha} = 128$ and $\tilde{\alpha}\tilde{\gamma} = 0.1$, i.e. for small memory effects. The blue curve shows the correlation function for $\tilde{\alpha} = 0.25$ and $\tilde{\alpha}\tilde{\gamma} = 10$, i.e. for large memory effects. The orange dashed line shows the zero line.

the susceptibility $\chi_1'(t-t_{st})$ increases strictly monotonically and reaches a saturation value at the end of the time domain. For $t-t_{st} \geq 6000\,\tau_c$ the susceptibility is then constant.

Figure (b) shows a similar behaviour, where the saturation value is already reached for $t-t_{st} \geq 4000\,\tau_c$. For all parameter combinations of $\tilde{\alpha} \in \{y | y = 0.25 \cdot 2^i, i \in \{0,1,...,9\}\}$ and $\tilde{\alpha}\tilde{\gamma} \in \{0.1, 1, 10\}$ the integrated susceptibility $\chi_1'(t-t_{st})$ reaches the saturation value for the time difference $t-t_{st} \geq 6000\,\tau_c$. Therefore, $\chi_1'(t=\infty)$ is calculated over the time average. The time average is calculated in the interval $t_b \leq t-t_{st} \leq t_e$, where $t_b = 6000\,\tau_c$ and $t_e = 10000\,\tau_c$. Let $t_n = t_{st}$ be as in section 6.2. Then the index n is given by $n = 10^6$. The value $\chi_1'(t=\infty)$ is thus approximated by

$$\chi_1'(t=\infty) \approx \overline{\chi}_1' = \frac{h}{t_e - t_b} \sum_{t_i \in I} \chi_1'(t_i - t_n) \tag{7.1}$$

where $I \in \{t_b, t_b + h, t_b + 2h, ..., t_e - h, t_e\}$. The numerical uncertainty $u[\overline{\chi}_1'(t)]$ of $\overline{\chi}_1'(t)$ is calculated by the variance. The value for $\mathrm{Cor}_{11}(0)$ is calculated numerically by calculating 10 times the correlation function according to equation (6.27) with $R = 10^4$ and from this 10 values the average is determined. The numerical uncertainty $u[\mathrm{Cor}_{11}(0)]$ of $\mathrm{Cor}_{11}(0)$ is estimated by the variance. The effective temperature $T_{\mathrm{eff},4}$ is then calculated with equation (5.10) where for the uncertainty with the gaussian error propagation

$$u[T_{\mathrm{eff},4}] = \sqrt{\left(\frac{1}{\overline{\chi}_1'} u[\mathrm{Cor}_{11}(0)]\right)^2 + \left(\frac{\mathrm{Cor}_{11}(0)}{\overline{\chi}_1'^2} u[\overline{\chi}_1']\right)^2} \tag{7.2}$$

applies. It still has to be justified numerically that $\mathrm{Cor}_{11}(t)$ vanishes for $t \to \infty$. Figure 7.12 therefore shows two correlation functions $\mathrm{Cor}_{11}(t-t_{st})$ as a function of time. The red curve shows the correlation function for $\tilde{\alpha} = 128$ and $\tilde{\alpha}\tilde{\gamma} = 0.1$, i.e. for small memory effects. The blue curve shows the correlation function for $\tilde{\alpha} = 0.25$ and $\tilde{\alpha}\tilde{\gamma} = 10$, i.e. for large memory effects. It is striking that the correlation function $\mathrm{Cor}_{11}(t-t_{st})$ depends only very weakly on the choice of the parameters α and $\alpha\gamma$. This is surprising, as one would expect a much larger correlation to exist for large memory effects. Since the same code as in chapter 7.1 was used for the numerical calculation of the correlation function, an implementation error can be excluded.

Figure 7.13 shows the effective temperature $T_{\mathrm{eff},4}$, defined in equation (5.10), as a function of the coefficient α for the three decay constants $\tilde{\alpha}\tilde{\gamma} = 0.1$, $\tilde{\alpha}\tilde{\gamma} = 1$ and $\tilde{\alpha}\tilde{\gamma} = 10$. The analytical

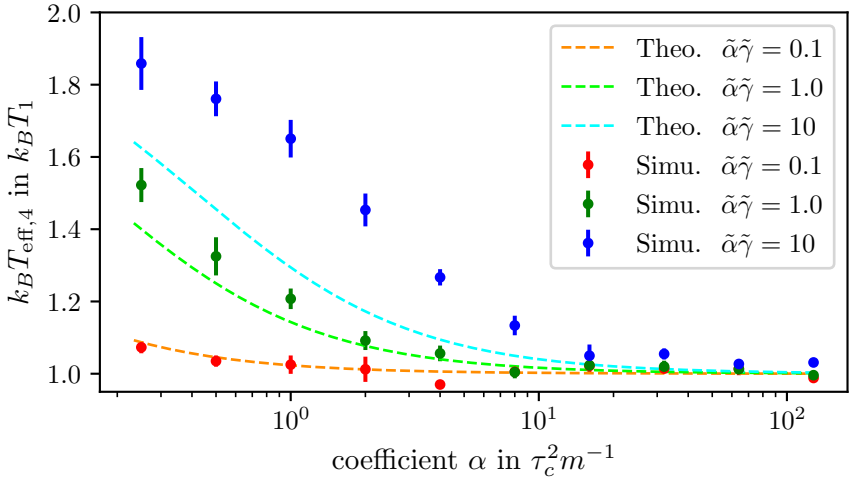

Figure 7.13: For the three decay constants $\tilde{\alpha}\tilde{\gamma} = 0.1$, $\tilde{\alpha}\tilde{\gamma} = 1$ and $\tilde{\alpha}\tilde{\gamma} = 10$ three effective temperature curves are shown depending on the parameter α. The points are the numerical results calculated with equation (5.10). The dashed lines are the analytical approximations according to equation (5.11). The analytical approximation is obviously not compatible with the numerical solution.

approximations from the Ornstein Uhlenbeck process are also shown as dashed lines in each case, which are calculated according to equation (5.11). For the decay constant $\tilde{\alpha}\tilde{\gamma} = 0.1$, the numerical solution still approximately agrees with the analytical approximation. However, for the decay constants $\tilde{\alpha}\tilde{\gamma} = 1$ and $\tilde{\alpha}\tilde{\gamma} = 10$, the numerical solutions and the analytical approximations do not agree. The effective temperature $T_{\text{eff},4}$ in equation (5.10) is thus not determined exclusively by the curvature of the minima of the double well potential. With the FDT, an effective temperature can be defined, which depends much more on the exact mathematical form of the meta-stable potential, compared to the effective temperature which is determined from the stationary distribution of the system according to section 7.4.1. The definition of the effective temperature via the FDT has another interesting property which is discussed in section 7.4.3.

7.4.3 Effective temperature with the Arrhenius factor

In this subsection, an effective temperature is determined from the Arrhenius factor. The parameters $\tilde{\Gamma}_0$ and ϵ are fixed to $\tilde{\Gamma}_0 = 4$ and $\epsilon = 2$. The energy barrier is varied for values $\tilde{E}_b \in \{5, 6, ..., 10\}$. For energy values $E_b/(k_B T_1) > 10$, the reaction rate Υ becomes so small that a numerical determination is only possible with extremely long simulation times. Ilg and Barrat have already pointed out this numerical problem in [5]. This thesis is therefore limited to the maximum value $\tilde{E}_b = 10$. According to section 4.2, the Arrhenius approximation is very good when $E_b/(k_B T_1) \gg 1$ holds. Therefore, $\tilde{E}_b = 5$ is chosen as the minimum value. The relation $\tilde{E}_b \gg 1$ is not really fulfilled. However, there are good reasons to believe that the Arrhenius dependence holds in a good approximation also for $\tilde{E}_b = 5$. In Figure 7.8, for the energy barrier $\tilde{E}_b = 5$, the Arrhenius approximation is shown as an orange dashed line. For a friction coefficient $\tilde{\Gamma}_0 = 4$, the analytically exact solution and the Arrhenius approximation are very close to each other. For an energy barrier of $\tilde{E}_b = 5$, the Arrhenius dependence seems to be satisfied to a good approximation. Note that this argument is only valid for small memory effects. For large memory effects, the simulation data will later show that the Arrhenius dependence is already very well fulfilled for an energy barrier of $\tilde{E}_b = 5$.

In Figure 7.14, the reaction rate Υ is shown as a function of the energy barrier E_b. The coefficient $\tilde{\alpha}$ is fixed at $\tilde{\alpha} = 0.25$. The reaction rate $\Upsilon(E_b)$ is calculated numerically with equation (4.45). The red curve shows the reaction rate for the decay constant $\tilde{\alpha}\tilde{\gamma} = 0.1$. The

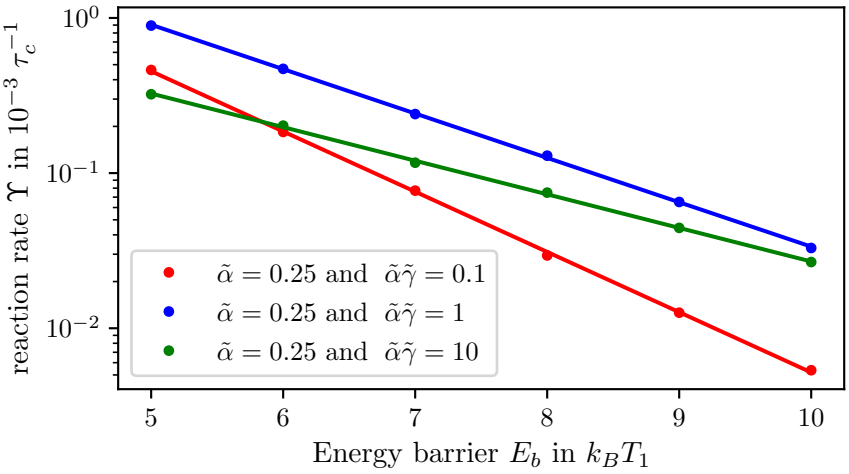

Figure 7.14: The red curve shows the reaction rate as a function of the energy barrier E_b for the combination $\tilde{\alpha} = 0.25$ and $\tilde{\alpha}\tilde{\gamma} = 0.1$. The dots are the numerical values, the solid line is the fit function. The blue curve shows the reaction rate as a function of the energy barrier for the combination $\tilde{\alpha} = 0.25$ and $\tilde{\alpha}\tilde{\gamma} = 1$ and the green curve shows the reaction rate for the combination $\tilde{\alpha} = 0.25$ and $\tilde{\alpha}\tilde{\gamma} = 10$.

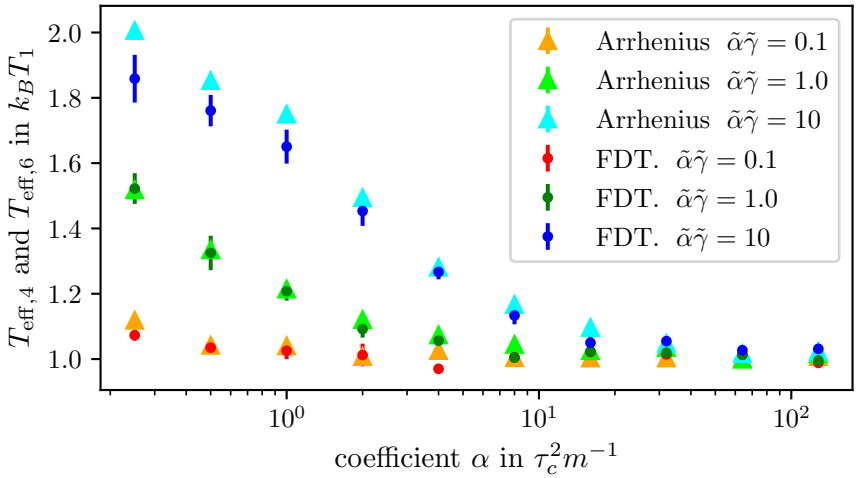

Figure 7.15: Depending on the coefficient α, the effective temperatures $T_{\text{eff},4}$ and $T_{\text{eff},6}$ are shown for the three decay constants $\tilde{\alpha}\tilde{\gamma} = 0.1$, $\tilde{\alpha}\tilde{\gamma} = 1$ and $\tilde{\alpha}\tilde{\gamma} = 10$. The triangles are the numerically calculated effective temperatures with the Arrhenius factor. The points with error bars are the numerically calculated effective temperatures with the FDT.

points symbolise the numerically calculated values. A fit function of the form $f(E_b) = b_0 - b_1 E_b$ is fitted to the 6 data points. The fit function is shown as a red solid line. The green points show the numerical reaction rate Υ for the decay constant $\tilde{\alpha}\tilde{\gamma} = 1$ and the green solid line is the corresponding fit function. In the same way, the blue curve shows the reaction rate for the decay constant $\tilde{\alpha}\tilde{\gamma} = 10$. The combination $\tilde{\alpha} = 0.25$ and $\tilde{\alpha}\tilde{\gamma} = 10$ corresponds to large memory effects. Since the blue curve has a linear behaviour, the Arrhenius dependence also applies to large memory effects.

From the $E_b - \Upsilon-$diagrams, the effective temperature $T_{\text{eff},6}$ can now be determined, which is defined in equation (5.12). For the fit parameter b_1, $T_{\text{eff},6} = 1/b_1$ then holds. In this way, the effective temperature $T_{\text{eff},6}$ is calculated for all parameter combinations $\tilde{\alpha} \in \{y | y = 0.25 \cdot 2^i, i \in \{0, 1, ..., 9\}\}$ and $\tilde{\alpha}\tilde{\gamma} \in \{0.1, 1, 10\}$. In Figure 7.15, the effective temperature $T_{\text{eff},6}$ for the decay constants $\tilde{\alpha}\tilde{\gamma} = 0.1$, $\tilde{\alpha}\tilde{\gamma} = 1$ and $\tilde{\alpha}\tilde{\gamma} = 10$ is shown as triangles depending on the coefficient α. The uncertainty of the effective temperature $T_{\text{eff},6}$ is calculated from the uncertainty of the fit parameter b_1 by gaussian error propagation. The uncertainty of $T_{\text{eff},6}$ is then less than $0.01\, k_B T_1$ and thus cannot be reasonably represented in Figure 7.15. At this point it must be noted that $T_{\text{eff},6}$ is only calculated for small energy barriers $E_b/(k_b T_1) \leq 10$. The uncertainty of $T_{\text{eff},6}$ could therefore be much larger. This methodological problem in the calculation of the effective temperature via the Arrhenius dependence has already been pointed out by Ilg and Barrat in [5]. For comparison, the effective temperatures $T_{\text{eff},4}$, which are calculated with the FDT, are plotted as points with error bars in Figure 7.15. For the decay constants $\tilde{\alpha}\tilde{\gamma} = 0.1$ and $\tilde{\alpha}\tilde{\gamma} = 1$, $T_{\text{eff},4}$ and $T_{\text{eff},6}$ agree quite well. Only for the decay constant $\tilde{\alpha}\tilde{\gamma} = 0.1$ do $\tilde{\alpha} = 0.25$ and $\tilde{\alpha} = 4$ lead to larger deviations between the two temperatures. For the decay constant $\tilde{\alpha}\tilde{\gamma} = 10$, however, there are larger deviations for the coefficients $\tilde{\alpha} \in \{0.25, 0.5, 1\}$ which seem to be systematic. For very large memory effects, the effective temperatures $T_{\text{eff},4}$ and $T_{\text{eff},6}$ probably no longer agree. The fact that the two effective temperatures for light to medium memory effects are identical is a sign that $T_{\text{eff},4}$ is a meaningful effective temperature. This is because a hallmark of activated processes is Arrhenius dependence and the effective temperature from the FDT coincides with the effective temperature from the Arrhenius factor.

8. Conclusions

Glassy systems play a very important role in today's technologised world [2]. However, a fundamental generally accepted physical description has not yet been achieved for amorphous solids. A promising concept could be effective temperatures. Therefore, the aim of this work was to investigate and compare three possible definitions of effective temperatures for the model system [6]. The central results can be summarised in the figures 7.10, 7.13 and 7.15.

The first definition of an effective temperature in this thesis is given by the stationary canonical distribution of the system according to section 5.1. What is interesting about this definition is that this effective temperature depends only weakly on the model form of the meta-stable potential. The central statement in section 7.4.1 is that the effective temperature of the double well potential is characterised by the curvature of the minima. This fact could be a hint that the effective temperature calculated by a stationary canonical distribution could be a meaningful effective temperature in experimental and theoretical terms, since the double well potential is only a model potential and real systems have only approximately this potential form. However, since the effective temperature depends to a very good approximation only on the curvature of the minima, meta-stable systems can often be modelled well by the double well potential.

The second definition of an effective temperature in this thesis is given by the FDT. For different system states, this effective temperature is shown in Figure 7.13. In section 7.4.2 it was shown that the first definition and the second definition of the effective temperature do not match for system settings where the system is far from thermal equilibrium and has medium to large memory. For glass systems which are always far from equilibrium, these two definitions represent truly different effective temperatures.

The third definition of an effective temperature uses the Arrhenius dependence of activated processes. For different system settings, this effective temperature is shown as triangles in Figure 7.15. Very interesting in this context is that the Arrhenius definition and the FDT definition coincide for system settings with small to medium memory effects. This connection between the two effective temperatures is an indication that the FDT definition is meaningful, since activated processes have the Arrhenius dependence as a trademark and the FDT definition matches the Arrhenius definition of an effective temperature. For large memory effects, however, some difference between the second and the third definition of effective temperature could be observed. With the applied methods in section 7.4.3 it could not be clarified conclusively whether for very large memory effects the second and the third definition agree or disagree. However, a precise answer to this question would be very interesting, since for glassy systems the case for large memory effects is particularly interesting.

9. Appendix

Lemma 1. *The stochastic force*

$$\xi(t) = \sqrt{\frac{k_B T_2}{\alpha}} e^{-\frac{1}{\alpha\gamma}t} + \int_0^t d\tau\, e^{-\frac{1}{\alpha\gamma}(t-\tau)} \zeta(\tau)$$

satisfies the relation

$$\langle \xi(t)\xi(s)\rangle = k_B T_2 \Gamma(t-s) = k_B T_2 \frac{1}{\alpha} e^{-\frac{1}{\alpha\gamma}(t-s)}$$

where ζ is a Gaussian white noise with $\langle \zeta(t)\rangle = 0$ and $\langle \zeta(t)\zeta(s)\rangle = 2k_B T_2 \delta(t-s)/(\alpha^2\gamma)$.

Proof. Be without limitation of generality $t > s$. For the correlation of ξ we get

$$\begin{aligned}
\langle \xi(t)\xi(s)\rangle &= \left\langle \frac{k_B T_2}{\alpha} e^{-\frac{1}{\alpha\gamma}(t+s)} \right\rangle + \left\langle \sqrt{\frac{k_B T_2}{\alpha}} e^{-\frac{1}{\alpha\gamma}t} \int_0^s d\tau_1\, e^{-\frac{1}{\alpha\gamma}(s-\tau_1)} \zeta(\tau_1) \right\rangle \\
&\quad + \left\langle \sqrt{\frac{k_B T_2}{\alpha}} e^{-\frac{1}{\alpha\gamma}s} \int_0^t d\tau_2\, e^{-\frac{1}{\alpha\gamma}(t-\tau_2)} \zeta(\tau_2) \right\rangle \\
&\quad + \left\langle \int_0^t d\tau_2 \int_0^s d\tau_1\, e^{-\frac{1}{\alpha\gamma}(t+s-\tau_1-\tau_2)} \zeta(\tau_1)\zeta(\tau_2) \right\rangle \\
&= \frac{k_B T_2}{\alpha} e^{-\frac{1}{\alpha\gamma}(t+s)} + \int_0^t d\tau_2 \int_0^s d\tau_1\, e^{-\frac{1}{\alpha\gamma}(t+s-\tau_1-\tau_2)} \langle \zeta(\tau_1)\zeta(\tau_2)\rangle \\
&= \frac{k_B T_2}{\alpha} e^{-\frac{1}{\alpha\gamma}(t+s)} + \int_0^t d\tau_2 \int_0^s d\tau_1\, e^{-\frac{1}{\alpha\gamma}(t+s-\tau_1-\tau_2)} \frac{2k_B T_2}{\alpha^2\gamma} \delta(\tau_1-\tau_2) \\
&= \frac{k_B T_2}{\alpha} e^{-\frac{1}{\alpha\gamma}(t+s)} + \int_0^s d\tau_1\, e^{-\frac{1}{\alpha\gamma}(t+s)} e^{\frac{1}{\alpha\gamma}(2\tau_1)} \frac{2k_B T_2}{\alpha^2\gamma} \\
&= \frac{k_B T_2}{\alpha} e^{-\frac{1}{\alpha\gamma}(t+s)} + \frac{k_B T_2}{\alpha} e^{-\frac{1}{\alpha\gamma}(t+s)} \left[e^{\frac{2}{\alpha\gamma}s} - 1 \right] \\
&= \frac{k_B T_2}{\alpha} e^{-\frac{1}{\alpha\gamma}(t-s)} = k_B T_2 \Gamma(t-s).
\end{aligned}$$

□

Lemma 2. *Let $\boldsymbol{x} = (x_1, x_2)^\intercal \in \mathbb{R}^2$ and $\boldsymbol{M} = (M_1, M_2)^\intercal \in \mathbb{R}^2$ be vectors and $\boldsymbol{\sigma} \in \mathbb{R}^{2\times 2}$ be a symmetric matrix. Then, for the probability distribution density*

$$p(\boldsymbol{x}, t|\boldsymbol{x}_0, t_0) = \frac{1}{\sqrt{(2\pi)^2 \det\boldsymbol{\sigma}}} \exp\left[-\frac{1}{2} (\boldsymbol{x}-\boldsymbol{M})^\intercal \boldsymbol{\sigma}^{-1} (\boldsymbol{x}-\boldsymbol{M}) \right] \tag{9.1}$$

the marginal probability distribution density $p(x_1, t|\boldsymbol{x}_0, t_0)$ is given by

$$p(x_1, t|\boldsymbol{x}_0, t_0) = \int_{\mathbb{R}} p(\boldsymbol{x}, t|\boldsymbol{x}_0, t_0) dx_2 = \frac{1}{\sqrt{2\pi\sigma_{11}}} \exp\left[-\frac{1}{2} \frac{(x_1 - M_1)^2}{\sigma_{11}} \right]. \tag{9.2}$$

Proof. If the matrix $\boldsymbol{\sigma}$ has the form

$$\boldsymbol{\sigma} = \begin{pmatrix} \sigma_{11} & \sigma_{12} \\ \sigma_{21} & \sigma_{22} \end{pmatrix} \tag{9.3}$$

then the inverse matrix is given by

$$\boldsymbol{\sigma}^{-1} = \frac{1}{\det\boldsymbol{\sigma}} \begin{pmatrix} \sigma_{22} & -\sigma_{12} \\ -\sigma_{21} & \sigma_{11} \end{pmatrix}. \tag{9.4}$$

For a more compact notation, set $\boldsymbol{y} = \boldsymbol{x} - \boldsymbol{M}$. Then it applies

$$\boldsymbol{y}^\intercal \boldsymbol{\sigma}^{-1} \boldsymbol{y} = \frac{1}{\det\boldsymbol{\sigma}} (y_1, y_2) \begin{pmatrix} \sigma_{22} & -\sigma_{12} \\ -\sigma_{21} & \sigma_{11} \end{pmatrix} \begin{pmatrix} y_1 \\ y_2 \end{pmatrix} = \frac{1}{\det\boldsymbol{\sigma}} (\sigma_{22} y_1^2 - 2\sigma_{12} y_1 x_2 + \sigma_{11} y_2^2) \tag{9.5}$$

using that the matrix $\boldsymbol{\sigma}$ is symmetric so $\sigma_{12} = \sigma_{21}$ holds. With qudratic complement the following applies

$$\begin{aligned} \sigma_{22} y_1^2 - 2\sigma_{12} y_1 y_2 + \sigma_{11} y_2^2 &= \sigma_{22} y_1^2 + \sigma_{11} (y_2^2 - 2\frac{\sigma_{12}}{\sigma_{11}} y_1 y_2) \\ &= \sigma_{22} y_1^2 + \sigma_{11} \left(y_2 - \frac{\sigma_{12} y_1}{\sigma_{11}} \right)^2 - \sigma_{11} \left(\frac{\sigma_{12} y_1}{\sigma_{11}} \right)^2 \\ &= \frac{1}{\sigma_{11}} \left(\sigma_{11}\sigma_{22} - \sigma_{12}\sigma_{12} \right) y_1^2 + \sigma_{11} \left(y_2 - \frac{\sigma_{12} y_1}{\sigma_{11}} \right)^2 \\ &= \frac{\det\boldsymbol{\sigma}}{\sigma_{11}} y_1^2 + \sigma_{11} \left(y_2 - \frac{\sigma_{12} y_1}{\sigma_{11}} \right)^2. \end{aligned} \tag{9.6}$$

For the marginal probability distribution we then get

$$\begin{aligned} p(x_1, t | \boldsymbol{x}_0, t_0) &= \int_{\mathbb{R}} \frac{1}{\sqrt{(2\pi)^2 \det\boldsymbol{\sigma}}} \exp\left[-\frac{1}{2} \boldsymbol{y}^\intercal \boldsymbol{\sigma}^{-1} \boldsymbol{y} \right] dy_2 \\ &= \int_{\mathbb{R}} \frac{1}{\sqrt{(2\pi)^2 \det\boldsymbol{\sigma}}} \exp\left[-\frac{1}{2} \frac{1}{\det\boldsymbol{\sigma}} \left(\frac{\det\boldsymbol{\sigma}}{\sigma_{11}} y_1^2 + \sigma_{11} \left(y_2 - \frac{\sigma_{12} y_1}{\sigma_{11}} \right)^2 \right) \right] dy_2 \\ &= \frac{1}{\sqrt{(2\pi)^2 \det\boldsymbol{\sigma}}} \frac{\sqrt{2\pi \det\boldsymbol{\sigma}}}{\sqrt{\sigma_{11}}} \exp\left(-\frac{1}{2} \frac{y_1^2}{\sigma_{11}} \right) = \frac{1}{\sqrt{2\pi\sigma_{11}}} \exp\left(-\frac{1}{2} \frac{(x_1 - M_1)^2}{\sigma_{11}} \right) \end{aligned} \tag{9.7}$$

□

Dialogue between two students:

Art student: I have to go to Berlin or Munich every 2 weeks. In Konstanz, my creativity simply can't unfold. I simply need the live style of the big city to be productive. How often do you get out of Konstanz?

Physics student: My mean escape rate fulfil $\Omega^\dagger \tau_m(x_0) = -1$.

List of Figures

Bibliography

[1] R. Mandal and P. Sollich, *How to study a persistent active glassy system*, J. Phys.: Condens. Matter **33** 184001 (2021)

[2] M. D. Ediger, C. A. Angell and S. R. Nagel, *Supercooled Liquids and Glasses*, J. Phys. Chem. 100, 13200-13212 (1996)

[3] L. Berthier and G. Biroli, *Theoretical perspective on the glass transition and amorphous materials*, Rev. Mod. Phys. **83**, 587 (2011)

[4] Th. M. Nieuwenhuizen, *Thermodynamics of the Glassy State: Effective Temperature as an Additional System Parameter*, Phys. Rev. Lett. **80**, 5580 (1998)

[5] P. Ilg and J.-L Barrat, *Driven activation vs. thermal activation*, EPL **79**, 26001 (2007)

[6] P. Ilg and J.-L. Barrat, *Effective temperatures in a simple model of non-equilibrium, non-Markovian dynamics*, J. Phys.: Conf. Ser. **40**, 76 (2006)

[7] F. Schwabl, *Statistische Mechanik*, 3. Auflage, Springer-Verlag, Berlin Heidelberg, 2006

[8] J. Honerkamp, *Stochastische Dynamische Systeme - Konzepte, numerische Methoden, Datenanalyse*, 1. Auflage, VCH Verlagsgesellschaft, Weinheim, 1990

[9] R. Zwanzig, *Nonequilibrium statistical mechanics*,1. Auflage, Oxford University Press, New York, 2001

[10] J. Schropp, Skript zur Vorlesung *Numerik stochastischer Differentialgleichungen*, WiSi 2020/21, `http://www.math.uni-konstanz.de/~schropp/numsto/skript.pdf`

[11] W. Dieterich, Skript zur Vorlesung *Stochastische Prozesse in der Physik kondensierter Materie*, SoSe 2000, `https://theorie.physik.uni-konstanz.de/dieterich/skripte/Stochastische-Prozesse_Skript.pdf`

[12] M. Maier, N. Ditz and N. Grimm, Skript zur *Vorlesung Nonequilibrium Physics* von Prof. M. Fuchs, SoSe 2021

[13] M. Gnann, M. Ring, T. Bissinger, M. Gruber and J. Häring, Skript zur Vorlesung *Stochastische Prozesse* von Prof. M. Fuchs, SoSe 2019

[14] P. Hanggi, *Escape from a metastable state*, J Stat Phys **42**, 105–148 (1986)

[15] M. Gruber, *Kramers Entweichrate am Beispiel des Doppelmuldenpotentials*, Projekt Praktikum (unveröffentlicht) 2013

[16] H. Risken, *The Fokker-Planck Equation Methods of Solution and Applications*, 2. Auflage, Springer-Verlag, Berlin Heidelberg, 1996

[17] P. B. Warren and R. J. Allen, *Malliavin Weight Sampling for Computing Sensitivity Coefficients in Brownian Dynamics Simulations*, Phys. Rev. Lett. **109**, 250601 (2012)

[18] P. B. Warren and R. J. Allen, Supplementary Material for the article Phys. Rev. Lett. **109**, 250601 (2012)